THE APPLICATION OF THREE-DIMENSIONAL OPTICAL TRANSFORMS TO CRYSTAL-STRUCTURE DETERMINATION.

A Thesis presented to the
University of Manchester
for the degree of
Doctor of Philosophy

By
K. WALKLEY

July 1968

ProQuest LLC.
789 East Eisenhower Parkway
P.O. Box 1346
Ann Arbor, MI 48106 – 1346

PREFACE

None of the work described in this thesis has been presented to another university in support of an application for a higher degree.

All the author's research experience since first graduating has been gained in the Physics Department of the University of Manchester Institute of Science and Technology. The following appointments have been held:-

October 1964 to October 1966 - SRC Research Studentship.

October 1966 to the time of writing - Temporary Demonstrator.

A paper, written jointly with Professor H Lipson, has been published describing part of the work:

"On the validity of Babinet's Principle for Fraunhofer Diffraction", Optica Acta, 1968, 15, 83-91.

A further paper, written jointly with Dr G Harburn and Professor C A Taylor, has also been published during the course of the work:

"Gas-phase Laser as a Source of Light for an Optical Diffractometer", Nature, 1965, 205, 1095-1096.

ABSTRACT

The thesis is divided into two main sections. In the first section (chapters 1-4 inclusive) is described how three-dimensional optical transforms can be obtained from three-dimensional models and used in the solution of crystal structures. In the second section (chapters 5-7 inclusive) the solution of the crystal structure of 2-diazoindane-1,3-dione is discussed. It was originally intended to link both halves of the work by using three-dimensional optical transforms in the solution of the structure of 2-diazoindane-1,3-dione. However, the structure was solved by conventional methods before this new technique could be developed.

Chapter 1 outlines the conventional optical-transform technique of solving crystal structures using two-dimensional diffraction screens to give corresponding sections of the reciprocal solid. Ways in which the complete three-dimensional optical transform could be used are indicated and Harburn's method of obtaining non-central sections of the reciprocal solid is outlined. Also discussed is the suggestion by Harburn, on which this work is based, that three-dimensional optical transforms could be formed from diffraction patterns of three-dimensional models utilising Babinet's principle.

Babinet's principle is examined critically in chapter 2 and the very restricted conditions under which it is applicable are laid down. It is shown that transforms of

three-dimensional models cannot be obtained in the way that Harburn supposes, because the diffraction pattern of the aperture of the diffraction instrument must always swamp the pattern given by the model.

Chapter 3 discusses how the difficulties associated with Babinet's principle might be overcome using the technique known as apodisation. The use of two-dimensional apodising screens is described but rejected on theoretical and experimental grounds. Then the application of apodising apertures is explored and they are found to give satisfactory results.

Chapter 4 then gives examples of the applications of the apodising-aperture method of producing optical transforms of three-dimensional models. Other possible uses of the method are also discussed.

In Chapter 5 the initial steps in the solution of the structure 2-diazoindane-1,3-dione are described. The chemical interest in the structure is first outlined and the derivation of the unit cell and the space group is described. The solution of the (001) projection of the molecule is obtained using a combination of optical methods and Fourier methods followed by a rigid-body minimum-residual refinement.

Chapter 6 describes the completion of the structure refinement. The solution of the (100) projection is obtained using the minimum-residual refinement method and difference maps. Then, all the available data is used in a least-squares refinement of the complete structure. The resulting structure is examined critically using difference maps.

Finally in Chapter 7 the refined structure is examined in detail. Bond lengths and angles are calculated and compared with the values that might be anticipated and the degree of planarity of the molecule is examined. The packing of the molecules is discussed and lastly the parameters of the thermal vibration ellipsoids are derived.

CONTENTS

PART 1

THREE-DIMENSIONAL OPTICAL TRANSFORMS FROM THREE-DIMENSIONAL ATOMIC MODELS USING BABINET'S PRINCIPLE

CHAPTER 1

THE OPTICAL-TRANSFORM METHOD AND ITS EXTENSION TO THREE DIMENSIONS

The optical-transform method is now a well known technique in X-ray crystal-structure determination and it is not proposed to give an exhaustive description of it here. However certain theoretical and practical aspects, that are necessary to present a coherent and logical introduction to this work, will be outlined. In addition, the notation to be used will be introduced. Further information concerning the optical-transform method can be obtained from the standard works on the subject - Lipson and Taylor (1958) and Taylor and Lipson (1964) - and, from a concise but comprehensive review article, Lipson and Taylor (1965).

1.1 THE ANALOGY BETWEEN X-RAY AND OPTICAL DIFFRACTION

Consider a parallel beam of monochromatic coherent radiation striking a body of some material which will both transmit and scatter the radiation (fig.1.1a). If $\underline{s}_o$ and $\underline{s}$ are unit vectors representing the incident and scattered beams respectively, then the wave scattered by an incremental volume dV at a distance $\underline{r}$ from some arbitrary origin O is given in amplitude and phase by

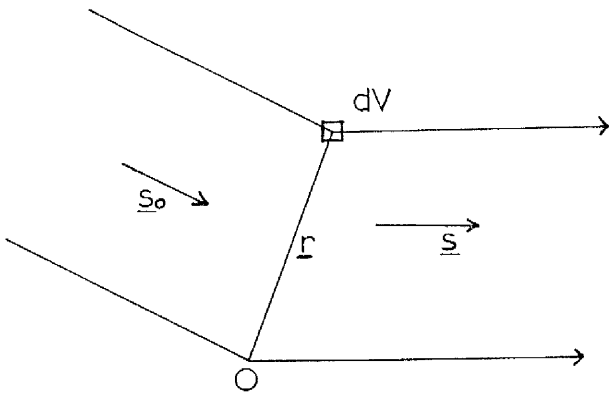

Fig1.1a

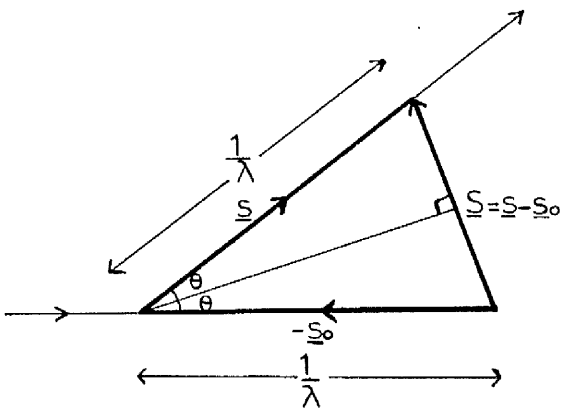

Fig.1.1b

$$dG(\underline{s}) = \rho(\underline{r}).dV.\exp[\frac{2\pi i}{\lambda}\,\underline{r}.(\underline{s} - \underline{s_o})]$$

The quantity $\rho(\underline{r})$ is the scattering density of the material at the element. If we now write $\underline{S} = \underline{s} - \underline{s_o}$, then the total scattering by the whole volume in the direction $\underline{s}$ is given by

$$G(\underline{S}) = \int_V \rho(\underline{r})\,\exp[\frac{2\pi i}{\lambda}\,\underline{r}.\underline{S}]dV \qquad (1.1)$$

It will immediately be seen that equation 1.1 has the form of a Fourier-transform relationship; that is, $G(\underline{S})$ is the Fourier transform of $\rho(\underline{r})$. $G(\underline{S})$ is a complex function which can be visualised as a "solid" reciprocal in nature to the scattering body $\rho(\underline{r})$ and existing in "reciprocal space", that is, $\underline{S}$ space. The term "reciprocal space" results from the inverse relationship between functions and their Fourier transforms; fine detail in the diffracting material, or "real space", is represented by large distances in reciprocal space.

Figure 1.1b is a vector diagram of the scattering process. No assumptions have so far been made about the amplitudes of $\underline{s}$ and $\underline{s_o}$ but it is convenient to make these $1/\lambda$, where λ is the wavelength of the radiation, so that the dimensions of reciprocal space are independent of λ; then $\underline{S} = \frac{2\sin\theta}{\lambda}$, where 2θ is the scattering angle and

$$G(\underline{S}) = \int_V \rho(\underline{r})\,\exp(2\pi i\,\underline{r}.\underline{S})dV \qquad (1.2)$$

The reciprocal-space variable $\underline{S}$, usually referred to simply as the reciprocal vector, has the dimensions of reciprocal length. If the incident beam is fixed but θ is allowed to take on all values, then the locus of the end of the vector $\underline{S}$ is the surface of a sphere of radius $1/\lambda$, the

sphere of reflection (fig.1.2). If the direction of the incident beam is now allowed to take on all possible values, it can be seen that the end of the reciprocal-lattice vector will occupy all points within a sphere of radius $2/\lambda$, the limiting sphere. The reciprocal solid may only be explored at points within this sphere (Lipson and Taylor 1958).

It will be noted that so far no mention has been made about the nature of the scattering material or the radiation. We shall, however, be concerned with the scattering of X-rays by electrons in crystals and of light waves by diffraction screens (under Fraunhofer conditions); although the mechanism of scattering is different, the above theory may be applied equally well to each. Since optical diffraction is usually carried out using two-dimensional screens, the analogy with three-dimensional X-ray scattering is often missed; however, even a strictly two-dimensional diffraction screen would produce a three-dimensional reciprocal solid, variable in two dimensions and constant along the other dimension.

One difference between optical and X-ray diffraction is extremely important. For X-rays diffracted by the atoms in a crystal, the relevant part of the reciprocal solid and the limiting sphere are of the same order of magnitude, since the wavelength of the radiation is about the same size as the atomic spacings. However, with the diffraction equipment used by the author the diffraction screens have dimensions about 10^4 times the wavelength of light and therefore the relevant detail in the reciprocal solid is much smaller (10^{-4} times) than the limiting sphere. In addition, the incident beam is fixed during observation of the optical

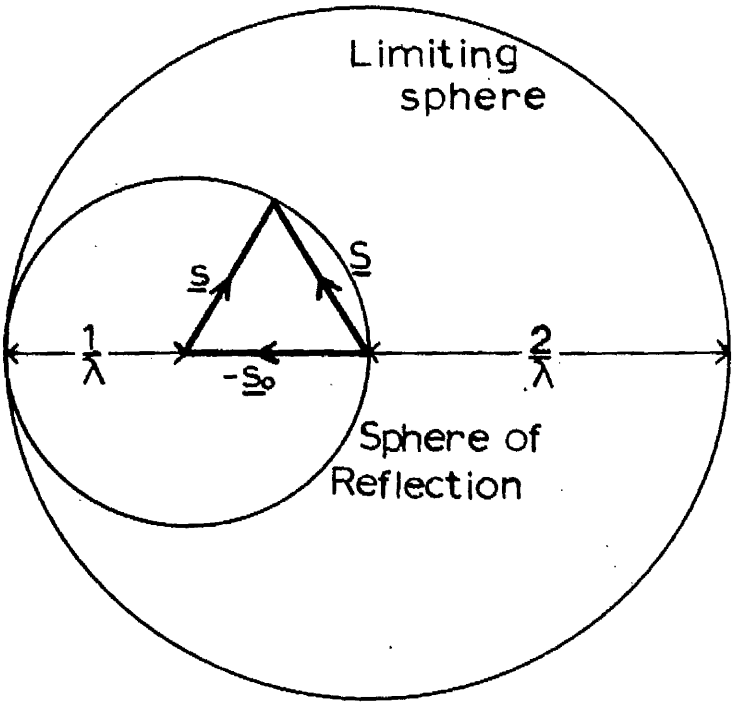

Fig.1.2

diffraction patterns and the diffraction angle θ is quite small ($\approx 10^{-3}$rad.). The total result is that, effectively, only a small cross-section of the reciprocal solid is observed, where it intersects the sphere of reflection; the cross-section appears planar because of the large radius of the sphere.

In the case of X-ray diffraction we shall normally only consider scattering by crystals whose lattices are perfectly ordered in three dimensions. The reciprocal solid is the familiar reciprocal lattice. Each reciprocal-lattice point represents a sampling of the continuous reciprocal solid obtained from a single unit cell of the real structure (Lipson and Taylor, 1958). We may therefore write the familiar X-ray scattering equation as

$$G(\underline{S}) = F(hkl) = \sum_{n=1}^{N} f_n \exp[2\pi i(hx_n + ky_n + lz_n)] \qquad (1.3)$$

The summation is taken over the N atoms of one unit cell and f_n is the scattering factor for the n^{th} atom with coordinates x_n, y_n and z_n expressed as fractions of the unit cell translations $\underline{a}$, $\underline{b}$ and $\underline{c}$. The indices h, k and l can assume whole number values only; they denote integral multiples of the reciprocal unit cell translations $\underline{a}^*$, $\underline{b}^*$ and $\underline{c}^*$ and specify the reciprocal-lattice points.

1.2 OPTICAL-TRANSFORM METHODS IN TWO DIMENSIONS

The similarity between X-ray diffraction and optical diffraction forms the basis of the optical-transform method of solving crystal structures. In this method X-ray data are compared with the optical diffraction pattern of a

representation of a possible structure. The representation of the structure is made by punching holes at atomic positions in an opaque card; it is only necessary to punch the projection of one unit cell of the structure (Hanson, Lipson and Taylor, 1953). The Fraunhofer diffraction pattern, or optical transform, is then formed, usually by means of an optical diffractometer (Hughes and Taylor (1953), Taylor and Thompson (1957)). The X-ray data are presented in the form of the relevant reciprocal-lattice section, drawn on transparent paper, and weighted at each reciprocal-lattice point with a black disc whose area is proportional to the X-ray amplitude at that point. (It is found convenient to use unitary structure factors rather than simple structure factors for the data). If the weighted reciprocal-lattice net is superimposed on a photograph of the optical transform of a trial structure the agreement may be tested and possible adjustments to the model suggested.

As was indicated above, the two-dimensional diffraction screen is a representation of a crystal structure projected onto a plane, and it has a transform which is constant in one dimension. The optical transform observed is a cross section of the transform perpendicular to the constant direction. What fraction of the total three-dimensional X-ray data can we compare with this optical transform therefore? The central section of the X-ray reciprocal solid (or lattice) parallel to the plane of projection of the structure is the relevant part. This may be shown simply if we let $O'S_xS_yS_z$ be an orthogonal set of axes in reciprocal space parallel to the axes Oxyz in real space. Equation 1.2 may be rewritten

$$G(S_x,S_y,S_z) =$$

$$\iiint_{xyz} \rho(x,y,z) \exp[2\pi i(xS_x + yS_y + xS_x)] \, dx \, dy \, dz$$

The complex amplitude distribution on the $O'S_xS_y$ plane ($S_z = 0$) is given by

$$G(S_x,S_y) =$$

$$\iiint_{xyz} \rho(x,y,z) \exp[2\pi i(xS_x + yS_y)] \, dx \, dy \, dz$$

i.e. $G(S_x,S_y) =$

$$\iint_{xy} \{\int_{z} \rho(x,y,z) \, dz\} \exp[2\pi i(xS_x + yS_y)] \, dx \, dy \qquad (1.4)$$

The term in curly brackets represents the projection of the real-space scattering density on to the Oxy plane. Therefore from equation 1.3 we can see that the transform of the projection of the scattering density in real space on to the Oxy plane is equal to the amplitude distribution on the parallel $O'S_xS_y$ plane in reciprocal space.

1.3 THREE-DIMENSIONAL OPTICAL TRANSFORMS - HARBURN'S METHOD

The optical-transform method is therefore essentially limited to two dimensions - projections in real space and corresponding sections in reciprocal space. However, as crystal structures are attempted which are more and more complex, this and other purely two-dimensional methods prove frequently inadequate. The usual reason for failure is that overlapping atoms in projection make interpretation of

two-dimensional electron density or Patterson maps difficult. Thus is has frequently been found necessary to use the full amount of information in the three-dimensional data and to use three-dimensional visualisations of the structure.

Many of the standard two-dimensional methods, for example, Patterson techniques [Buerger (1959)], have been readily extended to three dimensions. Three-dimensional weighted reciprocal lattices have been found to give useful information also (Iball and Mackay (1962)). Professor C A Taylor has therefore suggested that it might be valuable to attempt to extend the optical-transform method to three dimensions and a technique of producing diffraction patterns, representing non-central sections of reciprocal space, was evolved by Harburn and Taylor (1961) (also Harburn 1961). The basis of this method may be seen by rearranging equation 1.3, that is

$$G(\underline{S}) = \sum_{n=1}^{N} f_n \exp[2\pi i(hx_n + ky_n + lz_n)]$$

applying it here to diffraction of light by screens, so that f_n is the scattering factor of an aperture. We may rewrite the equation as

$$G(\underline{S}) = \sum_{n=1}^{N} f_n \exp[2\pi i(hx_n + ky_n)] \exp(2\pi i l z_n) \qquad (1.5)$$

If $l = 0$ this reduces to

$$G(\underline{S}) = \sum_{n=1}^{N} f_n \exp[2\pi i(hx_n + ky_n)] \qquad (1.6)$$

Equation 1.6 indicates that the zero layer of the reciprocal lattice (the central section of the reciprocal solid) may be represented by a two-dimensional mask equivalent

to the projection of the crystal structure. Equation 1.5 shows that, if l is not zero (a non-central section), we may still use the same mask but the phases of the light passing through each hole must be changed from zero to $2\pi lz_n$. Harburn produced these phase changes by rotating mica plates placed over each hole in the mask, which was illuminated by circularly polarised light.

1.4 THREE-DIMENSIONAL OPTICAL TRANSFORMS USING BABINET'S PRINCIPLE

Harburn and Taylor have also suggested a further method of producing three-dimensional optical transforms. The following quotation from Harburn (1961) outlines the idea:

> "Babinet's theorem states that, except at the centre, the intensity distributions in the Fraunhofer diffraction patterns of two complementary screens are the same; complementary screens have their clear and opaque areas interchanged. Utilizing this principle a trial structure could be represented in the parallel beam of a diffractometer by a model with small spherical balls representing the atoms and, except for the zero order, the optical transform of such an arrangement would be the same as that for a mask prepared in the conventional manner.
>
> If the various practical difficulties were overcome it would be possible, in theory, to build up the three-dimensional transform from a series of pictures taken with the model rotated a small amount about a chosen axis between exposures."

The optical transform is in each case a central section of the reciprocal solid; and we can scan the whole of the

solid by rotating the section. This is somewhat analogous to taking a rotation photograph in X-ray crystallography.

The attempt to achieve three-dimensional optical transforms in this way forms the first part of this thesis. It was realised early in the work that, in addition to practical difficulties, certain theoretical obstacles lie in the way of achieving the desired results. As will be shown in the following chapter, the view of Babinet's principle taken by Harburn and Taylor is misleading. It should be added that the same view is quite generally held to be correct.

1.5 NOTATION USED IN FRAUNHOFER DIFFRACTION WORK

The notation used up to this point is that commonly applied to X-ray crystallography and, although it can be useful in considering optical transforms, it is inconvenient to apply in the case of simple Fraunhofer diffraction of light. Figure 1.3 illustrates the notation to be used in discussing Babinet's principle (Chapter 2), and apodisation and its application to producing three-dimensional optical transforms (Chapter 3). The diagram is an idealised optical system of an optical diffractometer.

O_oOO_1 defines the common optic axis of the two lenses L_1 and L_2, O_o and O_1 being the focal points of L_1 and L_2 respectively. Oxyz defines an orthogonal set of axes at O, Oz lying along the optic axis. $O_1\xi'\eta'$ defines a two-dimensional set of axes at O_1, in a plane perpendicular to the optic axis. If a diffracting object is placed between L_1 and L_2 and illuminated by a monochromatic point source at

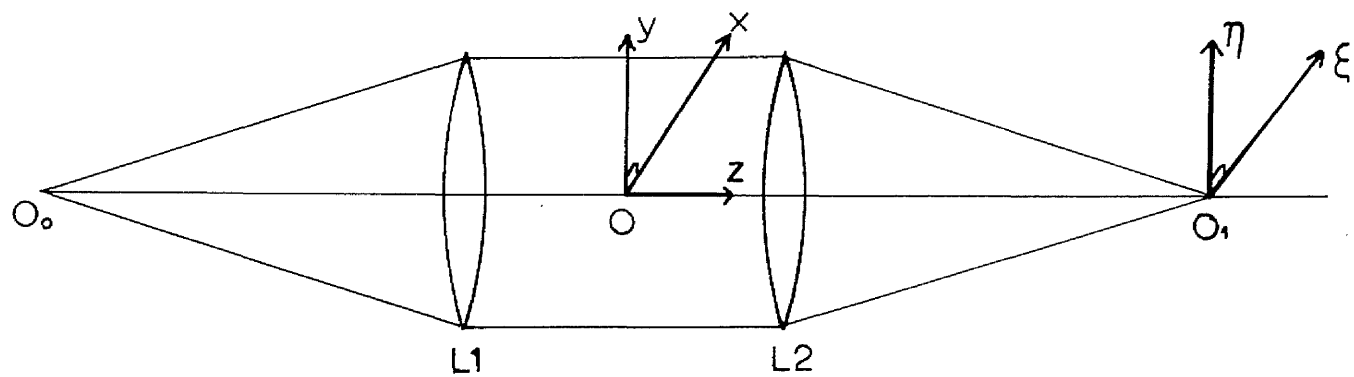

Fig.1.3

O_o, a Fraunhofer diffraction pattern is produced in the $O\xi'\eta'$ plane.

The Fourier-transform relation between a two-dimensional screen, with transparency distribution $T(x,y)$, and its diffraction pattern may be written

$$A(\xi',\eta') =$$

$$\iint_{xy} T(x,y) \exp\left[\frac{2\pi i}{p\lambda}(x\xi' + y\eta')\right] dx\, dy \qquad (1.7)$$

where p is the focal length of the lens L_2. It is usual to simplify this relation by writing

$$\xi = \frac{\xi'}{p\lambda} \quad \text{and} \quad \eta = \frac{\eta'}{p\lambda} \quad \text{so that}$$

$$A(\xi,\eta) =$$

$$\iint_{xy} T(x,y) \exp[2\pi i(x\xi + y\eta)] dx\, dy \qquad (1.8)$$

The similarity between the Fourier transform relationships in equation 1.8 and 1.2 can easily be seen. If the screen, and hence its diffraction pattern, has circular symmetry then we can write

$$A(\rho) = \int_r T(r)\, J_o(2\pi r\rho)\, 2\pi r\, dr \qquad (1.9)$$

where $\rho^2 = \xi^2 + \eta^2$ and $r^2 = x^2 + y^2$. Equation 1.9 is in the form of a Hankel transform relation and it is useful when considering apodisation.

We have already seen that if we have a three-dimensional transparency distribution

$$A(\xi,\eta) =$$

$$\iint_{xy} \{\int_{z} T(x,y,z)\, dz\} \exp[2\pi i(x\xi + y\eta)]\, dx\, dy \qquad (1.10)$$

the quantity in curly brackets represents the projection of $T(x,y,z)$ on to the plane $z = 0$.

1.6 SUMMARY

The purpose of the work described in the first part of this thesis may now be summarised. Many crystal-structure determinations are now carried out in three dimensions and therefore an extension of the optical-transform method to three dimensions could prove useful. One possible approach to achieving this aim has been suggested: that is to put actual three-dimensional models in the aperture of an optical diffractometer and photograph their diffraction patterns. We should expect to see optical transforms which correspond to those from a punched mask representation of a projection of each model. Babinet's principle indicates that this latter result should be valid; the following chapter examines this principle carefully and shows that the anticipated result does not in fact occur.

CHAPTER 2

BABINET'S PRINCIPLE

2 BABINET'S PRINCIPLE

While attempting to apply Babinet's principle in producing optical transforms of three-dimensional objects, as outlined in the previous chapter, the author was forced to look very closely at the limitations on the principle. This chapter is concerned mainly with the conclusions drawn from this investigation (see also Lipson and Walkley (1965)). Babinet's principle (Babinet (1837)) is an interesting example of an idea which has been changed almost out of recognition by the reinterpretations of later investigators; in addition a number of fallacies have become associated with it and these are pointed out. Although Babinet's principle is applied to both Fresnel and Fraunhofer diffraction the discussion is mostly concerned with the latter.

2.1 INTRODUCTION TO BABINET'S PRINCIPLE

Let us examine an account of Babinet's principle which might be given in the average textbook in optics. We consider a two-dimensional screen containing a large aperture and illuminated by a point source S of monochromatic light (fig. 2.1). At some point P, on the far side of the screen

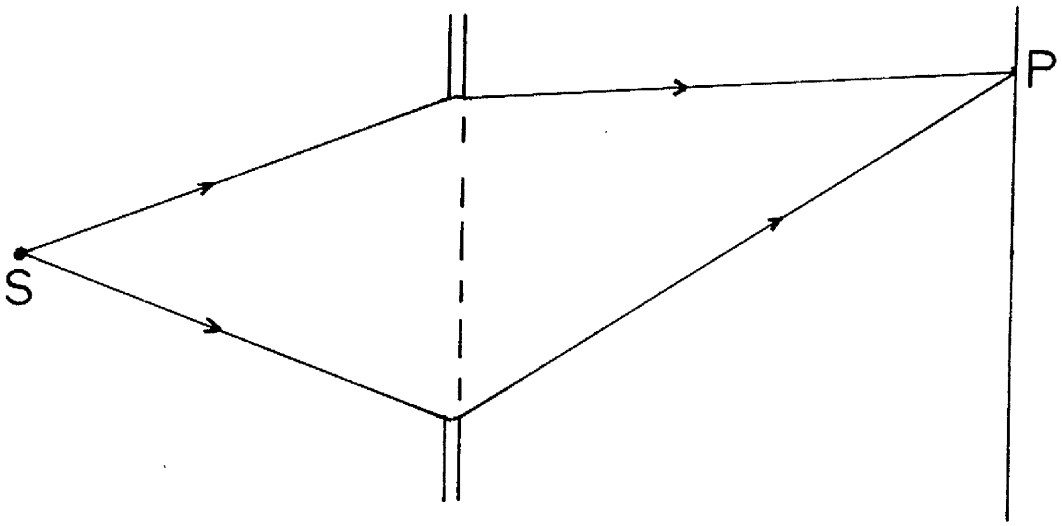

Fig.2.1

from the light source, we obtain a diffraction pattern of the aperture in the screen. Let us suppose that the vector amplitude is A_0 at P. The large aperture in the screen is then covered by another screen, containing a number of smaller apertures, giving a diffraction pattern with vector amplitude A_1 at P. This latter screen is then replaced by another in which the opaque portions correspond to clear portions in the first screen and vice-versa. (The two screens are said to be complementary). If the second screen gives amplitude A_2 at P, then by the vector addition property of light:-

$$A_0 = A_1 + A_2 \qquad (2.1)$$

If $A_0 = 0$ over most of the diffraction pattern then

$$|A_1|^2 = |A_2|^2 \qquad (2.2)$$

and therefore the diffraction patterns of the complementary screens will appear identical, having equal intensity distributions.

Equation 2.1 is given in many modern textbooks as a statement of Babinet's principle; however it is often regarded to be the statement that complementary screens produce identical diffraction patterns, i.e. equation 2.2. The difficulty arises because it is implicitly assumed that the two expressions are equivalent. Equation 2.1 is of course absolutely correct within the limits of Kirchhoff's diffraction theory but, as we shall see, complementary screens only rarely produce similar diffraction patterns. We shall in the following regard this latter statement as representing

Babinet's principle (although incorrect) since it is the traditional physical idea associated with the principle.

Equation 2.1 holds for both Fresnel and Fraunhofer diffraction. (In the case of Fraunhofer diffraction S and P may be considered to be at large distances from the screen). A number of textbooks, e.g. Meyer (1949) and Sommerfeld (1954), recognise that for Fresnel diffraction the quantity A_o will have large values over most of the points P not in the geometric shadow of the surrounding aperture (that is, effectively over the whole pattern). Hence the Fresnel diffraction patterns of complementary screens are not equivalent and Babinet's principle cannot be applied. For Fraunhofer diffraction, however, most optics textbooks assume that complementary screens produce identical diffraction patterns (see, for example, Michelson (1927), Sommerfeld (1954), Meyer (1949), Andrews (1960), Longhurst (1962), and Jenkins and White (1957)). The usual justification is that A_o is very small except for a small region near the centre of the pattern. (This particular idea is refuted in section 2.5.) However, complementary screens produce comparable Fraunhofer diffraction patterns only under certain limited conditions and the major part of this chapter is devoted to demonstrating this fact.

It is convenient to consider here one possible objection to the above consideration of Babinet's principle. It would be reasonable to consider a situation where there was no limiting aperture to the complementary screens. This would mean that there is no contribution A_o and hence $|A_1|^2 = |A_2|^2$ for the whole pattern. However this would not represent any physically real system. It is always necessary

to limit the extent of the diffraction screens if only to ensure coherent illumination over their total area (Taylor and Thompson (1957)).

2.2 HISTORICAL DEVELOPMENT OF BABINET'S PRINCIPLE

It has already been stated that Babinet's principle is a concept which has altered considerably from its original form. It is interesting to trace this development, as it sheds some light on how and when the various misconceptions have arisen.

Babinet's original paper (Babinet 1837) is concerned with an explanation of the occasional appearance of haloes surrounding the Sun and Moon. He interprets this phenomenon as being due to light diffracted by small spherical water droplets of roughly uniform size in the atmosphere.

Babinet states the principle thus (in translation):

> "Given a point of light producing its normal image at the back of the eye, if, outside the line joining the point and the eye, but fairly near to this line, we place a small opaque obstacle, the effect of this small opaque body will be exactly the same as that of a precisely similar aperture illuminated by incident light, so that to the extent that the globule would seem necessarily to produce opacity, in reality it produces illumination."

Babinet does not justify this statement beyond giving an explanation of the presence of light in the shadow of an opaque body in terms of half-period zones. It will be noted that the statement is quite vague and there is of course no mention of the idea of complementary screens.

The phenomenon that Babinet describes, of the diffraction of light by collections of small opaque bodies, had been previously observed by a number of investigators of whom Babinet mentions Newton and Young. Young (1845) used the effect in the device known as "Young's Eriometer" (see 2.6) to measure the diameters of thin fibres and small particles.

Babinet does not connect his statement with either Fresnel or Fraunhofer diffraction, although the phenomenon he describes obviously belong to the Fraunhofer class. Sommerfeld (1954) states that initially Babinet's principle was applied only to Fraunhofer diffraction. It is more probable, however, that the distinction had not been clearly drawn at that time between Fraunhofer and Fresnel diffraction.

Verdet (1869) describes a particular illustration of the principle. He derives the Fraunhofer diffraction pattern of a number of parallel threads of the same diameter (as in Young's Eriometer) and shows that this is the same as the diffraction pattern of its complementary screen (without using this terminology). He does not state whether he intends the principle to apply to Fresnel diffraction also, although he clearly distinguishes between the two types of diffraction in his book.

Mascart (1889) extends the concept of Babinet's principle beyond the simple idea of the similarity of the diffraction patterns of complementary screens, as described by Babinet and Verdet. He first defines the meaning of the term "complementary screens" (using this terminology) and gives an equation similar to 2.1 to describe the relation between their diffraction patterns. However he applied this equation only to Fresnel diffraction.

Drude (1902) also introduces an equation corresponding to 2.1, apparently applying it only to Fraunhofer diffraction. He defines Babinet's principle as follows:

> "The diffraction patterns which are produced by two complementary screens are identical excepting the central spot, which corresponds to the diffraction angle zero."

This statement is shown to be incorrect in the general case in section 2.5.

The statements associated with the above authors do not mean that they are necessarily the originators of these ideas. However it is possible to trace the evolution of Babinet's principle through them. It can be seen that by 1902 all the ideas now associated with Babinet's principle had been gathered. The concept began with the simple qualitative statement by Babinet and was then generalised, with the additional concept of complementary screens, into equation 2.1, and applied to both Fraunhofer and Fresnel diffraction. The additional idea was also accumulated that the Fraunhofer diffraction patterns of complementary screens are identical except for a small region at the centre.

2.3 EXPERIMENTAL INVESTIGATION OF BABINET'S PRINCIPLE.

A simple illustration of the workings (or non-workings) of Babinet's principle, as applied to Fraunhofer diffraction, is now given. Figures 2.2a and 2.2b show two simple complementary screens and figures 2.2c and 2.2d are their respective diffraction patterns. It can be seen that both transforms look very similar overall but that a point-to-point comparison

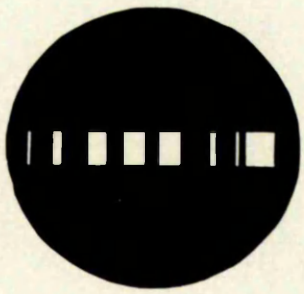

(a)

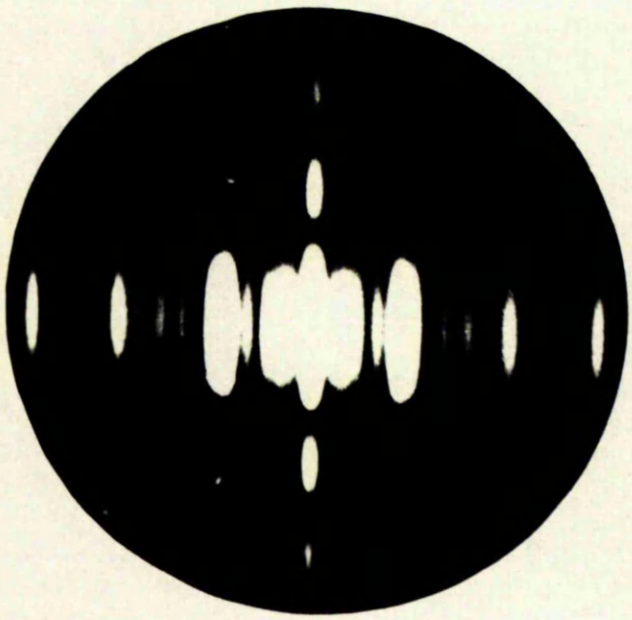

(c)

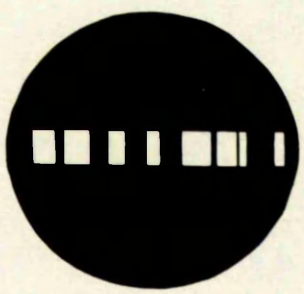

(b)

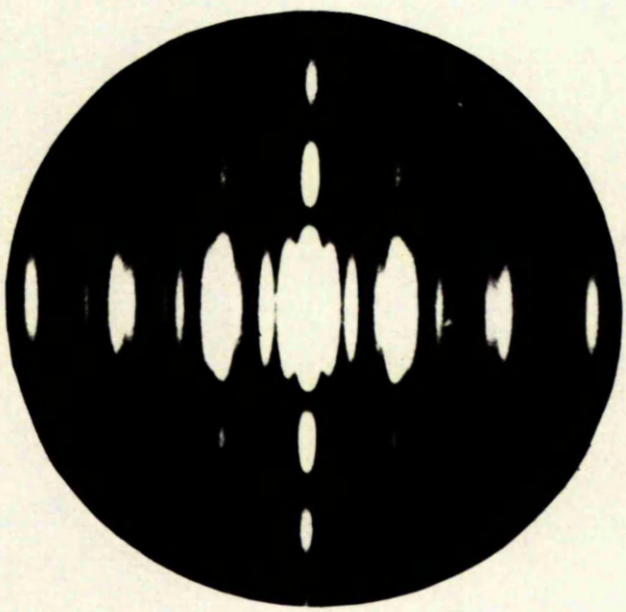

(d)

Fig.2.2

reveals considerable differences. A further example is given in figure 2.3 where two more-complex complementary screens are used. Figures 2.3c and 2.3d are the diffraction patterns of 2.3a and 2.3b respectively. Again we have the overall similarity between the two patterns and the point-to-point differences.

If we were to examine both sets of transforms on the points of a superimposed lattice, where the lattice points coincided with features on one or other of the patterns, we should find that the number of points of correspondence (positions of equal intensity) was greater for figures 2.3c and 2.3d than for 2.2c and 2.2d. This illustrates a general property of complementary screens that the more complex are the screens (i.e. the finer the detail), the more nearly do their diffraction patterns correspond. This is shown theoretically in the next section.

The screens of 2.2 and 2.3 have been carefully constructed to ensure that the clear areas of each pair of complementary screens are equal. This is also another necessary condition to obtain similar diffraction patterns. Figure 2.4 illustrates a case in which the diffraction patterns of the complementary screens are very different because the clear areas are not equal (see section 2.5).

After examining figures 2.2 and 2.3 and many other pairs of complementary screens the author was forced to conclude that Babinet's principle does not hold with any great accuracy in the general case. In fact, figures 2.2 and 2.3 are rather favourable examples since the differences in the two diffraction patterns are often greater. If, therefore, Babinet's principle does not hold in the general case, are there any special conditions under which it does hold? The author

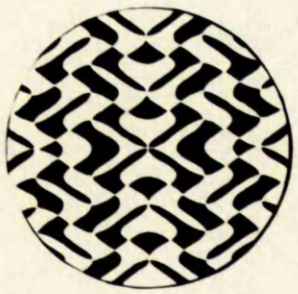

(a)

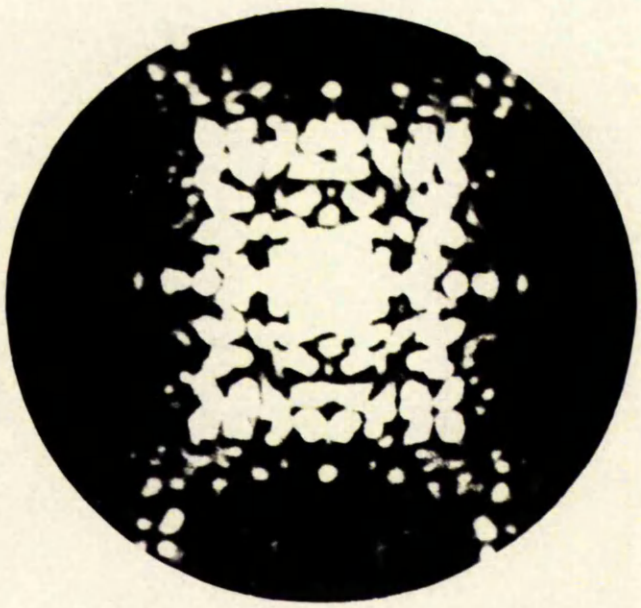

(c)

(b)

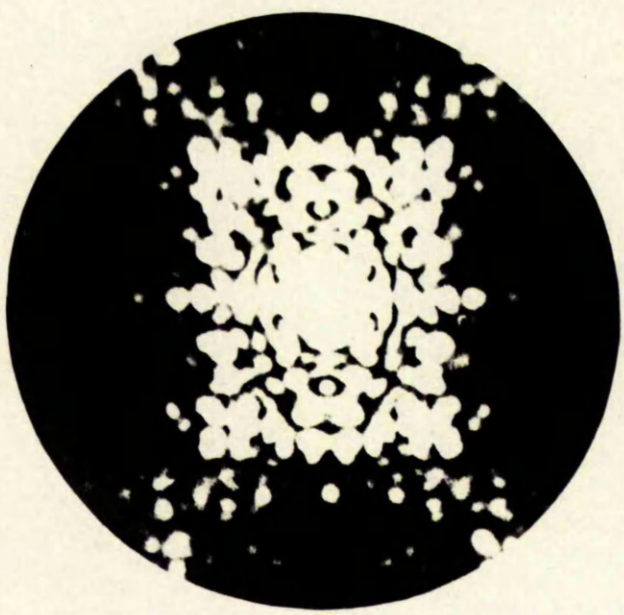

(d)

Fig. 2.3

arrived at the following conditions, under which Babinet's principle is most nearly obeyed, by a trial and error process, when examining various types of complementary screens:

(1) The two screens must each obstruct approximately half the total aperture.

(2) The detail in the screens must be small compared to the dimensions of the aperture.

(3) The detail must be evenly distributed throughout the aperture.

Of all the optics textbooks referred to by the author only Ditchburn (1963) seems to be aware of these limitations. Hosemann and Bagchi (1962) do point out some of these limitations, although their work is concerned mainly with disordered structures and is not a textbook in optics.

2.4 THEORETICAL INVESTIGATION OF BABINET'S PRINCIPLE

We may derive these conditions theoretically at least for the quite general case of centrosymmetric complementary screens in a centrosymmetric aperture. We have seen above that the condition for the diffraction patterns of complementary screens to be the same at any point is that

$$|A_1|^2 = |A_2|^2$$

(equation 2.2) will hold. This will be so if $A_o = 0$ in equation 2.1, i.e.

$$A_o = A_1 + A_2$$

However A_o depends on the shape of the aperture and in

general will be zero at a very limited number of points. (The conditions under which it is zero over a large number of points will be explored in Chapter 3). It is possible to derive a further condition on the complementary screen function, which will result in similar diffraction patterns.

From equation 2.1 we may write

$$|A_2|^2 = A_2 A_2^*$$

$$= A_1 A_1^* + A_o A_o^* - A_1 A_o^* - A_o A_1^*$$

$$|A_2|^2 = |A_1|^2 + A_o A_o^* - A_1 A_o^* - A_o A_1^* \qquad (2.3)$$

If at any point equation 2.1 holds then

$$A_o A_o^* - A_1 A_o^* - A_o A_1^* = 0 \qquad (2.4)$$

We may simplify this expression by considering a centrosymmetric aperture and centrosymmetric screens, then:

$$A_o = A_o^* \quad \text{and} \quad A_1 = A_1^*$$

and equation 2.4 becomes

$$A_o(A_o - 2A_1) = 0 \qquad (2.5)$$

If we ignore the solution $A_o = 0$ then equation 2.5 becomes

$$A_o - 2A_1 = 0 \qquad (2.6)$$

We may write A_1 as:

$$A_1 = \sum_{n=1}^{N} f_n \cos(2\pi r_n \cdot \rho) \qquad (2.7)$$

if the diffracting screen 1 consists of a centrosymmetric arrangement of N apertures each with scattering factor f_n and position vector r_n. The vector $\underline{\rho}$ is the position vector in the plane of the diffraction pattern.

A_o and A_1 are two independent oscillating functions of $\underline{\rho}$. From equations 2.6 and 2.7 therefore, equation 2.2 can be satisfied for the largest number of values of $\underline{\rho}$ if:

(a) $|A_o|_{max}$, the maximum value of A_o, and $2|A_1|_{max}$ are approximately equal,

(b) $(A_o - 2A_1)$ oscillates through zero as frequently as possible.

Since $|A_o|_{max}$ is proportional to S, the area of the aperture enclosing the screens, and $|A_1|_{max}$ is proportional to ϵS, the clear area of screen 1, then condition (a) implies that $\epsilon = \frac{1}{2}$ (condition (1) above).

Condition (b) implies that A_1 must oscillate as rapidly as possible, if we assume that A_o is fixed. In general the oscillation of A_1 is more rapid for larger values of N, since the number of spatial frequency components in the diffraction pattern is increased. Also, if the apertures are widely distributed, the oscillations of A_1 are again more rapid since the average period of these spatial frequency components is decreased. Thus condition (b) implies conditions (2) and (3).

Hosemann and Bagchi (1962) derive similar theoretical conclusions but only for one particular set of complementary screens in one particular aperture (a square lattice of holes - or round obstacles - inside a square aperture). The above treatment given by the author is therefore more general.

2.5 BABINET'S PRINCIPLE FOR LARGE APERTURES.

It has been indicated above that a number of authors (for example Drude (1902), Jenkins and White (1957), and Michelson (1927)) put forward the idea that the Fraunhofer diffraction patterns of complementary screens are identical except for a small region near the centre (the image of the source). Other authors extrapolate from this and suggest that for very large apertures the source image is very small (see Longhurst (1962) and Meyer (1949)) and hence conclude that better approximations to similarity are obtained for large apertures. This can simply be disproved by actually performing the experiment.

Figure 2.4a illustrates a hexagonal arrangement of diffracting obstacles which are placed in successively larger apertures (dotted circles). Figure 2.4b shows the complementary screen. Figures 2.4c, d and e respectively show the diffraction patterns of 2.4a for each aperture. Figure 2.4f is the diffraction pattern of the complementary screen 2.4b. There is a vague similarity between 2.4f on the one hand and 2.4c, d and e on the other (they have the same hexagonal symmetry). As the aperture size is increased however, the diffracted light from the aperture increasingly dominates the whole pattern and the similarity decreases.

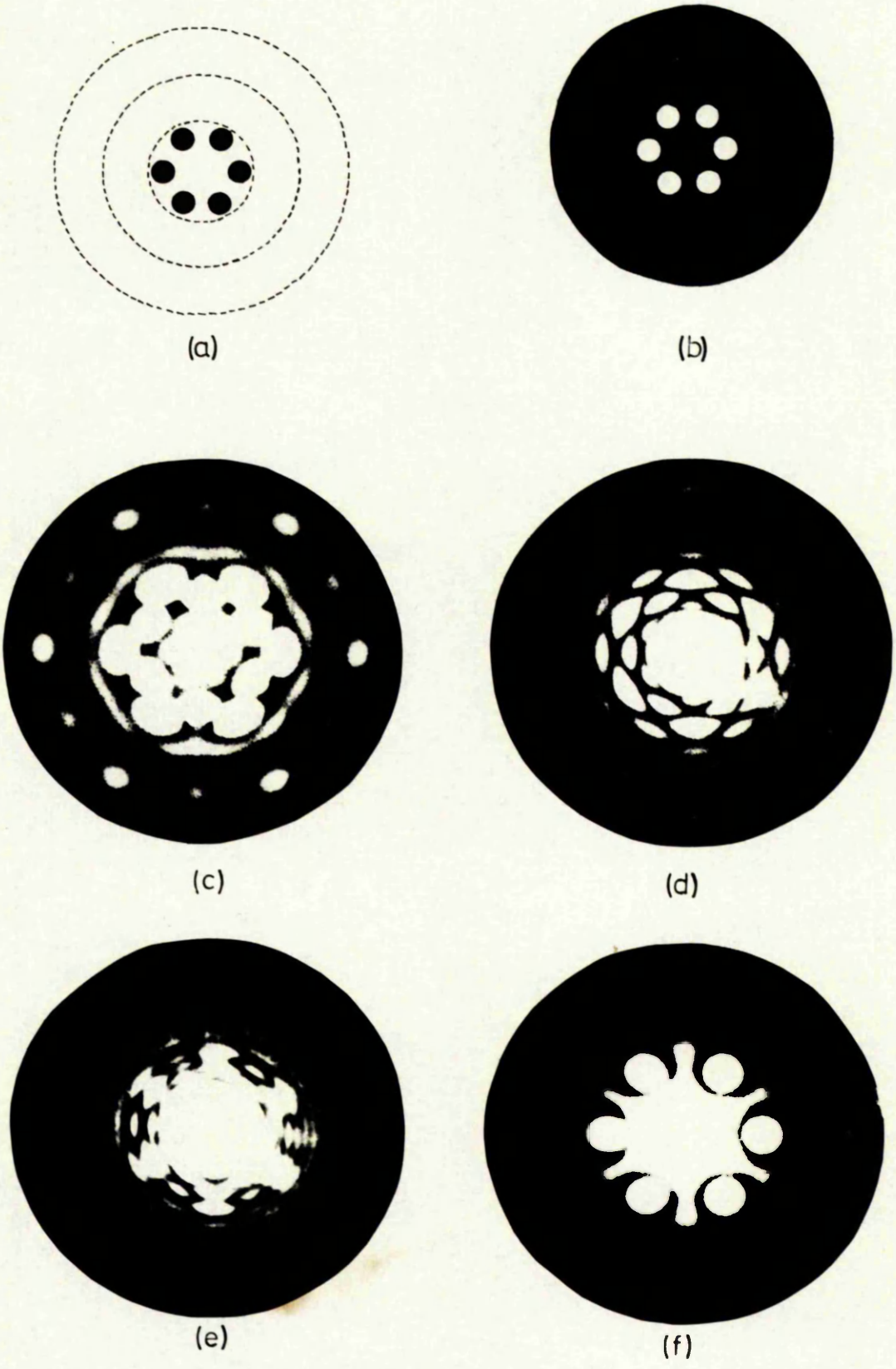

Fig. 2.4

This result can be shown theoretically. Let us consider the case of a circular aperture whose diffraction pattern is given by the familiar relation derived by Airy:

$$A(\rho) = 2\pi a^2 J_1(2\pi\rho a)/(2\pi\rho a) \qquad (2.8)$$

where a is the radius of the aperture and ρ is the distance from the centre of the diffraction pattern. Now the Bessel function $J_1(z)$ may be approximated by

$$J_1(z) \approx \sqrt{(\frac{2}{\pi z})} \cos(z - \tfrac{3}{4}\pi)$$

(Handbook of Mathematical Functions) for large values of z, the error being of the order of z^{-1}. Substituting in equation 2.8 we obtain

$$A(\rho) \approx \frac{1}{\pi\rho} \sqrt{(\frac{a}{\rho})} \cos(2\pi\rho a - \tfrac{3}{4}\pi) \qquad (2.9)$$

Therefore the peak height of the pattern is given by the modulus of the right hand side of equation 2.9

$$|A|_{max} \approx \frac{1}{\pi\rho} \sqrt{(\frac{a}{\rho})}$$

Hence, as the radius of the aperture increases, the average peak height of the pattern at any point at a distance ρ from the centre of the pattern also increases (as the square root of the radius). Therefore the diffraction pattern of any obstacles placed within this aperture will increasingly be swamped as the size of the aperture is enlarged. The author derived this result after performing the experiments of figure 2.4 but later found that it had already been noted by

Boersch (1951), who did not illustrate it experimentally however.

2.6 YOUNG'S ERIOMETER

The device known as Young's eriometer is often quoted in textbooks as an example of Babinet's principle (Ditchburn (1963) and Longhurst (1962)). Unfortunately this assertion is extremely suspect.

The device consists of a plate drilled with a number of small holes on the circumference of a circle of about 20cm. diameter. At the centre of the circle is a larger hole of about 2mm diameter. The back of the plate is illuminated by an extended monochromatic source, usually a sodium lamp. If the central hole is now viewed through a glass plate sprinkled with fine particles of the order of 10μm. diameter, a diffraction pattern is seen, which has the appearance of the familiar Fraunhofer diffraction pattern of a circular hole. The pattern is in fact that which would be produced by a hole which has the average diameter of the powder particles.

It is possible to line up the dark rings of the pattern with the ring of small holes surrounding the central aperture and hence deduce the angular diameter of each dark ring. These results may then be used to calculate a value for the average diamter of the powder particles.

The explanation usually given in optics textbooks of the diffraction pattern is that, because of Babinet's principle, the random arrangement of powder particles produces the same pattern as the complementary random arrangement of apertures.

The explanation then shows that the diffraction pattern of a random arrangement of similar holes is the same as that of a single hole, multiplied N times in amplitude, where N is the total number of holes.

This illustration of Babinet's principle appears to be perfect with no interference from a limiting-aperture diffraction pattern. Unfortunately, the explanation is wrong at two points. First the diffraction pattern of a random array of holes does not have the appearance suggested (Stone 1963), particularly at points near the centre of the pattern. Secondly, the diffraction pattern that is observed is not a Fraunhofer diffraction pattern in the normally accepted sense. It can be simply shown that, with the experimental arrangement given above, good coherence is obtained only between points separated by a few particle diameters (i.e. not over the whole area of the glass plate containing the particles). The calculation is that which is normally used to derive the degree of coherence between points in the mask plane of the optical diffractometer (Taylor and Thompson, 1957). The particles are therefore scattering independently and the diffraction pattern is that of an individual particle, multiplied N times in intensity. No interference pattern due to a limiting aperture is observed, as this would have dimensions of such a size that it would be incoherently illuminated.

2.7 CONCLUSIONS CONCERNING BABINET'S PRINCIPLE

The main conclusion that can be drawn is that Babinet's principle does not hold generally. The principle is only true for a limited class of complementary screens, unless a

particular type of limiting aperture is used (see Chapter 3). However, the equation

$$A_o = A_1 + A_2$$

which is sometimes regarded as an expression of Babinet's principle, is true, but it has no great physical significance if it does not imply that complementary screens have identical diffraction patterns.

The conditions that must be obeyed by complementary screens are that they must each obstruct about one half the total aperture and must consist of fine detail evenly spaced over the screen. Increasing the size of the limiting aperture does not improve the similarity between the two diffraction patterns, as is often supposed. The most frequently quoted example of Babinet's principle, Young's eriometer, is not a straightforward application of the principle, as the diffracting mask (the powder particle distribution) is not coherently illuminated.

These restrictions on Babinet's principle are not generally appreciated, although some of them have been pointed out by other workers. For this reason it was felt necessary to treat the subject fully before continuing with the main subject of this thesis, the application of Babinet's principle to the production of transforms of three-dimensional objects.

CHAPTER 3

3 THE APPLICATION OF APODISATION IN OBTAINING OPTICAL TRANSFORMS OF THREE-DIMENSIONAL OBJECTS

The work outlined in the previous chapter indicates that there is no simple way to obtain the required optical transform of a three-dimensional crystal-structure model. If we were to place such a model directly in the aperture of an optical diffractometer, the diffraction pattern of the model would in general be completely distorted by the light diffracted (A_o) from the aperture of the instrument. Therefore the obvious conclusion is that A_o must be made zero, or negligible, over the major part of the diffraction pattern of the model; and thus, in some way, the transmission characteristics of the aperture must be altered to produce this effect. A somewhat analogous problem, that of reducing the "diffraction ripple" surrounding images formed in optical instruments, has been solved by the technique known as "apodisation"; the author was led to explore the possibilities of using apodisation to eliminate the diffraction ripple represented by the quantity A_o.

The first attempt to use apodisation with two-dimensional apodising screens was unsuccessful and the reasons for its failure are discussed. The second attempt, using apodising apertures, did succeed and some examples of its use are given.

3.1 APODISATION

Most optical instruments are assessed on their ability to resolve two equally bright objects; however, there are circumstances in which the instrument is required to separate two objects one of which is much fainter than the other. In such a case the ring system, or more generally the pattern of diffracted light that surrounds the brighter image, can obliterate the faint image. Examples may be found in astronomy - the observation of the companion of Sirius by Sinton (1952) -, in spectroscopy - the observation of faint satellite lines or lines of rare isotopes - and in many branches of optics, particularly microscopy, where the resolution of high contrast detail is required.

A method of spatial-frequency filtering has been developed to suppress the side maxima or 'feet' of the main image and this is known as 'apodisation' (from the greek α, to take away and ποδος, foot). It may be easily shown that the form of the transmission function of the spatial-frequency filter must be such that its Fourier transform consists of one single maximum (in practice it is possible to achieve only an approximation to this).

The most general type of apodisation - two-dimensional apodisation - is achieved by placing an absorbing screen with rotational symmetry in the aperture of an instrument. The radial transmission function of such a screen is, in general, entirely real and decreases gradually from the centre outwards. The Fourier transform of the screen will approximate to a peak function (in two dimensions), although the width of the peak must of course be finite. The

actual function in the transform plane is given by equation 1.9:-

$$A(\rho) = \int_r T(r)\, J_o(2\pi r\rho)2\pi r dr$$

T(r) being the transmission function of the apodising screen. We may write the reverse Hankel (Fourier) transform equation to equation 1.9 as:

$$T(r) = \int_\rho A(\rho)\, J_o(2\pi r\rho)2\pi\rho d\rho \qquad (3.1)$$

It may appear, at first sight, that equation 3.1 implies that we can choose some suitable approximation to a peak function for $A(\rho)$ and, hence, calculate the necessary apodising screen function T(r). However, the Hankel transform of any bounded function for $A(\rho)$ will transform to an unbounded function T(r), and of necessity T(r) must be bounded by the instrumental aperture; thus, $A(\rho)$ cannot be chosen a priori. Therefore an indirect solution to the problem must be sought.

One approach is that of Lansraux and Boivin (1961) who, instead of assuming T(r) to be any general function of r, limit themselves to all possible linear combinations of n basic functions $f_p(r)$. T(r) is then a function of n parameters which are the coefficients a_p of the linear combination

$$T(r) = \sum_{p=o}^{n-1} a_p f_p(r) \qquad (3.2)$$

The basic functions $f_p(r)$ are chosen so that their Hankel transforms $\psi(\rho)$ are known analytically, thus

$$A(\rho) = \sum_{p=o}^{n-1} a_p \psi_p(\rho) \qquad (3.3)$$

A condition, maximising the diffracted energy within a circle of some arbitrary radius ρ_m, and by implication producing apodisation, is then applied to equation 3.3; and a system of linear equations is obtained, which may be solved for $a_o \ldots a_p, \ldots a_{n-1}$, hence T(r) is completely determined.

Lansraux and Boivin choose

$$f_p(r) = (1 - 4r^2)^p \qquad (3.4)$$

hence, $$\psi(\rho) = \frac{\pi}{4} \frac{\Lambda_{p+1}(\rho)}{p+1} \qquad (3.5)$$

where, $$\Lambda_p(\rho) = 2\Gamma(p+1) \frac{J_p(\pi\rho)}{(\pi\rho)^p}$$

Γ being the factorial function and $J_p(x)$ the Bessel function of order p. Figure 3.1a illustrates some of the results of Lansraux and Boivin for the function T(r) and figure 3.1b gives the corresponding values of $A(\rho)$ (actually $A(\rho)^2$) compared with the results for a uniform (unapodised) pupil. The scale for $A(\rho)^2$ is plotted linearly for small values of ρ and then logarithmically for larger values.

The values of $A(\rho)$ were computed by the author and compare well with the published graphs of Lansraux and Boivin. Equation 3.3 was reduced by means of equation 3.5 to a summation with terms of the type $b_p J_p(\pi\rho)/\pi\rho$ (b_p constant). An Atlas-autocode library program, which evaluates $J_o(x)$ and

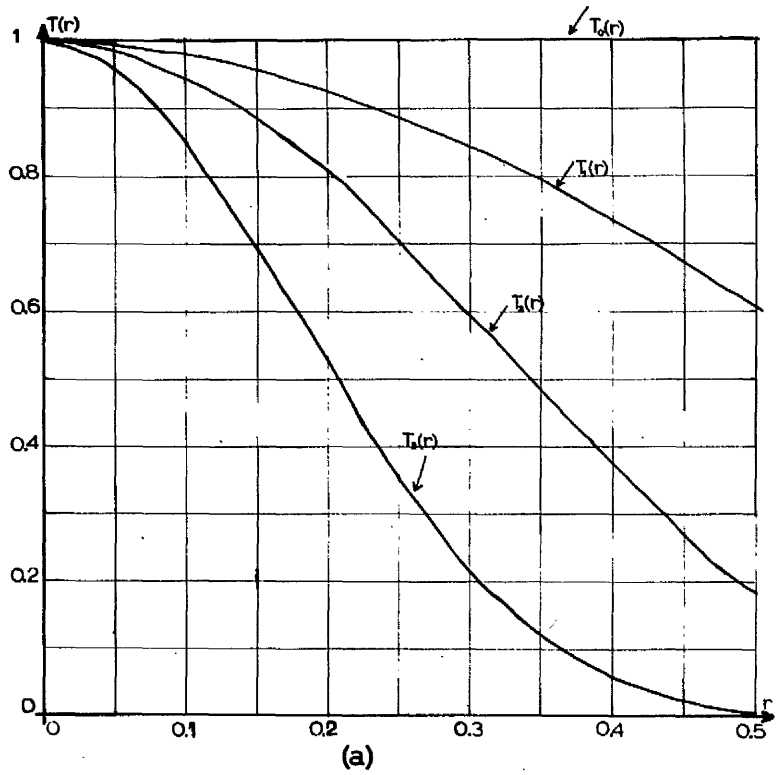

(a)

$T_0(r)=1$

$T_1(r)=0.609+0.326(1-4r^2)+0.065(1-4r^2)^2$

$T_2(r)=0.181+0.426(1-4r^2)+0.257(1-4r^2)^2+0.136(1-4r^2)^3$

$T_3(r)=0.068+0.290(1-4r^2)+0.371(1-4r^2)^2+0.156(1-4r^2)^3+0.114(1-4r^2)^4$

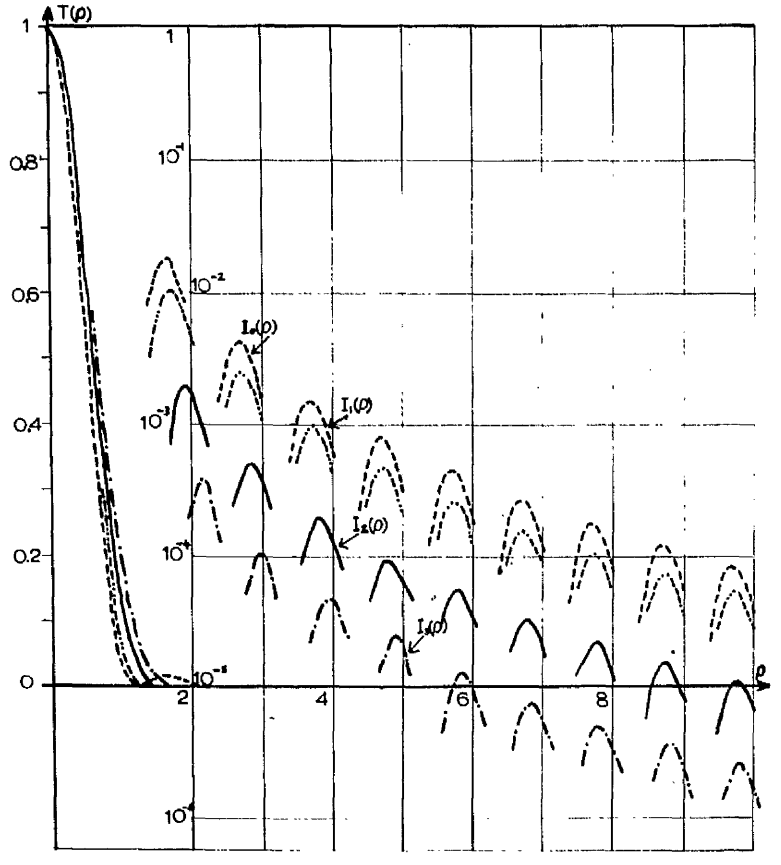

(b)

Fig.3.1

$J_1(x)$ by means of a polynomial approximation, was made use of and higher order Bessel functions were calculated by means of the recurrence relation.

$$J_p(x) = (2(p - 1)/x)J_{p-1}(x) - J_{p-2}(x)$$

(Handbook of Mathematical Functions)

In certain circumstances circularly-symmetric apodising screens are unnecessary - for example, in the observation of spectral lines. This particular case requires apodisation only in directions perpendicular to the length of the line; and the requirement may be satisfied by an absorbing screen whose transmission function T(x) varies parallel to one axis in its plane and is constant along the perpendicular axis. Expressions for T(x) have been calculated by Dossier et al. (1950) in the form,

$$T(x) = \sum_{p=o}^{n-1} a_p \cos(2p\pi x) \qquad (3.6)$$

using a method similar to that described above for two-dimensional screens. Screens of this type are known as 'one-dimensional apodising screens'.

A further more-restricted case of apodisation is that produced by placing an aperture of the type shown in figure 3.6a in the instrument. The apodisation is now only obtained along a single line, figure 3.6b (the Fraunhofer diffraction pattern), and could be used, for example, in spectroscopy if there is a point source or in the problem of resolving two stars, if their relative orientations are known. The form of the contour of such an aperture is given by the one-dimensional apodisation functions of Dossier.

Apodising screens with non-uniform absorption are made by evaporating chromium on to glass. The glass plate is placed behind a suitable mask and moved during evaporation according to the type of screen; the one-dimensional screen is moved back and forth (Jacquinot,1950), and for screens with circular symmetry the plate is rotated (Giacomo et al., 1964). Apodising apertures can be cut from an opaque screen under a binocular microscope (Dossier et al.,1950) or made by photo-engraving on thin metallic sheets (Huet, 1960).

The above description of apodisation is of necessity brief and incomplete. However, further information may be obtained from a comprehensive review of the whole subject by Jacquinot and Roizen-Dossier (1964).

3.2 THE APPLICATION OF TWO-DIMENSIONAL APODISATION TO PRODUCE OPTICAL TRANSFORMS OF THREE-DIMENSIONAL OBJECTS

3.2.1 Theoretical considerations

Apodisation, therefore, appears to offer a way of eliminating the troublesome diffraction contributions from the aperture when we attempt to observe the optical transform of a three-dimensional object.

Let us consider what would happen if we place a two-dimensional apodising screen (transmission function $T_a(r)$) in the aperture of an optical diffractometer together with a model representing a crystal structure. The total transmission through the aperture may be written,

$$T_t = T_a(r) - T_m(x, y) \tag{3.7}$$

where $T_m(x, y)$ is the transmission function of the two-dimensional screen complementary to the projection of the model. The transform of the apodising screen approximates to a peak function and we write this as $\Delta(\rho)$. If the transform of T_m is $A_m(\xi, \eta)$, then

$$A_t = \Delta(\rho) - A_m(\xi, \eta) \tag{3.8}$$

Thus the total diffraction pattern consists of the pattern of the screen complementary to the model (with a negative phase), plus a peak-like function at the origin; if the apodising screen is somewhat larger than the model, the width of the peak function will be negligible and it will overlap little of the diffraction pattern of the model. An undistorted diffraction pattern of the model should now be visible with a bright spot at the centre.

However, this view is simplified since we have implicitly assumed that the model will be uniformly illuminated and, of course, the presence of the apodising screen will ensure that this is not so; but, if the model is small compared to the dimensions of the screen, then the differences of illumination over the area of the model will also be small.

Another way of looking at this difficulty is by means of the idea of the convolution of two functions (Bracewell, 1965). Equation 3.7 should really be written as a product

$$T_t = T_a(r)[1 - T_m(x, y)]$$

thus:

$$T_t = T_a(r) - T_a(r)\, T_m(x, y) \qquad (3.9)$$

Therefore equation 3.8 becomes:

$$A_t = \Delta(\rho) - \Delta(\rho) * A_m(\xi, \eta) \qquad (3.10)$$

The second term on the right hand side of equation 3.10 represents a convolution product. If $\Delta(\rho)$ were a true peak function, then

$$\Delta(\rho) * A_m(\xi, \eta) = A_m(\xi, \eta)$$

and equation 3.10 reduces to the ideal case of equation 3.8. When, however, the width of $\Delta(\rho)$ is finite but small compared to the spatial frequencies in $A_m(\xi, \eta)$, then the effect will be to produce a slight blurring (or smoothing) of the function $A_m(\xi, \eta)$; the result may be compared to the scanning of a spectrum by the slit of a spectrophotometer, producing a representation of the spectrum with a slight loss of resolution. The condition on the width of $\Delta(\rho)$ of course implies that the diameter of the apodising screen is large compared to the extent of the model.

Summing up, therefore, provided that the apodising screen is large compared to the model, we shall see a transform corresponding to that desired of the model with perhaps a slight loss of detail; and at the centre of the pattern there will be a narrow bright peak.

3.2.2 PRACTICAL CONSIDERATIONS

The author, having deduced that the method was feasible, sought a simple experimental demonstration of this fact. The primary difficulty is that of making a two-dimensional apodising screen simply. To use the method of Giacomo unfortunately requires a comparatively elaborate piece of apparatus. However, diffraction screens with continuous transmission functions have been made in optical-transform work by a technique similar to the method of reproducing newspaper photographs using half-tone screens (Harburn et al.,1965); the apodising screen of figure 3.2a was made with this idea in mind. The screen is actually a photographic negative of a drawing of a large number of dots on the points of a two-dimensional lattice; the diameters of the dots (apertures) decrease in size with increasing distance from the centre, to reproduce the function

$$T(r) = 0.068 + 0.290(1 - 4r^2) + 0.371(1 - 4r^2)^2 + 0.156(1 - 4r^2)^3 + 0.114(1 - 4r^2)^4 \quad (3.11)$$

(T_3 of fig. 3.1a). (An order-of-magnitude calculation suggested that this function would be adequate for the purpose). The representation is very approximate as only eleven hole sizes were used in successive circular zones. The diameter of the screen was 3cm.

As a test object the familiar hexagonal arrangement of obstacles was used, figure 3.2b - actually, 1/16in. balls stuck to a glass plate and in the form of a hexagon of 0.23cm. side. If the photographic plate of the apodising screen and the glass plate with the obstacles were placed directly in to the optical diffractometer, differences in phase

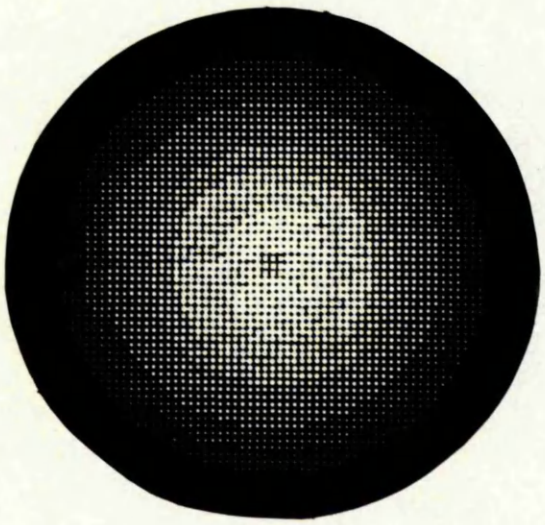

(a)

(b)

(c)

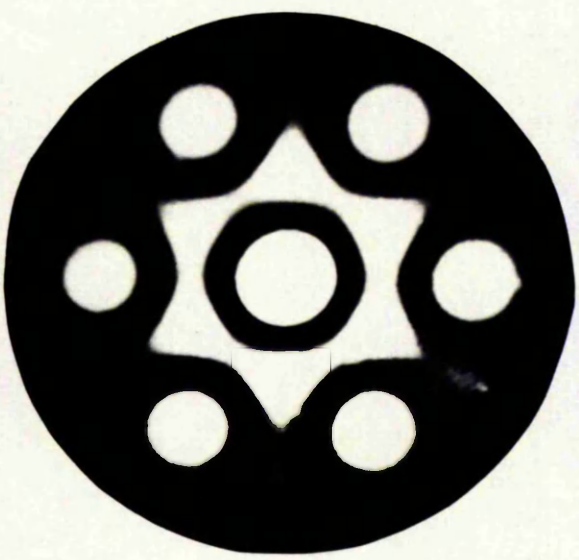

(d)

Fig.3.2

across the aperture would be introduced due to non-uniformity in their thicknesses. Therefore the screen and the obstacles are immersed in cedar-wood oil contained in a tank having an optical flat as its base.

The optical transform of the screen plus the obstacles is given in figure 3.2c and may be compared with the ideal result in figure 3.2d. The transform is recognisable in broad detail but the finer detail is not reproduced.

The author was encouraged by the relative success of this rather crude apodising screen and concluded that a continuous-tone screen would give much better results. It should be stated here that this conclusion was based on very approximate order-of-magnitude calculations which later proved inadequate.

It was decided to try to make continuous-tone apodising screens by a photographic method rather than to use the experimentally more difficult chromium-deposition method of Giacomo. (The lack of a large enough vacuum-evaporation plant was a major disincentive to using this method).

Therefore, the author made the piece of apparatus, illustrated in figure 3.3a, to produce these photographic apodising screens and it is in fact an optical analogue of Giacomo's apparatus. The photographic plate is mounted on a large (7in. o.d.) bearing and rotated beneath a stationary mask (a photographic reproduction) of the type shown in figure 3.3b. While it is rotated, a light source above the apparatus is used to expose the plate. The mask is attached to the bottom side of a perspex sheet, and slots (not shown) cut into the sheet and the baseplate enable the lateral position of the mask to be adjusted. The exact form

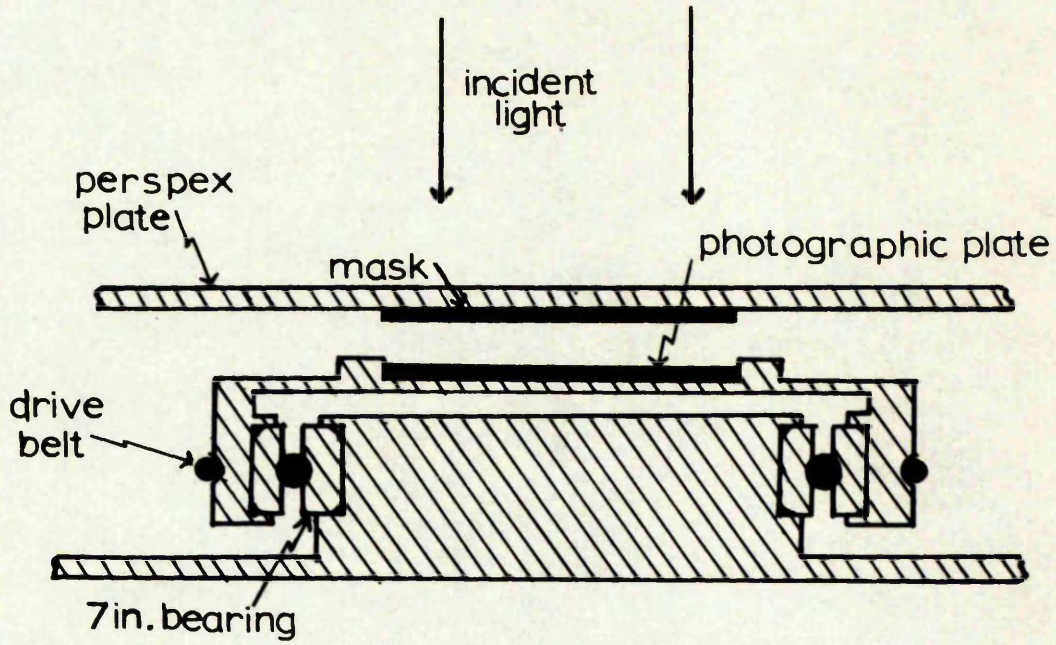

Fig.3.3a

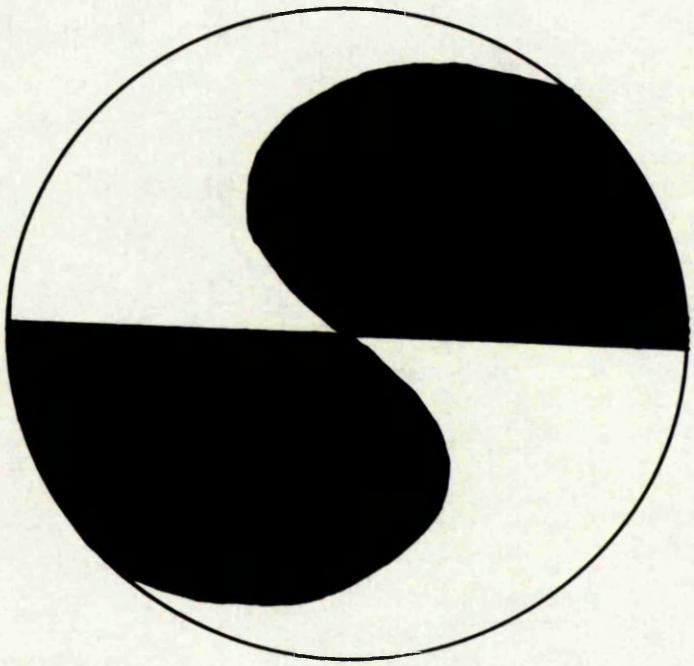

Fig.3.3b

of the stationary mask may be found empirically, using first of all a standard mask to produce a known (e.g. linear) intensity distribution across the photographic plate and measuring the resulting density distribution.

It is important that the rotation axis of the photographic plate be colinear with the centre of the mask. This alignment was carried out by replacing the photographic plate by a card with a number of parallel lines drawn on it; when this is rotated, a series of concentric rings is observed and the centre of the mask may be easily made to coincide with the rotation axis, which is at the centre of the rings.

The rotational speed of the photographic plate must also be chosen carefully. If a single exposure is broken up into a number of short exposures (using the same intensity), the amount of blackening produced is not the same as that produced by the continuous exposure; this effect is known as "intermittency failure". Webb (1933) has shown, however, that if the flash rate is high enough the blackening produced will be that given by the equivalent continuous exposure. For this reason it is necessary to rotate the plate rapidly and a speed of 1500 r.p.m. was chosen.

The development of the photographic plate is perhaps the most critical part of the process. The temperature of the developer, its concentration and degree of agitation, and the development time, must be carefully controlled to get reproducible results.

The photometric measurements were made using a rather crude densitometer built by Hinde (1951), replacing the original selenium photo-voltaic cell with a modern silicon

type (Ferranti MS2BE) to increase the sensitivity. A heat filter was added, since the silicon cell is very sensitive to infra-red radiation, and also a spectral filter, of the type used in the optical diffractometer, to simulate the normal working conditions of the apodising screen.

A 35mm. photographic enlarger was used as a source of light; this was convenient since the intensity could be adjusted by means of the variable aperture on the lens. This method of illumination was unsatisfactory for two reasons: first the output of the light source was not stabilised; secondly strict parallelism of the light striking the mask and photographic plate was not achieved, therefore the distribution of intensity across the plate was incorrect. The second of these defects was alleviated by masking the separation between the mask and the plate as small as possible ($\sim \frac{1}{8}$in.) and the distance of the light source as large as possible. It was hoped to correct these drawbacks after a few preliminary trials of the apparatus.

The function

$$T(r) = 0.105 - 0.057(1 - 4r^2) + 0.777(1 - 4r^2)^2 - 0.047(1 - 4r^2)^3 \qquad (3.12)$$

was used as an initial test of the apparatus. This function gives slightly improved apodisation to the function of equation 3.11 and has a smaller range of values of T(r), hence it can be more easily reproduced in an apodising screen. The expression was calculated by Jacquinot and Roizen-Dossier (1964), who adopted a criterion of apodisation slightly different to that of 3.11.

The actual range of the intensity transmission function $(T(r)^2)$ to be reproduced is therefore about 50:1 and this

requires a reasonably high-contrast photographic plate. Kodak B4 plates were chosen but no special care was taken over the choice of processing chemicals, those readily available were used for this preliminary trial. The plates were developed after exposure in Kodak D163, a normal to high-contrast developer mainly intended for photographic paper, and this was diluted 1 part to 3 of water and maintained at 20°C during processing. The comparatively dilute state of the developer and the consequently extended development time assists even blackening over the whole plate. During development the surface of the plate was stroked regularly with a soft brush to remove the products of the reaction, which would otherwise accumulate, slowing the development and producing uneven blackening. The plates were rinsed for 30 seconds in a 2% acetic acid solution after development and fixed in Ilford IF9 fixer (actually an X-ray film fixer) for 10 minutes. They were then washed in running water for 30 minutes and rinsed in filtered water containing a wetting agent before being dried.

As indicated above the plates were calibrated using a mask which gave a uniform decrease of illumination along the radius. A series of calibration plates were made with various total exposure times and a continuous curve of the intensity transmission function against time was plotted. It is then a simple matter to deduce the form of the mask, fig. 3.3b, which is required to obtain the correct function $T(r)$ (or $T(r)^2$), from the curve.

Although several short-cuts were taken for this preliminary trial of the apparatus, quite a reasonable reproduction of the desired function was obtained in the

apodising screen. Figure 3.4a shows the theoretical function $(T(r)^2)$ and the experimental fit of the apodising screen function. Since only relative values of the transmission function of the apodising screen could be obtained, it was necessary to artificially fit the experimental points to the theoretical curve and this was done by arranging that one of the experimental values ($r = 0.2$) should lie on the theoretical curve.

The fit for low values of r is not very good and this is due to a faint ring pattern at the centre of the screen, probably caused by the axis of rotation of the photographic plate not being coincident with the centre of the stationary mask. However, the fit over most of the screen is quite reasonable.

Again the familiar test object was used of a hexagonal arrangement of diffracting obstacles - $\frac{1}{8}$in. discs on a hexagon of 0.47cm. side. The apodising screen was 8cm. in diameter so that the obstacles lay within the region for which $T(r) > 0.9$ of the maximum transmission. Both the screen and the obstacles were immersed in cedar-wood oil as before. Figure 3.4b shows the diffraction pattern of the screen plus the obstacles. There is a very intense maximum at the centre, as might be expected, and the six main peaks of the diffraction pattern of the obstacles show up clearly. Yet the result is disappointing since the interference effect of the surrounding aperture is still clearly visible as the ripple pattern on the main peaks of the transform of the obstacles; obviously some improvement is required in the amount of apodisation achieved. Comparing this result with that of the half-tone screen, no great improvement can be observed, although it must be taken

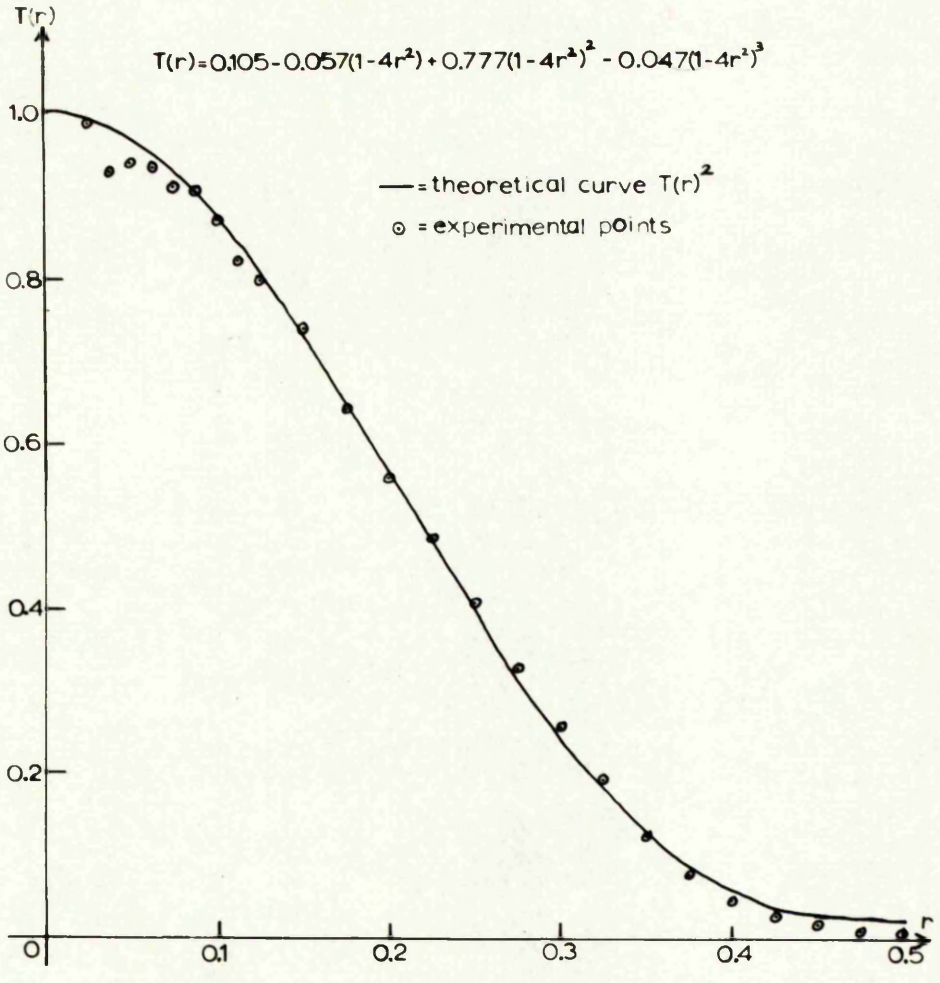
T(r)
T(r)=0.105-0.057(1-4r²)+0.777(1-4r²)²-0.047(1-4r²)³
1.0
0.8
0.6
0.4
0.2
0
0.1
0.2
0.3
0.4
0.5
r
——=theoretical curve T(r)²
⊙ = experimental points

(a)

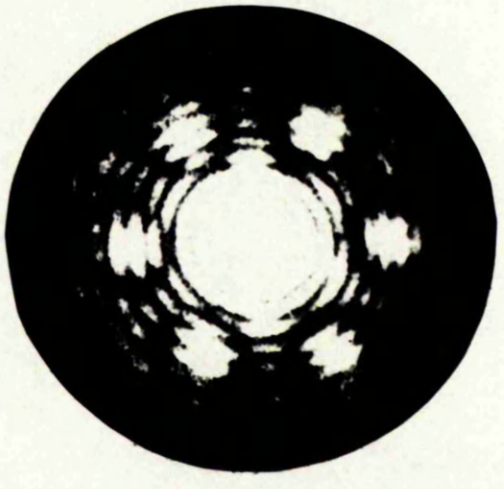

(b)

Fig.3.4

into account that, there, the diffracting obstacles occupied relatively twice as much of the area of the screen.

3.2.3 NUMERICAL INVESTIGATION

The inadequacy of the apodising screen could be explained in one of two ways, either the screen was not a good enough approximation to the theoretical function, or the theoretical function did not give sufficient apodisation. This question could obviously be decided by calculating the optical transform of the theoretical screen and comparing it with that of the hexagonal obstacle-arrangement. It was decided not just to do this for one particular screen but to choose several screens, with varying degrees of apodisation, and to compare their performances.

The problem of calculating the optical transforms of two-dimensional apodising screens has been dealt with in section 3.1 and the same program could be easily adapted for use here. The transform of the hexagonal arrangement of obstacles is the same as that of its complementary screen of holes. From equation 1.8 we have

$$A(\xi, \eta) = \iint_{xy} T(x, y) \exp[2\pi i(x\xi + y\eta)] \, dxdy$$

The transform of the obstacles may therefore be written as the summation,

$$A(\xi, \eta) = \sum_{x_n} \sum_{y_n} f \exp[2\pi i(x_n\xi + y_n\eta)] \, dxdy \qquad (3.13)$$

where x_n and y_n are the positional coordinates of the six obstacles (holes) and f is the scattering Factor for each.

Thus,

$$f = 2\pi a^2 \frac{J_1(2\pi\rho a)}{2\pi\rho a}$$

Since the arrangement is centrosymmetric,

$$A(\xi, \eta) = \sum_{x_n} \sum_{y_n} f \cos[2\pi(x\xi + y\eta)] \qquad (3.14)$$

where the summation is taken over a centrosymmetric half (three obstacles). The values of $A(\xi, \eta)$ were calculated from equation 3.14 by means of a simple computer program written by the author.

For the purposes of the calculation it was assumed that the hexagonal arrangement of obstacles consisted of discs of 1mm. diameter on a hexagon of 0.23cm. side which, if we use the normal scale of optical transform work (1/6cm. = 1Å), represents a benzene ring of side 1.4Å; distances in the transform can therefore be given as $Å^{-1}$. The sizes of the apodising screens were adjusted so that the obstacles lay just within the region in which $T(r) > 0.9$ of the maximum transmission.

The results of the calculation are given in figure 3.5. The apodising screen functions that were used are those of figure 3.1, T_0 being the uniform (unapodised) pupil and T_1, T_2 and T_3 being unapodised functions in order of increasing degree of apodisation. The graphs represent cross-sections through the modulus of the transform of each screen (full lines) compared with the modulus of the transform of the obstacles (dotted lines). The cross-section of the transform of the obstacles is taken through one of the six main peaks.

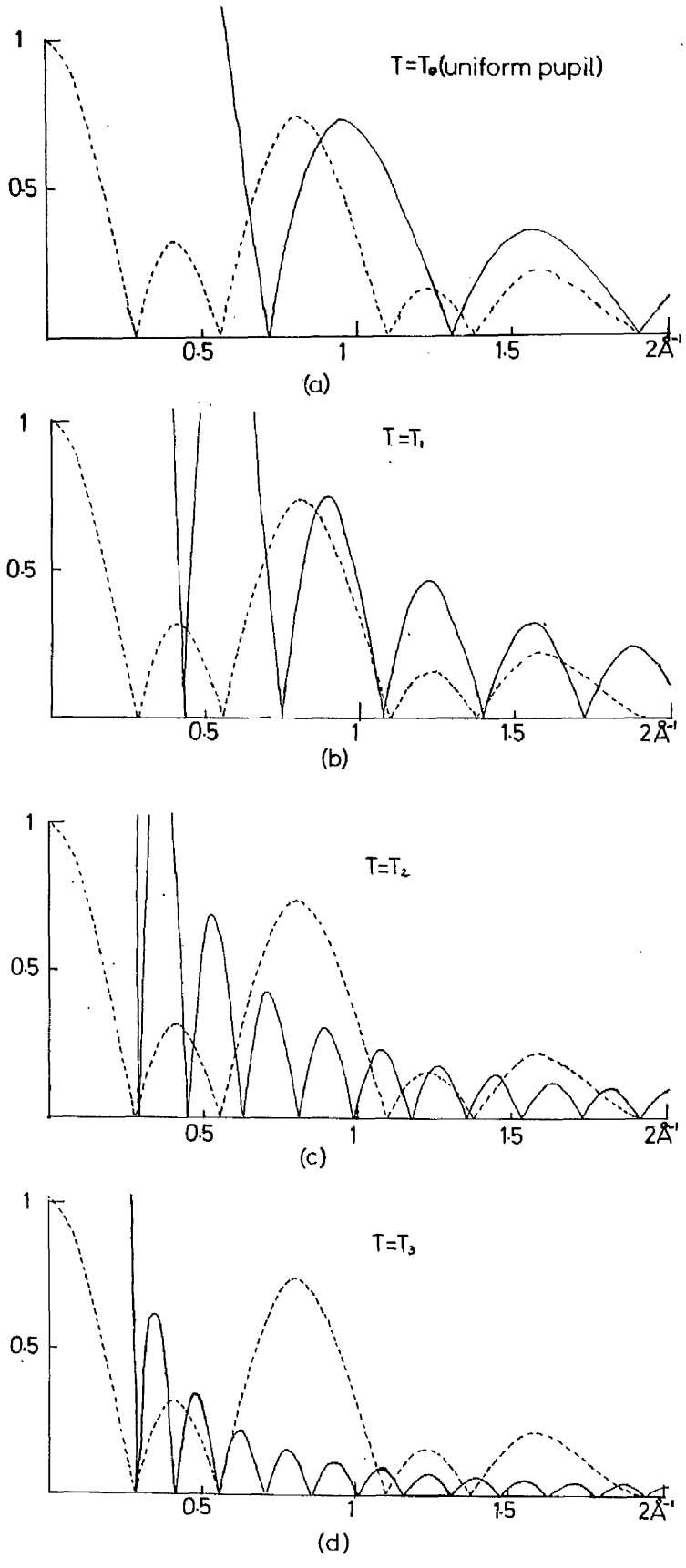
1
0·5
T=T₀(uniform pupil)
0·5
1
1·5
2Å⁻¹
(a)
1
0·5
T=T₁
0·5
1
1·5
2Å⁻¹
(b)
1
0·5
T=T₂
0·5
1
1·5
2Å⁻¹
(c)
1
0·5
T=T₃
0·5
1
1·5
2Å⁻¹
(d)
—— = apodising screen transform
------ = transform of obstacles

Fig.3.5

The most striking feature of these results is the slow rate of fall of the peaks of the transforms of the apodising screens as we progress from the least to the most effective screen. The reason for this is not difficult to see. As we increase the effectiveness of the apodising screen, the function T(r) falls off more rapidly, hence the size of the screens must be increased (and thus their relative diffracting power is also increased) so that the obstacles remain within the region $T(r) > 0.9$.

The function used for the experimental screen gives results very similar to the last screen (T_3) of figure 3.5 and this can be seen to be barely adequate. Thus the experimental screen would seem to give a result which is not too far from theoretical expectations. Evidently an apodising screen function T(r) must be used which will give a greater degree of apodisation. Unfortunately, such a function would give a degree of apodisation which is excessive for normal optical applications and therefore it has not been calculated by previous workers, as far as can be ascertained from the literature. There seems to be no reason, however, why such functions should not be calculated by the present methods.

3.2.4 OBJECTIONS TO THE METHOD

Although the first experimental trial of the method was not clearly successful, it is still theoretically feasible. In addition we can expect better results for models larger (i.e. with more atoms) than the simple benzene ring. If the models are larger and the apodising screen

is enlarged, so that the models remain within the region $T(r) > 0.9$, then the large peaks of the screen transform will move closer to the centre and away from the region of interest, say 0.25Å^{-1} to 2.0Å^{-1} (see figure 3.5). It might also be possible to slightly relax the condition $T(r) > 0.9$ to obtain a better result.

Yet, although the method is feasible, there are certain experimental difficulties which make it awkward to use in practice. The new function $T(r)$, which is required to give improved apodisation, would almost certainly have a larger difference between the maximum and minimum values of $T(r)$. Thus the range of contrast of the photographic reproduction would be greater and therefore more difficult to control. Also, if the screens were to be so much larger ($\approx 5x$) than the extent of the model, so that it would lie within the region $T(r) > 0.9$, then either the models must be made very small or the screens very large. Very small models (say 1cm. across) would entail difficulties in construction and this would clash with the essential features of optical methods - speed and simplicity. Large screens would require equally large (say 30cm. diameter) optical flats for the oil-immersion process and these would be prohibitively expensive.

3.3 THE APPLICATION OF APODISING APERTURES TO PRODUCE OPTICAL TRANSFORMS OF THREE-DIMENSIONAL OBJECTS

3.3.1 INTRODUCTION

Two-dimensional apodising screens would seem to offer a way of obtaining optical transforms of three-dimensional

objects but the method is rather cumbersome in practice. However, while examining the optical transforms of various apodising apertures, the author came upon a much simpler method and the idea of using two-dimensional screens was dropped in favour of this.

Apodising apertures, that give apodisation along a single line in their transforms, have already been mentioned in section 3.1. Figure 3.6a is an example of such an aperture and figure 3.6b is its optical transform. The striking feature of this optical transform is that, not only is there apodisation along a horizontal line through the centre of the transform, but the intensity appears to be zero also over two symmetrical fan-shaped regions, of which this line is the bisector. The angle of the fan may be altered by adjusting the relative dimensions, length to breadth, of the aperture; in the example shown the ratio is 3:1, which gives an angle of about 110^{o}. The equation of the aperture contour may be written

$$T(x) = 0.413 + 0.499 \cos(\frac{2\pi x}{3}) + 0.087 \cos(\frac{4\pi x}{3}) \qquad (3.15)$$

which is a 'stretched' version of a function (equation 3.6) given by Dossier et al. (1950).

The application of these apertures to producing optical transforms of three-dimensional objects is quite simple. Suppose, for example, we place the usual hexagonal arrangement of obstacles within the aperture of the diffractometer, together with the apodising aperture of figure 3.6a. In the fan-shaped regions of the optical transform the contribution (A_o) from the apodising aperture is very small and we shall be able to see that part of the optical trans-

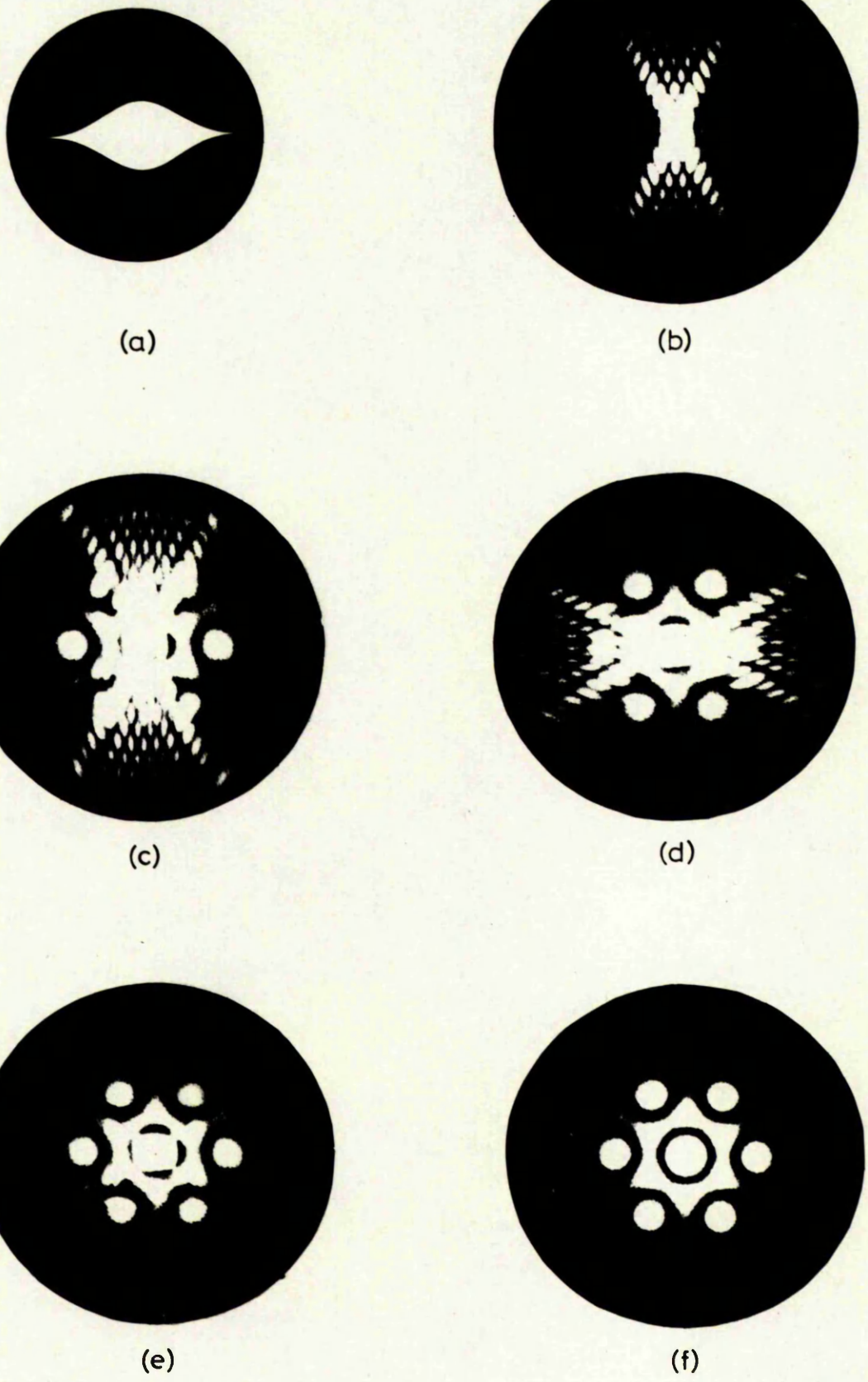

Fig.3.6

form of the obstacles that lies in this region, figure 3.6c. Now, if the aperture is rotated until it is perpendicular to its original orientation, the remainder of the obstacle transform may be observed, figure 3.6d. If photographs are taken with the aperture in both positions, a composite photograph, figure 3.6e, may be assembled of the total optical transform of the obstacles. This compares extremely well with the transform of the complementary screen in figure 3.6f.

The advantages of this method over that using two-dimensional apodising screens are immediately apparent. First, it obviously works experimentally! Secondly, the apertures may be made much more easily than the photographic absorbing screens (methods of making the apertures are discussed later). Thirdly, we have no problems with uneven illumination over the area of the model. Fourth, the screens need not be immersed in cedar-wood oil - a rather awkward procedure. The only disadvantage of this method, compared to the two-dimensional screen method, is that the complete transform of the three-dimensional object cannot be viewed, or photographed, at any one instant; however, a possible way of overcoming this problem is suggested in the next chapter.

3.3.2 NUMERICAL RESULTS

It is obviously of some interest to compare the numerical results for the apodising qualities of the aperture of figure 3.6a with the results for two-dimensional screens

obtained in section 3.2.2. In order to do this it is necessary to calculate the distribution of amplitude in the diffraction pattern of the aperture, i.e. figure 3.6b.

It is quite simple to calculate the amplitude distribution along the line in the pattern for which the aperture is designed to give apodisation. If we write the contour function of the aperture as:

$$T(x) = \sum_{p=o}^{n-1} a_p \cos(2b_p \pi x) \qquad (3.16)$$

where a_p and b_p are constants (see equation 3.15), then, along the ξ axis of the optical transform, we may write the amplitude distribution in the form of a Fourier-transform integral:-

$$A(\xi) = 2\int_{-l}^{l} T(x) \exp(2\pi x\xi)\, dx$$

This may be reduced, since T(x) is even, to:

$$A(\xi) = 4\int_{o}^{l} T(x) \cos(2\pi x\xi)\, dx$$

2l is the horizontal distance between the tips of aperture of figure 3.6a. When the integral is evaluated we obtain:

$$A(\xi) = \sum_{p=o}^{n-1} \frac{a_p}{\pi}\left[\frac{\sin(4\pi l(b_p + \xi))}{b_p + \xi} + \frac{\sin(4\pi l(b_p - \xi))}{b_p - \xi}\right] \qquad (3.17)$$

Obviously $A(\xi)$ may easily be calculated from equation 3.17, by hand or with a simple computer program, provided that care is taken at the discontinuities, i.e. when $\xi = b_p$.

The two-dimensional transform is much more difficult to evaluate; the amplitude distribution is given by the two-dimensional Fourier-transform integral:

$$A(\xi, \eta) = \int_{-1}^{1} \int_{-T(x)}^{T(x)} \exp 2\pi i(x\xi + y\eta)\, dx\, dy \qquad (3.18)$$

We may reduce this to:

$$A(\xi, \eta) = 4\int_{0}^{1} \int_{0}^{T(x)} \cos(2\pi x\xi) \cos(2\pi y\eta)\, dx\, dy \qquad (3.19)$$

Integrating over y, equation 3.19 may be written:

$$A(\xi, \eta) = \frac{2}{\pi\eta} \int_{0}^{1} \sin(2\pi T(x)\eta) \cos(2\pi x\xi)\, dx \qquad (3.20)$$

The author could find no analytic solution to the integral of equation 3.20 and therefore a numerical method of integration was sought.

When considering numerical methods of integrating equation 3.20, two conflicting requirements are evident. In the apodised region the values of $A(\xi, \eta)$ will be very small and therefore high accuracy must be sought. However, as we must evaluate the integral at a large number of values of ξ and η, a very efficient method is needed. Obviously simple numerical-integration methods such as the trapesoidal rule and Simpson's rule are not suitable.

The numerical-integration method known as "Gaussian quadrature" (Lanczos, 1957), which gives high accuracy with a minimal number of sampling points, was therefore applied. Effectively, a Legendre polynomial is fitted to the function to be integrated and the area under this curve is then

found. In practice, if we wish to integrate the function:

$$I = \int_a^b f(x)\, dx \qquad (3.21)$$

we replace this by the summation:

$$I = \frac{b - a}{2} \sum_{i=1}^{n} w_i f(x_i)$$

where x_i is a function of the position of the ith zero of the Legendre polynomial of order n and w_i is a function of the differential of this polynomial at the position of the ith zero. Both the positions of the ith zero and the values of the differential of the polynomial are tabulated for various values of n (Handbook of Mathematical Functions, also Kronrod,1965), thus w_i and x_i may be determined and hence the value of the integral. It will be noted that the sampling points x_i are not equally distributed along the interval a to b, as with the trapesoidal rule and Simpson's rule, and it may be shown that the increased accuracy results from relaxing this condition.

In using Gaussian quadrature, it is necessary to decide upon the minimum number of sampling points necessary to achieve the desired degree of accuracy. There are analytical methods of estimating this quantity but the usual procedure employed is to actually perform the integration several times, increasing the number of sampling points on each occasion; the process is halted when the changes in the value of the integral, as the number of sampling points is increased, are less than the maximum-allowable error.

The function to be integrated in equation 3.20 is sinusoidal in form. The average period of the function decreases as ξ and η are decreased; therefore, it is obviously not sensible to use the same number of sampling points for all values of ξ and η. However, if we examine the function to be integrated, we can see that the maximum number of zeroes of the function is the integral part of $(2l\xi + 2T_m\eta + 1)$, where T_m is the maximum value of $T(x)$ in the range $x = 0$ to 1. If we now divide the function into a number of equal ranges, where the number of ranges is given by the number of zeroes in the total range, we shall be approximately dividing the function into a number of half periods of a sinusoid. It is then a simple matter to estimate the number of Gaussian sampling points necessary to integrate one half period of a sinusoid.

A test program was written to evaluate the integral of $\sin(x)$ in the range $x = 0$ to π by Gaussion quadrature. It was found that seven sampling points were necessary to achieve a result accurate to 11 significant figures - the full decimal accuracy of the store of the Atlas computer. An Atlas-autocode program was then written by the author to evaluate the integral of equation 3.20. The function was divided into ranges as indicated above for each value of ξ and η and Guassian quadrature with seven sampling points was performed in each range and the total for all ranges was then found. It was arranged that these totals for various values of ξ, η should be output on a lineprinter in the form of a map of results, so that contours could be directly drawn, in an exactly similar way to the normal procedure for crystallographic electron density maps.

If we examine the function to be integrated in equation 3.20, it is obvious that care must be exercised when $\eta = 0$. Here we have that:

$$A(\xi, \eta = 0) = 4\int_0^1 T(x) \cos(2\pi x\xi)\, dx$$

which is the simple one-dimensional case of the amplitude distribution along the line for which apodisation is required, as discussed above, and an analytic solution is possible - equation 3.17. However, a step was included in the program to perform this integration numerically so that the results could be compared with those obtained by evaluating the analytic solution of equation 3.17. The agreement was perfect, at least up to the 6th decimal place of the normalised values of $A(\xi, \eta)$, and may have been better as the results of the analytic integration were not calculated any more accurately. Thus a further check was made on the accuracy of the results (and of the program).

For the purposes of the calculation, it was assumed that the size of the aperture was such that it would just enclose the obstacles, arranged in the form of a hexagon, used in the numerical calculation for the two-dimensional apodising screens in section 3.2.3; thus, a direct comparison of the two methods may be made from the results. The actual dimensions of the aperture were 1.7cm.(10.2Å) by 0.57cm.(3.4Å). Figure 3.7 shows the results of the integration in the form of a contour map of the function $\log_{10}[A^2(\xi, \eta)]$, the contours being at unit intervals ($A^2 = 10^{-1}$). The results are normalised to give a value of $A(\xi, \eta) = 1$ at the centre of the map (i.e. $\log_{10}(A^2(\xi, \eta)) = 0$). As

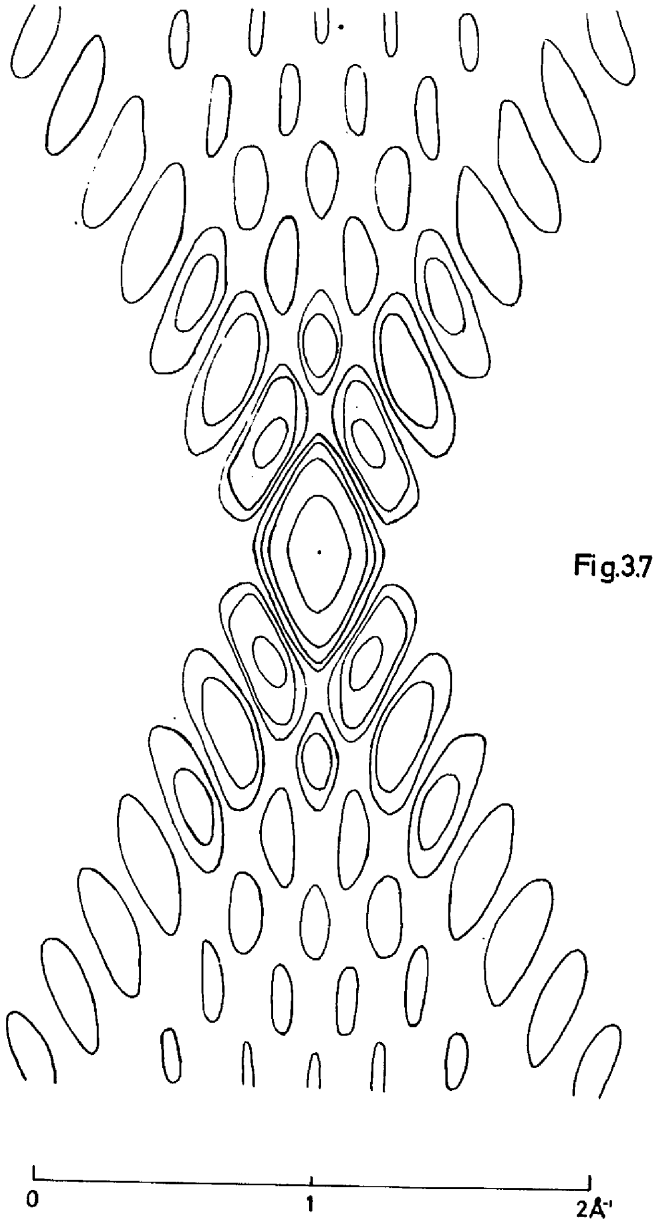

Fig.3.7

with the transforms of figure 3.5 the scale is given in $\mathring{A}^{-1}$. Figure 3.7 compares well with the optical transform of the apodising aperture in figure 3.6b - a further indication of the validity of the numerical results. The existence of the large region of very low intensity is also confirmed - the lowest contour shown represents an intensity of 10^{-4} of the intensity at the centre of the pattern.

However, it is difficult to assess the worth of the apodising aperture from figure 3.7 and to compare its usefulness with that of the two-dimensional screens. In figure 3.8 it has been supposed that the apodising aperture has been used to obtain the optical transform of the obstacles in the form of a benzene ring - placing the aperture in two orientations at right angles. The modulus of the scattered light from the screen, which overlaps into the apodised region (i.e. within the sector of angle 90°), is then plotted for both orientations. Thus, figure 3.8 shows the total interference pattern of the light from the apodising aperture for the simple benzene-ring transform; these results may now be directly compared with the results for two-dimensional apodising screens in figure 3.5. The contours of the central peak correspond to unit intervals on the vertical scale of the graphs of figure 3.5, while the remaining contours correspond to intervals of 0.1 units.

A comparison of the results for the best screen in figure 3.5 and the results of figure 3.8 reveals that only at a small number of points is the performance of the aperture inferior and that it is generally superior over

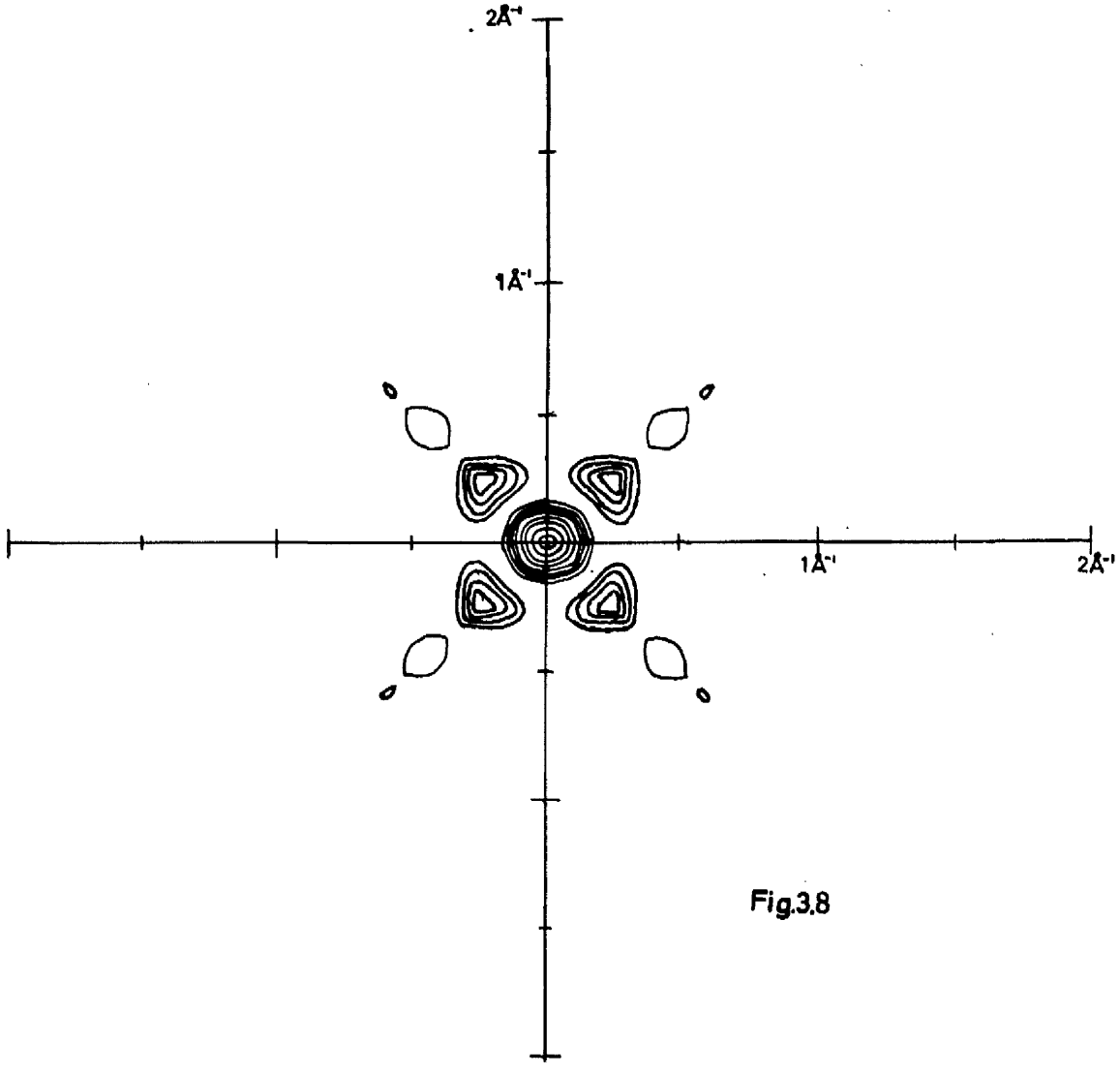

Fig.3.8

most of the optical transform. Furthermore, since accurate reproduction of the aperture function is much simpler than that of the two-dimensional function, we should expect the experimental results of the aperture method to compare even more favourably. Again, as with two-dimensional screens, we may anticipate better results for models with a larger number of atoms.

Before leaving this discussion of the evaluation of the theoretical transforms of apodising apertures, it may be noted that further investigations in this direction might be useful. Only one particular contour function has been tried and further functions may give better results. This particular function is in fact the most effective one, quoted by Dossier et al. (1950), for one-dimensional apodisation. Again, the relative dimensions, length to breadth, have been chosen empirically and ideal dimensions might be deduced theoretically. The author has not pursued this investigation; first, because the present aperture is sufficient for the purpose; and secondly, because the numerical integration program uses a considerable amount of computer time and the investigation would require frequent use of this program.

3.3.3 PRACTICAL DETAILS

Apodising apertures are clearly an effective way of obtaining optical transforms of three-dimensional objects and examples of their use are described in the next chapter. It is therefore convenient to introduce here some practical details of the method.

Frequent use has been made of the large optical diffractometer described by Taylor and Lipson (1957), since it enables larger structure models to be made. It has an aperture of 38cm. compared with the 13cm. of the more usual diffractometer. Differences in the size and the design of the large and the small diffractometers result in differences in experimental technique and these are pointed out when necessary.

Two methods of manufacturing the apodising apertures have been used. Large apertures, suitable for use with the big optical diffractometer, are made by plotting the required function on graph paper and then cutting it out. Smaller apertures, suitable for use with the normal-size diffractometer, are made in thin copper sheets by the photoetching process of Harburn, Taylor and Yeadon (1965). Printed-circuit board, consisting of a thin sheet of copper laminated to a plastic backing, is coated with an ultra-violet sensitive emulsion. A photographic plate, of a reproduction of the aperture in black, is then used to make a contact print on to the sensitised surface of the board. The region of the emulsion exposed to the ultra-violet radiation is hardened, while the unexposed region may be easily dissolved away, enabling the underlying copper to be attacked by an etching solution, leaving a representation of the aperture in the copper sheet. The plastic backing may then be removed by soaking in potassium cyanide solution.

Photography of the optical transforms using apodising apertures is not straightforward, since the transform of the apodising aperture is so much brighter (particularly at

the centre) than the transform of the obstacles. The diffraction patterns of figure 3.6 were produced using the technique of overexposing the film and then underdeveloping it, thus enhancing the faint detail. However, this method is not very satisfactory and obviously a stop is necessary to block out the diffraction pattern of the aperture. Figure 3.9a shows an example of such a stop for use with the aperture of figure 3.6a. The angle of the clear segments is 100°, although in theory it need only be 90°; however, a certain amount of overlap is advisable to allow for experimental errors. The overall diameter of the stop is about 0.5cm. The width of the central portion depends on the size of the apodising aperture - it must be large enough to block the central maximum of the diffraction pattern of the aperture but small enough not to obscure relevant detail in the diffraction pattern of the three-dimensional model - it is typically 0.2mm. Such stops are made by the photoetching process described above.

One rotational movement and two non-parallel translational movements in the plane of the diffraction pattern are required to make the stop coincide with the transform of the apodising aperture. The stop is mounted on a cylindrical cap, which fits snugly on to the focussing drum of the diffractometer (figure 3.9b) and gives the necessary rotational movement. (The reader may find it useful to refer to the details of the construction and use of the optical diffractometer given by Taylor and Lipson, 1964 and Hughes and Taylor, 1958). Translational movements of the optical transform of the aperture can be made, in the case of the small diffractometer, by adjusting the

(a)

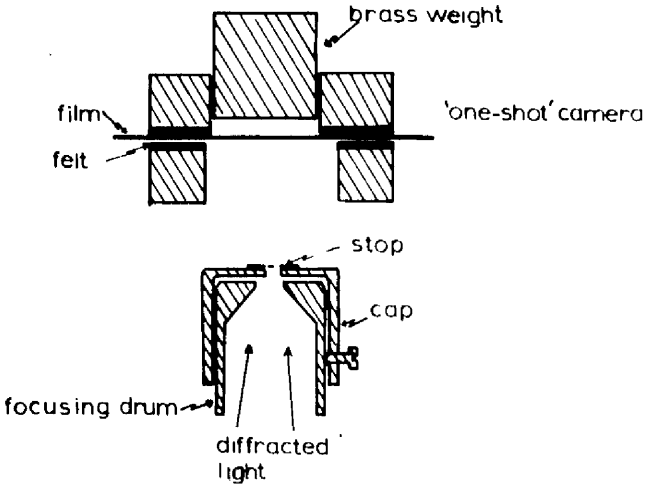
brass weight
film
felt
'one-shot' camera
stop
cap
focusing drum
diffracted light

(b)

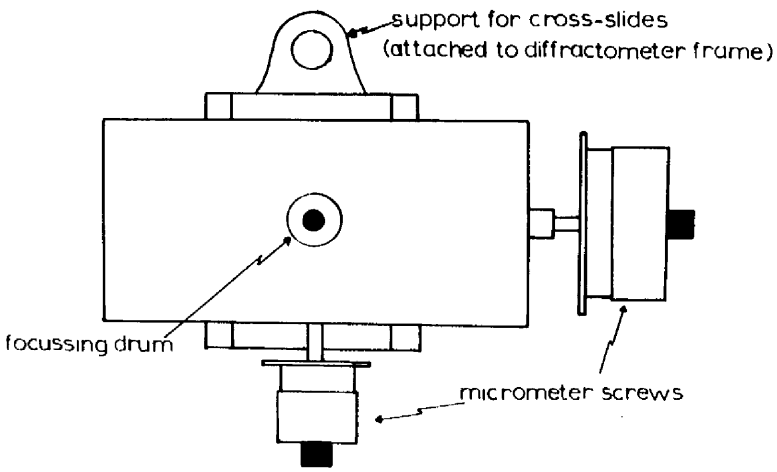
support for cross-slides
(attached to diffractometer frame)
focussing drum
micrometer screws

(c)

Fig.3.9

inclination of the mirror which reflects light received from the lenses to the focussing drum. However, the large optical diffractometer does not have such a mirror and a cross-slide arrangement is used to translate the stop; the focussing drum is then mounted on the cross-slide as shown in Figure 3.9c.

The normal type of camera for taking photographs of optical transforms is unsuitable here, since the spring-loaded platform in the camera, that holds the film against the focussing drum during exposure, displaces the drum slightly and hence also displaces the stop. A light-weight single-exposure camera is therefore used, figure 3.9b, having a brass block held in by an elastic band to push the film against the stop.

One difficulty that may be mentioned here is the problem of the accurate fitting-together of the photographic prints representing the two halves of the optical transform of the three-dimensional object. No really satisfactory method of orientating the two halves has been found but a reasonable fit may be obtained, if there are details in the transform common to both halves, that can be made to overlap. It is always advisable to ensure that such common detail exists when taking the photographs. Uneven shrinkage (i.e. non-isotropic) of the photographic paper during processing also causes matching difficulties, but this can be overcome if the main shrinkage axis of the paper is made to coincide with a prominent direction in the transform for both component parts of the photograph.

The complete transform of the three-dimensional model may be scanned either by rotating the aperture or by rotating

the model. In practice it is found simpler to rotate the aperture, since movement of the model may easily upset its alignment.

Using these experimental techniques outlined above, quite accurate optical transforms may be obtained from three-dimensional models. Figure 3.10 illustrates such a result. The transform is that of a mask representing the structure decanamide (Brathovde and Lingafetter, 1958). Figure 3.10a shows the optical transform of a distribution of discs fixed to an optical flat representing the 010 projection of the structure; figure 3.10b shows the corresponding optical transform of a punched-mask representation. The two transforms are almost identical.

3.4 SUMMARY

The main conclusions of this chapter may now be stated. Apodisation clearly offers a way of eliminating the contribution (A_o) from the instrumental aperture to the total diffraction pattern, if we attempt to observe the optical transform of a three-dimensional model. The use of two-dimensional apodising screens is feasible but apodising apertures give better results.

The next chapter is devoted to illustrating examples of possible applications of both the apodising aperture method and optical transforms of three-dimensional objects in general.

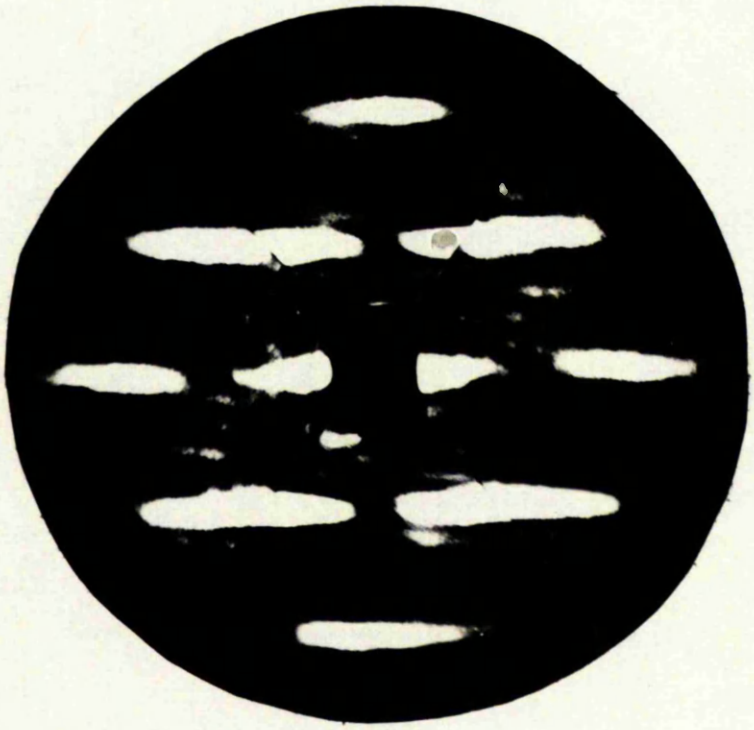

(a)

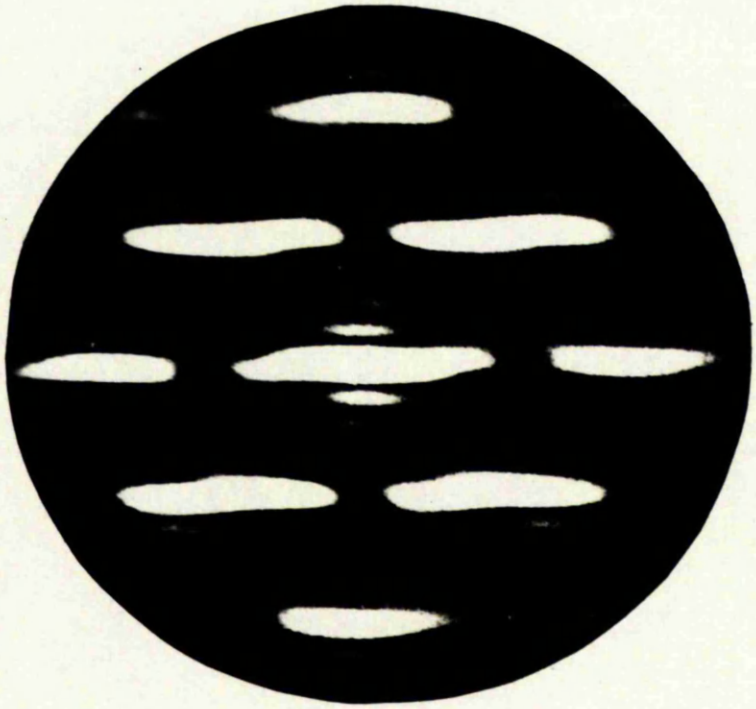

(b)

Fig.3.10

CHAPTER 4

OPTICAL TRANSFORMS OF THREE-DIMENSIONAL CRYSTAL-STRUCTURE MODELS OBTAINED USING APODISING APERTURES

This chapter is mainly devoted to illustrating and exploring the possible applications of optical transforms of three-dimensional molecular-structure models, obtained by the apodising aperture method. The factors influencing the building of suitable crystal-structure models are first discussed; then, examples of transforms are given. Finally, future possibilities of using and improving the method are mentioned.

4.1 THE MANUFACTURE OF SUITABLE CRYSTAL-STRUCTURE MODELS

The most important factor to be considered, when building simple molecular-structure models, is their scale. The size of the models must obviously be such that they are easily accommodated within the aperture of an optical diffractometer. Furthermore, if an apodising aperture of the type shown in figure 3.6a is also to be included within the aperture of the diffractometer, the largest dimension of the model must be less than one third the distance between the tips of the apodising aperture. The lower limit on the size of the model is set purely by the difficulties in constructing it; very small balls are difficult to drill

accurately and small, thin bonds between the balls distort easily. The scale that is normally used for punched-mask representations of structures in smaller diffractometers is 1/6cm. = 1Å; making 'ball and bond' models to this scale would be difficult and time-consuming (attributes incompatible with optical methods of structure solution). In fact, ball and bond models on any scale, suitable for use with the combination of an apodising aperture and the smaller type of diffractometer, must have a maximum diameter of about 4cm. Making such models would present a number of practical difficulties, unless there are only a few atoms in the structure. However, the scale normally used with the large diffractometer in this department, that is 1cm. = 1Å, is much more promising; components for building models to this scale can be obtained commercially (Beevers, 1965). Beevers molecular models have been used, together with the large optical diffractometer, to produce the optical transforms illustrated in this chapter.

One difficulty, encountered with ball and bond models, is that light is diffracted from the bonds as well as from the balls, and so distortions of the optical transform are inevitably produced. A solution, that has been suggested to the author, would be to use transparent bonds and to immerse the model in a liquid, whose refractive index matches that of the bond material. However, so that phase distortions need not be introduced in the illuminating and diffracted beams at the liquid-air interface, two of the sides of the container for the liquid must be optical flats.

Quite large optical flats would be needed (≈ 40cm. diameter), if Beevers models with transparent bonds are to be used, and such flats would be prohibitively expensive.

Fortunately, if the bonds are thin compared to the ball diameter, the effect is small in the author's experience - only fainter details near the edge of the pattern are seriously affected. The wire normally used for bonds with Beever's models is 0.040in. diameter and this is rather thick; therefore, the models used had bonds made from 0.022in.diameter wire. With wire of this latter diameter and the 6.9mm. diameter balls used in Beever's models, for a typical carbon-carbon single bond, the ratio of the ball to bond scattering is about 30:1 in amplitude. In order to fit the 0.022in. bonds in to the 0.040in. holes in the balls plastic sleeves were placed over both ends of each bond, which was then cemented into position with 'Araldite'. This assembly process is very tedious but there seems to be no reason why, in future experiments, the models could not be built much more quickly, if balls with holes of the correct size were used.

Having chosen the scale of the model a further factor must be considered and that is the suitability of the ball diameter for this particular scale. The useful extent of the optical diffraction pattern of an arrangement of similar balls in a model is governed by the size of the individual ball, since the transform of the arrangement is modulated by the function representing the transform of each ball. Thus, the limit of the useful extent of the diffraction pattern is the point at which the transform of the ball

becomes zero for the first time. Ideally, all the X-ray diffraction data should be represented in the optical transform; therefore, the first zero of the optical transform should not correspond to a point nearer to the origin than the edge of the limiting sphere for the X-ray data (see section 1.1).

We may write the amplitude distribution in the diffraction pattern of a ball of radius a as

$$A(\rho) = 2\pi a^2 \frac{J_1(2\pi a\rho)}{2\pi a\rho}$$

The first zero of the pattern occurs when

$$2\pi a\rho = 3.832$$

(the second zero of the Bessel function $J_1(x)$).
Rearranging this expression we may write the distance of this zero point from the origin of reciprocal space as

$$\rho = \frac{3.832}{2\pi a}$$

Now if the scale of the model is such that mcm. = 1Å then:-

$$\rho = \frac{3.832\ m}{2\pi a}\ \text{Å}^{-1}$$

If this value of ρ corresponds to the edge of the limiting sphere then:-

$$\rho = \frac{2}{\lambda} = \frac{3.832\ m}{2\pi a} \qquad (4.1)$$

where λ is the wavelength (in Å) of the radiation used to give the X-ray diffraction pattern, which we are simulating optically. Thus, from equation 4.1 we may write the maximum value of the radius of the ball, that would enable all the X-ray pattern to be simulated optically, as

$$a_{max} = \frac{3.832\ m\lambda}{4\pi} \qquad (4.2)$$

For the Beevers models where m = 1, if λ = 1.541Å (CuKα radiation), then the maximum diameter of the balls that may be used can be deduced from equation 4.2 to be 9.4mm; thus, the actual diameter of 6.9mm. is quite adequate under these conditions. (In the case of the small optical diffractometer, where m = 1/6, it is interesting to note that the corresponding maxinum diameter of the apertures that may be used is 1.57mm.).

The diameter of the balls is also partly influenced by the problem of 'overlap'. In certain projections of most models one or more pairs of atoms overlap and the corresponding optical transform is partly incofrect, since the double scattering is not properly represented. The use of small balls helps to reduce the probability of overlap occuring.

Overlap has not been an important problem in any of the examples examined by the author. Obviously, whether or not the difficulty is serious, depends partly on the structure of the model and partly on the particular area of the transform being considered.

4.2 EXAMPLES OF OPTICAL TRANSFORMS OF THREE-DIMENSIONAL MODELS

When we wish to examine the optical-transform corresponding to a particular projection of a molecular-structure model, it is necessary to orientate the model so that the plane of projection is perpendicular to the optic axis of the optical diffractometer. The device shown in figure 4.1 was constructed by the author for this purpose.

The base of the device is a simple carriage which moves along, and may be clamped to, the rail shown, which in turn is fixed across the aperture of the diffractometer. The horizontal disc with the circular scale, together with the remainder of the structure fixed on top of the disc, is connected by means of a ball bearing to the carriage and may rotate freely in the plane of the disc. The model is clamped in the structure above the disc; and the two perpendicular rotations (shown in figure 4.1) given by this structure, enable the orientation of the model to be adjusted.

The direction of the optic axis of the optical diffractometer at points between the lenses of the instrument is clearly marked by the light beam, if a large bright source is used. The orientation of the model, with respect to the optic axis, can easily be determined from the shadow cast by the model in the beam. Thus, using the device in figure 4.1, the required projection of the model may be made perpendicular to the optic axis as follows:-

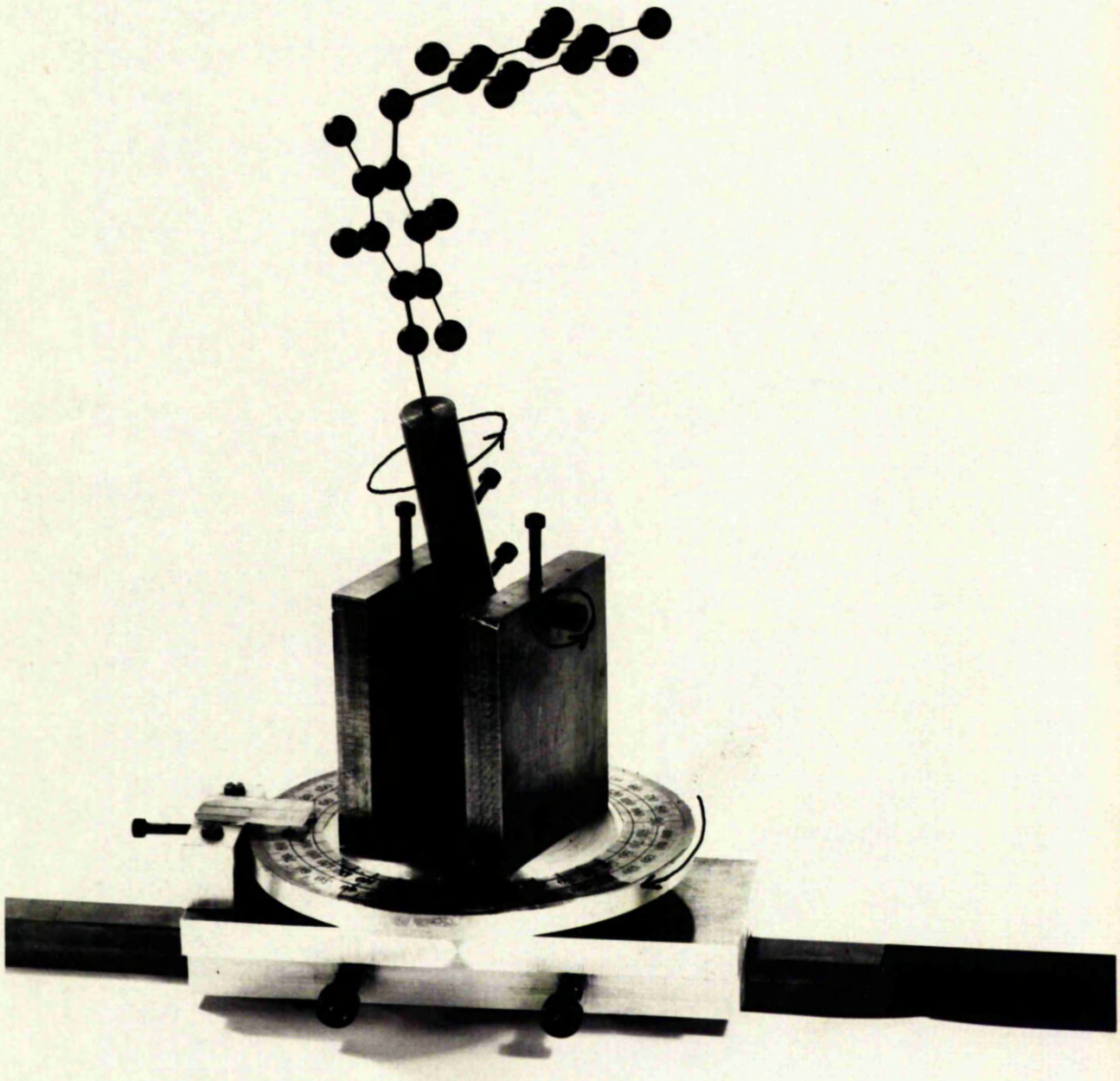

Fig.4.1

(i) An axis in the model, parallel to the required plane of projection, is marked with a straight piece of wire. The orientation of the model is then adjusted, using the two perpendicular rotations, until the marking wire remains parallel to the axis of rotation of the ball bearing, when the model is rotated on the device about this axis.

(ii) The bar supporting the device is then rotated about its length, until the rotation axis of the ball bearing (and hence the marking wire) is perpendicular to the optic axis. This is done by placing a straight piece of capillary tube on the horizontal disc and rotating the rail, until the beam of the diffractometer shines straight down the bore of the tube. (It is usual to repeat this procedure for several non-parallel positions of the tube on the disc to obtain a 'best fit').

(iii) The model is then rotated on the bearing axis until the desired projection is reached, as seen from the shadow cast by the model in the beam of the diffractometer.

The above procedure may be applied in any general case. However, in specific cases, it may be possible to orientate the model much more simply.

4.2.1 CORONENE

Coronene (Robertson and White, 1945) was selected as a first example of the method of obtaining optical transforms of three-dimensional crystal-structure models. The bond lengths and angles were idealised for the model actually made, figure 4.2, so that each bond length was 1.4cm. and each bond angle 120°. Since, in addition, the molecule is planar, the model is quite easy to construct.

Figure 4.3 shows, on the right-hand side, the optical transforms of the model in three different orientations. On the left-hand side of figure 4.3 are given the optical transforms of the punched masks corresponding to each position of the model. The three orientations of the model are obtained by rotating it about the axis in the molecular plane as indicated in figure 4.2. Transforms 4.3a and 4.3b correspond to the model viewed perpendicular to the molecular plane. In transforms 4.3c and 4.3d the molecule is rotated 30° out of this plane and for 4.3e and 4.3f, 60° out of the plane.

Comparison of the two corresponding sets of transforms provides a critical test of the apodising aperture method. If account is taken of the difficulty of obtaining equivalent exposure levels for corresponding transforms, then the two sets can be seen to be reasonably comparable. The intense detail near the centre of the pattern is always reproduced, but the fainter detail near the edge of the pattern is sometimes suppressed and sometimes enhanced (see particularly figures 4.3a and 4.3b). This effect is probably caused by

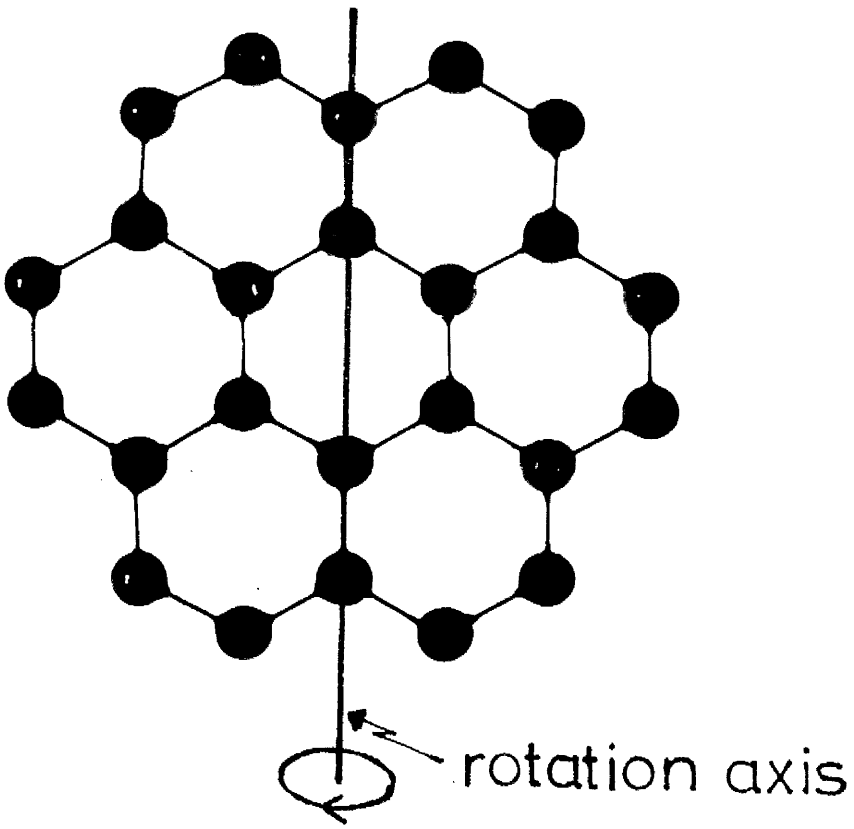

Coronene

Fig.4.2

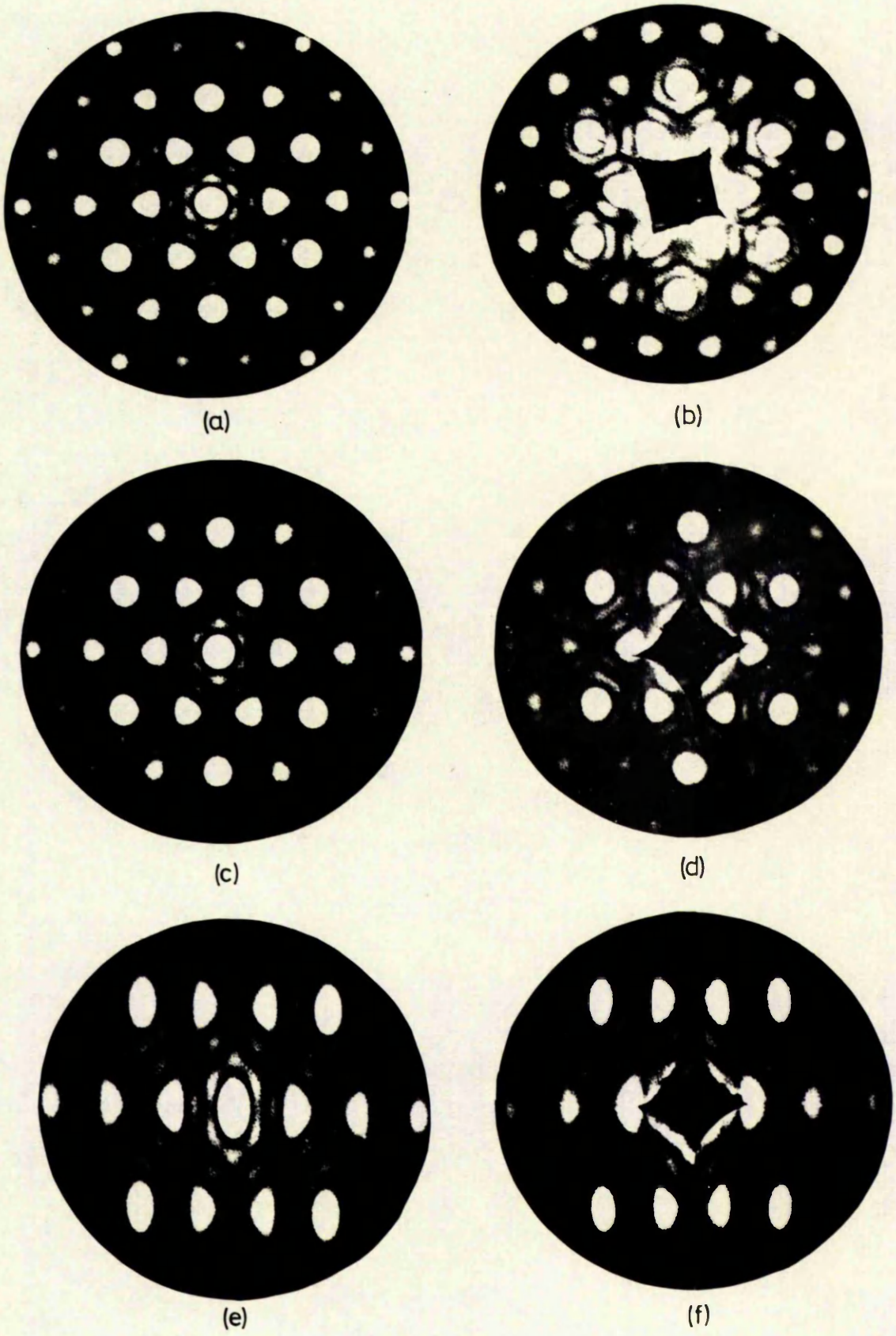

Fig.4.3

the interference of light scattered from the bonds. The scattering function of the bonds, along a perpendicular to the length of each bond, will fall off much more slowly than that of the balls; and thus, at the edge of the optical transform the scattering from the bonds may not be negligible compared to that from the balls. However, over most of the region of interest, the suppression of the fainter detail is usually not so great that it cannot be made visible by increasing the exposure a little. This procedure would be reasonably satisfactory in structure-solution work by optical-transform methods, since we are usually more interested in the presence or absence of detail rather than the absolute intensities of various parts of the pattern. In this connection it may be noted that the normal fall-off in intensity of the optical transform towards the edge also distorts the relative levels of the detail in the pattern; however, in a similar way this may be allowed for and it is usually not disadvantageous.

4.2.2 BIHYDROXYDURYLMETHANE

In contrast to the essentially planar structure of coronene the second example, bihydroxydurylmethane (Chaudhuri and Hargreaves, 1956), is truly three-dimensional (see figure 4.4). Again an idealised model of the structure was made with all bond angles 120° and all bond lengths 1.4Å (apart from those bonds linking the benzene rings to the central carbon atom which were made 1.54Å). Great care was taken to make the relative orientation of the planes of the benzene rings as near as possible to the structure found by

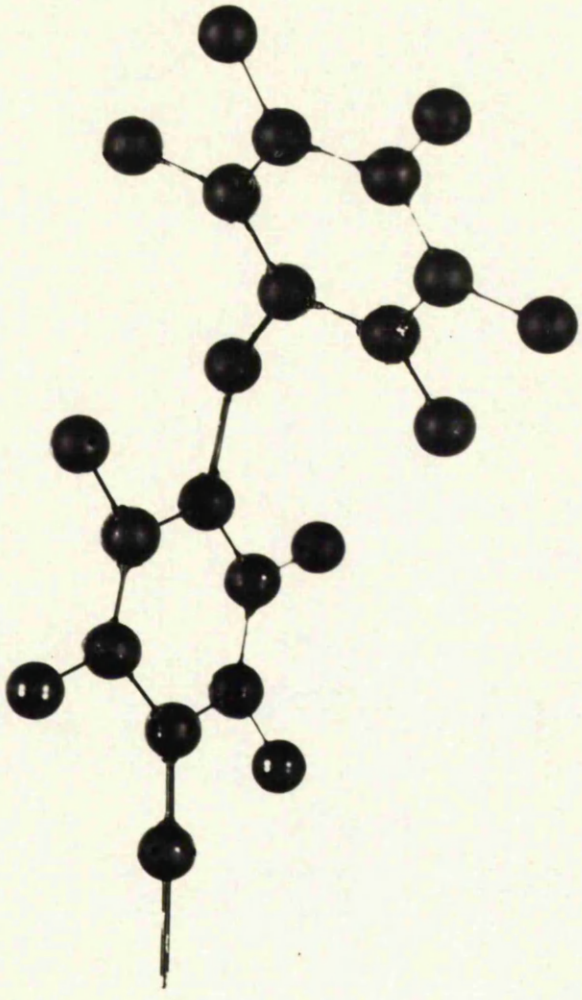

Bihydroxydurylmethane

Fig. 4.4

Chaudhuri and Hargreaves. The inaccuracies, introduced by the approximations made in building the model, make this model such that it might correspond to a trial structure.

Figure 4.5a is the optical transform of the projection of the molecule corresponding to the hOl data, which are given in the superimposed weighted reciprocal lattice. The agreement is quite good. This projection of the model corresponds well with the final structure obtained, as can be seen from a comparison of the shadow projection with a drawing of the final structure (as obtained by Chaudhuri and Hargreaves).

Figure 4.5b is the optical transform of the projection of the model corresponding to the hkO data. The agreement with the superimposed weighted reciprocal lattice is poor, although the correct symmetry is present in the pattern. The fit of the shadow projection of the model in this orientation with the final structure is not very good, since the inaccuracies in the model tend to show up badly in this projection.

4.2.3 A HYPOTHETICAL DISORDERED STRUCTURE

In recent years, there has been considerable interest in using optical-transform techniques in investigating various types of disordered structures and, in particular, fibre structures (e.g. Stern, 1966). Quite crude models are often useful for these structures; for example, Taylor (1965) has used collections of orientated springs to simulate the structure of a fibre and has produced optical

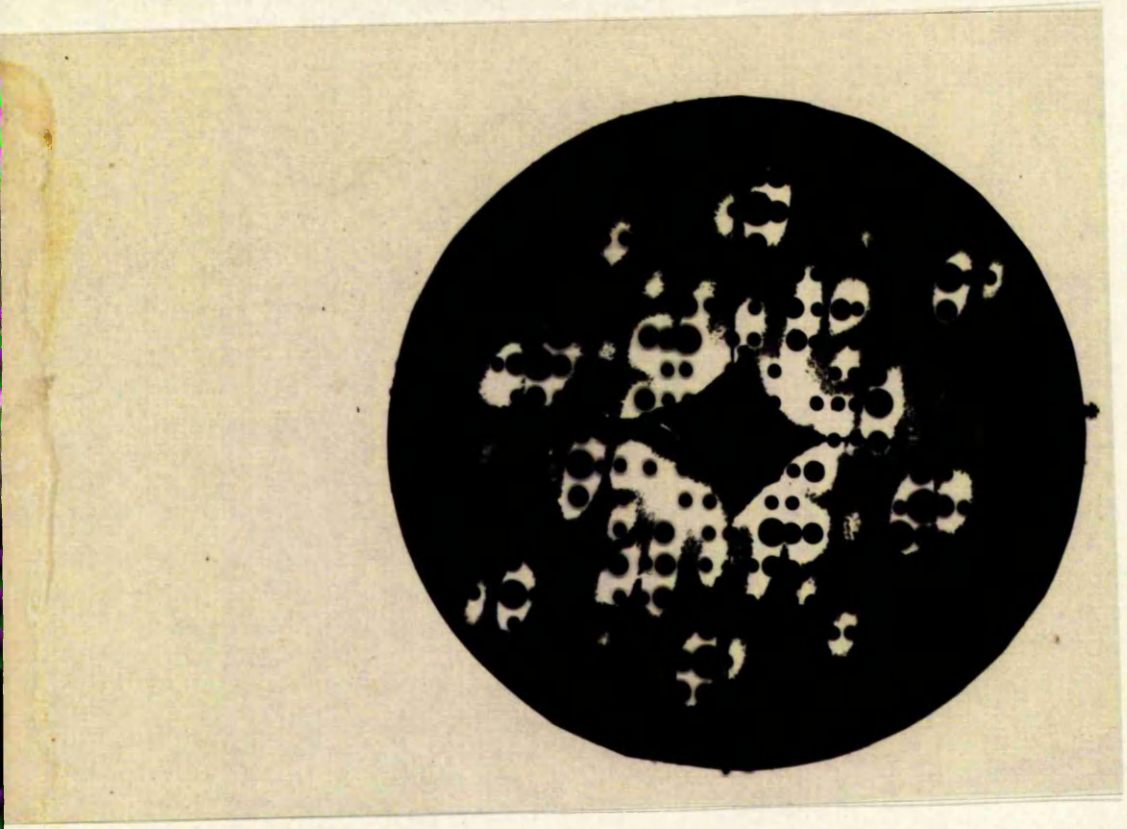

(a)

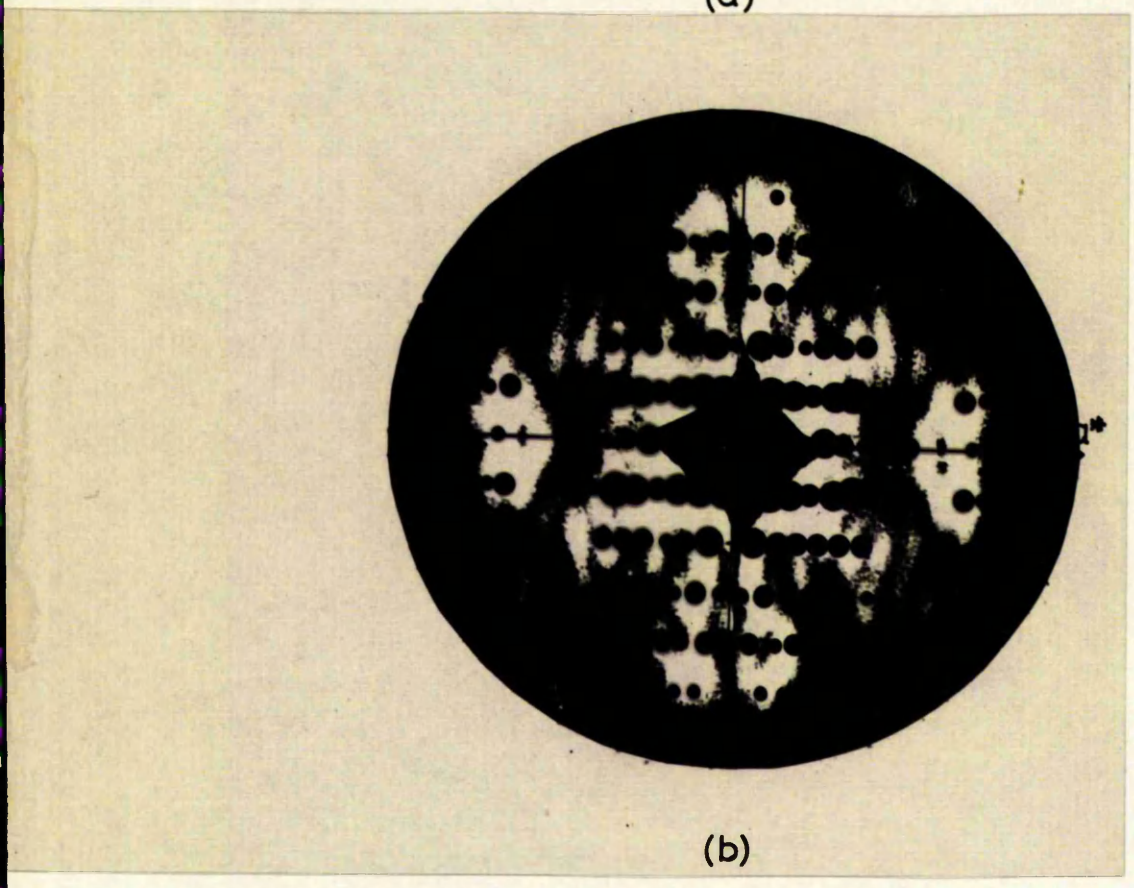

(b)

Fig. 4.5

transforms from photographic reproductions of this model.

Obviously, the apodising aperture technique could be used to obtain optical transforms directly from such models, without the need for the intermediate photographic process. Figure 4.6 shows such a model consisting of roughly parallel strings of balls, which might represent the grouping of one-dimensionally ordered polymer molecules in a fibre. The balls are threaded on wires fixed to a Dexion framework.

The transform of the model is a series of parallel streaks, figure 4.7. The spacing between the streaks is proportional to the repeat distance between the balls on each wire. The diffuseness of the pattern along the streaks is due to the lack of order in the spacings between the strings of balls.

4.3 CONCLUSIONS CONCERNING THE USE OF THE APODISING APERTURE METHOD AND ITS FUTURE POSSIBILITIES

The preceding examples show that the method of using one-dimensional apodising apertures to obtain the diffraction patterns of models of molecular structures can produce reasonably good results, although some inaccuracies may occur due to light scattered from the bonds in the model. Possibly, the primary source of error is in the actual construction and orientation of the model, particularly if some complex three-dimensional structure is involved. This suggests that the method might be used at very early stages of structure solution, when rough three-dimensional details, for example the position and orientation of atomic groups, are being determined. Later detailed refinement could be

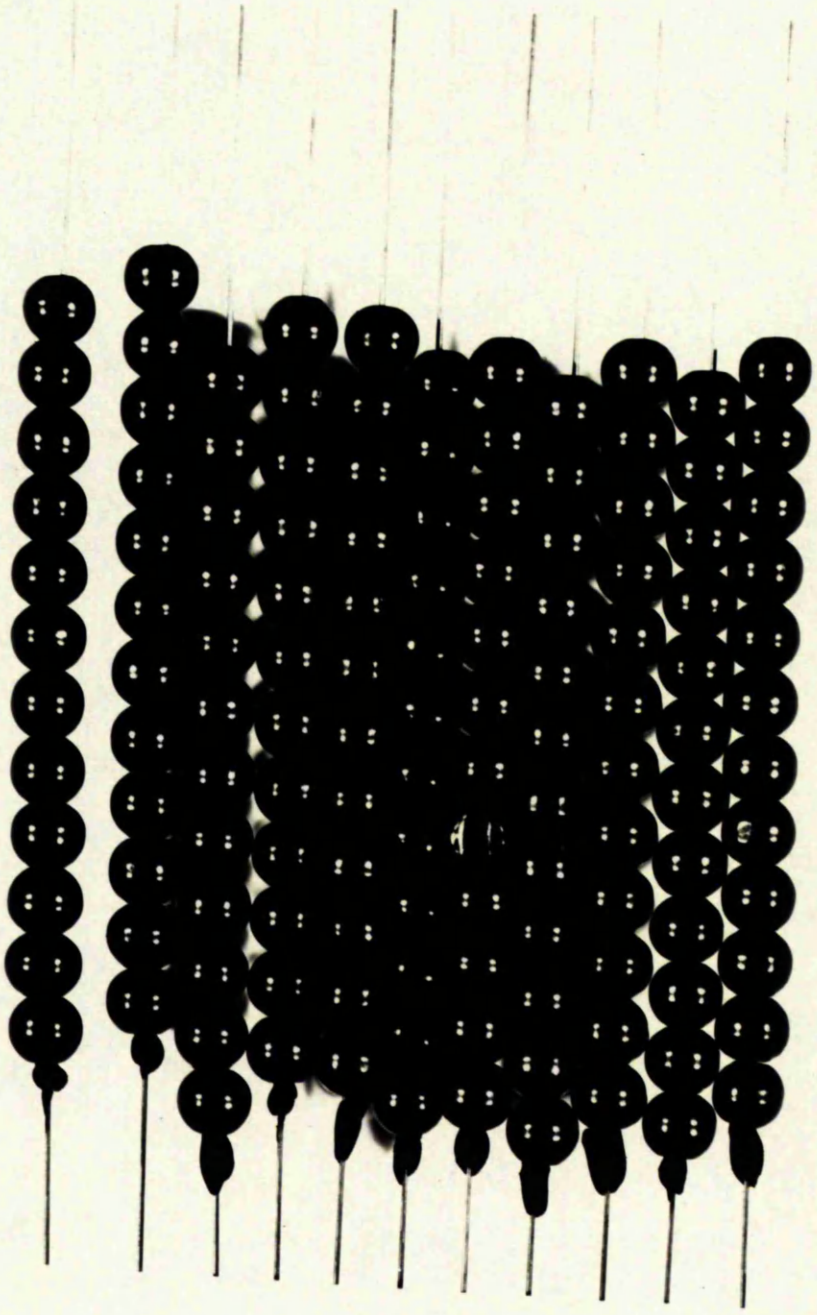

Disordered structure

Fig.4.6

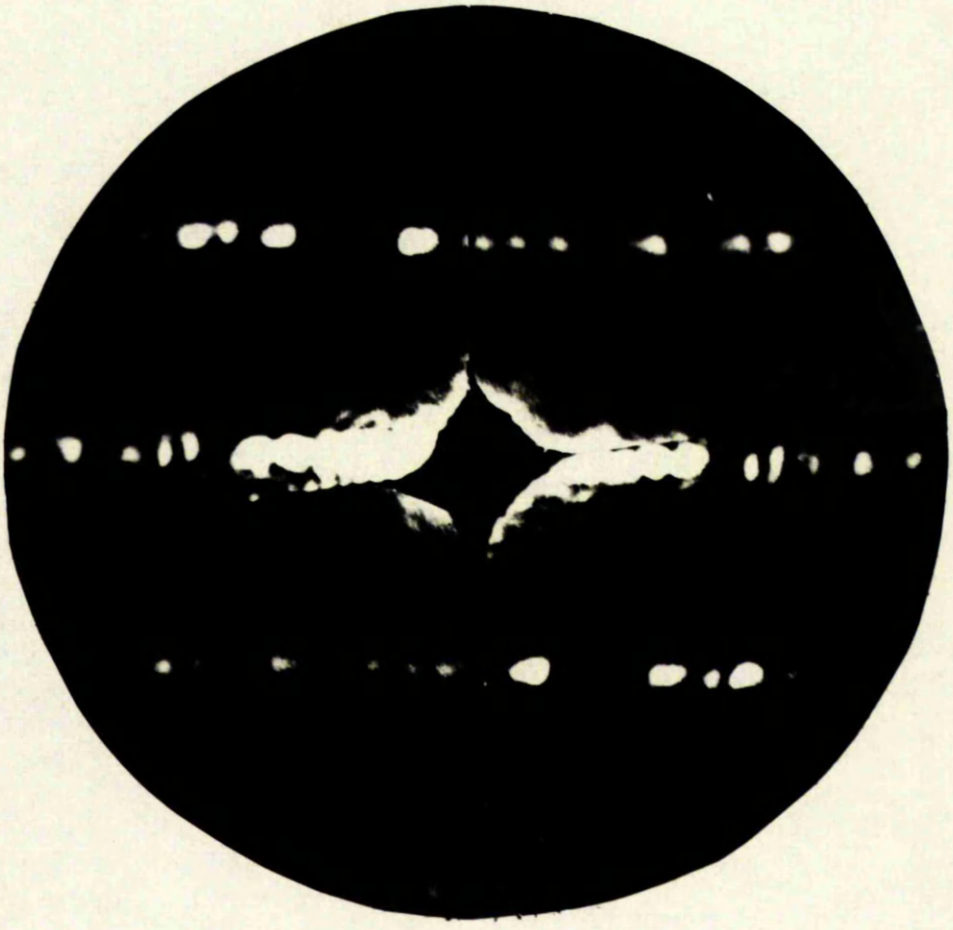

Fig.4.7

carried out in projection using more conventional optical methods.

Although no attempt has been made by the author to construct an actual three-dimensional optical transform, as suggested by Harburn (see section 1.4), this is now quite feasible. The amount of work involved would be similar to that when constructing a three-dimensional Patterson map.

The application of the method to disordered structures, as in section 4.2.3, would also be quite useful. Simple ideas about rough structural details can easily and quickly be tested. In addition, it is possible to simulate structures, in which there is rotational disorder, by building models which actually rotate in three-dimensions.

Possibly the most useful improvement to the apodising-aperture method would be to eliminate the necessity of a double exposure to obtain a complete transform. If the apodising aperture was oscillated between the two mutually perpendicular orientations, at which the two photographs of the transform are taken, then the model transform would be continuously scanned. If, in addition, this motion was linked to a corresponding motion of the stop in the transform plane, only the transform of the three-dimensional model need be seen. It would, of course, be impossible to clamp a film against this moving stop, to photograph the complete transform as it is scanned, but a re-imaging system could overcome this problem.

In conclusion, one possible industrial use of the apodising aperture method may be noted. Redman (1968) has described how the dimensions of machined products, such as

fuel cans for nuclear reactors, may be checked by examining the optical transform of the actual three-dimensional object. He envisages simply putting the object in the aperture of a diffractometer to obtain a transform, but the use of apodising apertures would certainly give better results.

PART 2

THE CRYSTAL AND MOLECULAR STRUCTURE OF 2-DIAZOINDANE-1,3-DIONE

CHAPTER 5

2-DIAZOINDANE-1,3-DIONE: PRELIMINARY INVESTIGATION AND THE SOLUTION OF THE (001) PROJECTION

5.1 INTRODUCTION

The preceding chapters have described the search for a method of obtaining optical transforms of three-dimensional molecular-structure models so that complete three-dimensional optical transforms could be formed. At the beginning of the investigation it was hoped that, when this new optical approach was developed, it would be possible to apply it in solving an unknown crystal structure. Accordingly, X-ray diffraction data were collected for the structure 2-diazoindane-1,3-dione. However, the problem of obtaining optical transforms of three-dimensional objects proved somewhat intractable at first and, before the method was sufficiently developed, it was found that the structure could be solved conveniently by conventional methods.

It was decided, before the structure was investigated, that it would be useful to try to achieve the solution by purely physical means (and in particular by optical methods) without recourse to any chemical information apart from the empirical formula $C_9N_2O_2H_4$. Such determinations have been attempted successfully in the past (Crowder et al., 1959). While this approach is quite instructive, suggesting ways of tackling problems where the information is wrong or incomplete,

it does lengthen the process of structure solution. As in the present case, if the full information about the conformation of the molecule is not known and if few clues can therefore be deduced about its likely mode of packing, the derivation of a trial structure suitable for refinement can be extremely time-consuming. About half the atoms in the molecule could be located by purely physical information; however, it was found necessary to use chemical information on the likely conformation of the molecule as a source of 'inspiration' to locate the remaining atoms.

5.2 THE CHEMICAL SIGNIFICANCE OF 2-DIAZOINDANE-1,3-DIONE

The previously unknown compound 2-diazoindane-1,3-dione was discovered almost simultaneously by Holt and Wall (1965) and Regitz and Heck (1964) using different synthetic routes. It is interesting in that it is one of the first diazodiketones to be prepared and the very first of the type 2-diazo 1,3 dione. It is also related to the 1,3 indanone compounds which are used as anti-tremor agents.

Regitz and Heck give the structure of 2-diazoindane-1,3-dione as a resonance of the two extreme forms

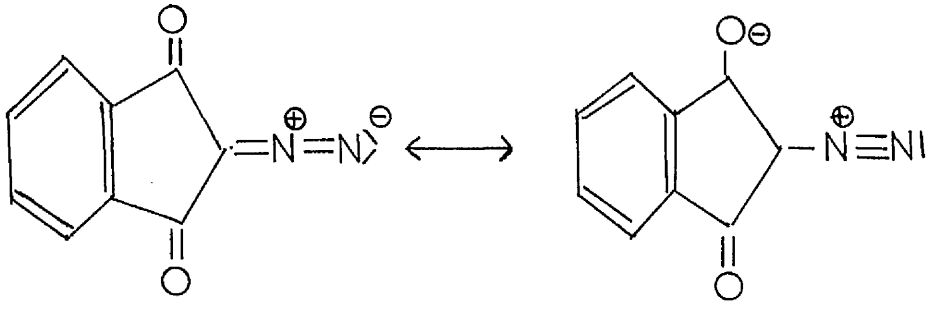

The synthesis of Holt and Wall involved a novel type of cyclisation reaction and it is of some interest to check the structure of the substance,obtained by them, by X-ray diffraction. In addition the resonance structure proposed by Regitz and Heck may be confirmed.

5.3 PRELIMINARY INVESTIGATION (UNIT CELL AND SPACE GROUP)

A sample of the substance (m.p.105-106°C) was provided by Dr G Holt in the form of colourless needle crystals, which had been recrystallised from hot water. These crystals proved suitable for X-ray examination without further treatment.

It was found that under exposure to the atmosphere and X-rays the substance changed into some unknown form, becoming brownish in colour. The X-ray reflections from the crystals became gradually weaker, as this process continued, until after a period of several weeks no sharp reflections could be obtained at all. The crystals also had an annoying tendency to drop out of the mounting adhesive, when exposures were being made, and this effect may well have been connected with the change in structure. It was found that a thin coating of shellac over the crystal and its mounting slowed the change and prevented it dropping off.

Since the end faces of the crystal, perpendicular to the needle axis, were small and not usually well-shaped, it was impossible to deduce the crystal form. The cross section, perpendicular to the needle axis, appeared to be a parallelogram with angles near 90° (often almost square).

The crystals were soft and it was difficult to cut them without producing distortion; thus, the preparation of suitable specimens for X-ray examination was extremely tedious.

An X-ray investigation of the crystals revealed that the symmetry was monoclinic and that the unique (b) axis lay perpendicular to the needle axis of the crystal and along one of the diagonals of the cross section. The two remaining axes (a and c) were chosen such that c lay along the needle axis and, since β was almost 90^{o}, a lay along the other diagonal of the cross section. The unit-cell sides - measured from rotation photographs about all three axes - and the β angle - measured on a Weissenberg photograph of the h0l layer of the reciprocal lattice - were found to be:

$$a = 9.67\text{Å}$$
$$b = 10.55\text{Å}$$
$$c = 7.93\text{Å}$$
$$\beta = 92.1^{o}$$

The following conditions for reflection were deduced from the systematic absences on Weissenberg photographs of the h0l, h1l and h2l layers of the reciprocal lattice:

hkl:	$h + k + l$	$= 2n$
h0l:	l	$= 2n \quad (h = 2n)$
0k0:	$(k$	$= 2n)$

Two possible space groups are indicated $I\frac{2}{c}$ (centrosymmetric) and Ic (non-centrosymmetric). It may be noted that these two space groups correspond to $C\frac{2}{c}$ and Cc, which are the forms in which they are given in International Tables for X-Ray Crystallography Vol.1. The (001) projections of the two

space groups have the two-dimensional symmetries cmm (centrosymmetric) and cm (non-centrosymmetric) respectively. A statistical test may therefore be applied to the hk0 data to determine whether there is a centre of symmetry present in this projection, and thus, whether one is present in the three-dimensional structure.

Wilson (1949, 1950) has examined theoretically the distribution in reciprocal space of the intensities of the X-ray reflections from a crystal with a unit cell containing a reasonably large number of atoms. The atoms are assumed to have approximately equal weights and to be arranged at random. Wilson shows that the distributions resulting from centrosymmetric and non-centrosymmetric crystals are quite different. If $P(I)\delta I$ is the proportion of the intensities lying between I and $I + \delta I$, then for a non-centrosymmetric crystal we have:-

$$_1P(I)\delta I = \frac{\exp(-I/S)\delta I}{S}$$

and for a centrosymmetric crystal:-

$$_1^-P(I)\delta I = \frac{\exp(-I/2S)\delta I}{(2\pi SI)^{\frac{1}{2}}}$$

S is a distribution parameter which depends on the particular set of reflections being considered; for general hkl reflections from a primitive lattice we have:

$$S = \sum_{j=1}^{N} f_j^2$$

where the summation is taken over all the atoms in the unit cell. From these results Howells et al. (1952) have shown that the fraction N(z) of the reflections, whose intensities are equal to, or less than, a fraction z of the local average intensity, is given, for a non-centrosymmetric crystal, by the function:

$$N(z) = 1 - \exp(-z)$$

and, for a centrosymmetric crystal, by the function:

$$N(z) = \mathrm{erf}(\tfrac{1}{2}z)^{\frac{1}{2}}$$

These expressions form the basis of the zero moment (or N(z)) statistical test for determining the presence or absence of a centre of symmetry in a crystal structure; figure 5.1 shows both functions (continuous lines).

Figure 5.1 also shows the experimental points (dotted) for the N(z) distribution of the **hk0** data, obtained using the method suggested by Lipson and Cochran (1966). The reflections are first grouped into three ranges of sin θ containing approximately equal amounts of data, rejecting very low-angle reflections (sin θ < 0.2) and the 0k0 and h00 reflections. The average intensity (I av.) in each range of sin θ is then determined. The data within each sin θ range are divided into subsets such that the intensities within each subset are less than, or equal to, some specific fraction of the average intensity (I av.). The numbers of reflections in corresponding subsets in each sin θ range are then summed together and expressed as fractions of the total

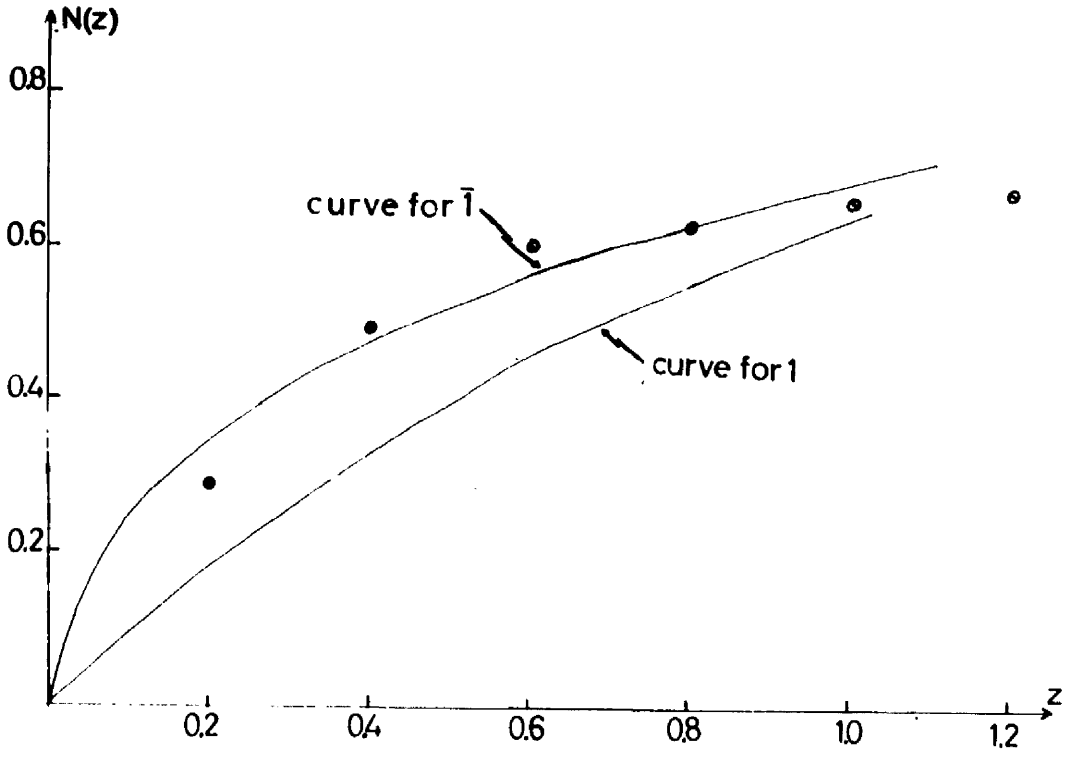

hk0 data: zero moment test

Fig.5.1a

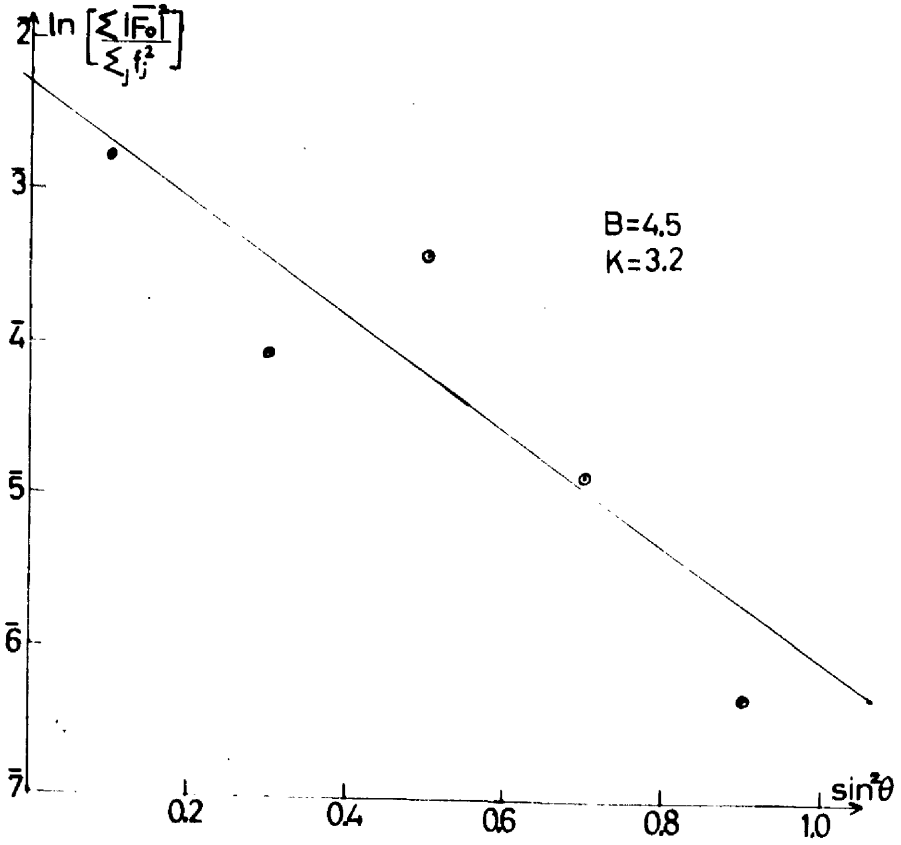

hk0 data: Wilson plot

Fig.5.1b

number of hk0 reflections. These fractions are the experimental values of N(z) for each range of z.

The points in figure 5.1 lie much closer to the centrosymmetric distribution curve than the non-centrosymmetric curve. The space group may thus be deduced with reasonable confidence to be $I\frac{2}{c}$.

Figure 5.2a gives the symmetry diagrams for the space group $I\frac{2}{c}$. It will be noted that, although the space group is centrosymmetric, a centre of symmetry is not chosen as the origin, but the point at the intersection of the 2-fold axis and the c-glide plane is used. Figure 5.2b shows the symmetry diagrams for cmm, the symmetry of the special projections (001) and (100), used in the structure determination. The origin for the projection (100) is shifted $\frac{1}{4}$ of a lattice translation along the b axis relative to the origin of the three-dimensional space group. It will be observed that in contrast to the three-dimensional space group the two-dimensional space group cmm <u>has</u> a centre of symmetry at the origin.

The density of the crystal was measured as 1.35gm cm^{-3} by flotation in zinc iodide solution, the density of the solution being determined with a specific-gravity bottle. Then, using this value for the density and the cell dimensions given above, the number of molecules per unit cell may be calculated to be 3.82, which gives 4 as the nearest integer. The space group $I\frac{2}{c}$ has 8 general positions and it is therefore evident that the molecule of 2-diazoindane-1,3-dione must be specially situated with respect to the symmetry elements in the unit cell. In fact, there is a 2-fold axis

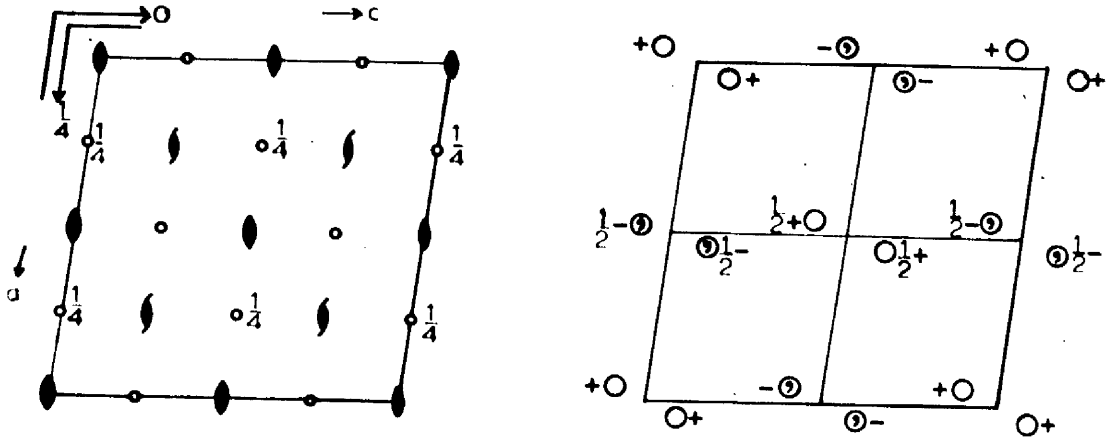

Three-dimensional space group: $I\bar{4}2$

(a)

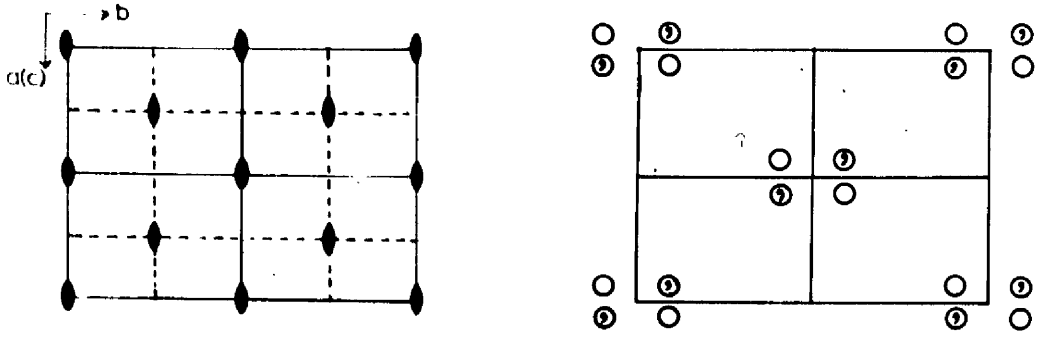

Two-dimensional space group: cmm

(b)

Fig.5.2

in the molecule which follows the line of the C-N-N group and relates the two halves of the molecule; and this 2-fold axis in each molecule is coincident with a 2-fold axis in the unit cell. A knowledge of the structure would have enabled this deduction to be made at once, but, as indicated above, this information was not available and so the conclusion was arrived at by a roundabout method.

5.4 THE SOLUTION OF THE (001) PROJECTION

5.4.1 THE COLLECTION AND PROCESSING OF THE hkO DATA

A crystal of length 0.63mm (needle axis) and cross section 0.099 by 0.073mm was selected. The X-ray intensities were measured using a Unicam Weissenberg camera with Ni-filtered CuKα radiation. Two packs of five films were used with exposure times of 120 hours for films 1 to 5 and 24 hours for films 6 to 10. The tube current was not stabilised but averaged 15ma and the potential across the tube was kept at approximately 40KV.

The intensities were measured visually against an arbitrary scale of spots which varied linearly in intensity from x = 1 (just visible) to x = 20. The sets of values for each particular reflection, obtained from several films, were scaled together by a method described by Darlow (1960). Empirical scale factors for scaling from the $n-1^{th}$ film to the n^{th} film were calculated as $S_n = (\Sigma x_{n-1})/(\Sigma x_n)$, including only intensities measured on both films. All the values of S_n were averaged (except for S_5, which connects the two packs) with weights proportional to Σx_n.

Now, since the intensity, x_n, of a spot on the n^{th} film can be measured to an accuracy of $\pm$ 1, the intensity of this spot scaled up to the most heavily exposed film is given by $I_n = C_n(x_n \pm 1)$, where $C_n = S_1 . S_2 \ldots\ldots S_n$. A mean value for the intensity for several spots on adjacent films, each spot being weighted by the reciprocal of the accuracy of the measurement, is given by Iobs. $= (\Sigma_r x_n)/\Sigma_r 1/C_n)$. This latter expression is extremely easy to calculate.

Measurements were made of 45 independent reflections out of a maximum possible of 75. Each unobserved reflection was given an intensity of 0.5 of the faintest spot recorded.

No absorption correction was applied to the data. The maximum error due to absorption was less than 1% and, neither the accuracy of the data, nor that of the available absorption-correction computer programs, justified taking this step. However, the usual Lorentz and polarisation corrections were applied to the data and the values of $|F_o|$, the observed structure factor (on an arbitrary scale), were calculated.

An overall temperature factor (B) and a scale factor (K) were then found by the familiar method due to Wilson (1942). Wilson has shown, for a reasonably random atomic distribution, that:

$$\ln\left(\frac{|\bar{F}_o|^2}{\sum_j f_j^2}\right) = -\ln(K^2) - \frac{2B}{\lambda^2}\sin^2\theta \qquad (5.1)$$

where, $|\bar{F}_o|$ is the local average value of $|F_o|$ at a given value of sin θ, f_j is the scattering factor of the j^{th} atom

in the unit cell, and K is such that $|F_c| = K|F_o|$. From the straight-line graph of $\ln(|\bar{F}_o|^2/\Sigma_j f_j^2)$ against $\sin^2\theta$, B may be calculated from the gradient and K from the intercept. Figure 5.1b shows the Wilson plot derived from the hk0 data by the technique described by Buerger (1960). The reflections are divided into a number of ranges at equal intervals of $\sin^2\theta$. The average intensity in each range is then found, counting zero intensities and extinguished reflections as points present but having zero intensity. Similarly $\Sigma_j f_j^2$ is calculated for each reflection and the average found in each $\sin^2\theta$ range. Then, the average values of $\ln(\bar{F}_o^2/\Sigma_j f_j^2)$ can be found for each range, and also the average values of $\sin^2\theta$ within the ranges; and both quantities are then used as coordinates for the points on the Wilson plot. Values of 4.5 for B and 3.2 for K were obtained from the hk0 data.

5.4.2 SUMMARY OF THE PROGRESS OF THE REFINEMENT OF THE (001) PROJECTION

As was indicated above, the solution of structure of 2-diazoindane-1,3-dione was attempted initially without any prior knowledge of its conformation. However, it was found necessary to use some of the chemical information about the structure in order to proceed with the refinement. Two incorrect models were proposed before the final correct structure was deduced.

From the weighted reciprocal lattice of the hk0 data a benzene ring was identified in the structure and the

orientation of this ring could be determined. The benzene ring was placed in what was later found to be an incorrect position in the unit cell. Then, using the chemical information on the probable conformation only as a guide, the remainder of the atoms in the molecule were positioned one by one from the peaks on successive Fourier maps. This first model of the structure proved to have a substantially correct conformation but to be wrongly positioned in the unit cell. The reasons why such a reasonably convincing model could be derived and yet be incorrect are quite interesting and are discussed in section 5.4.5.

A second model was deduced merely by changing the position in the unit cell of the molecule derived for the first model. However, this model also proved to be incorrect as the positions of the two nitrogen atoms were wrong.

A final correct model, with the nitrogen atoms repositioned, was proposed. This model then refined rapidly using a minimum-residual program, which enabled certain rigid-body constraints to be applied to the molecule.

5.4.3 THE cmm FOURIER PROGRAM AND THE MINIMUM-RESIDUAL PROGRAM USED IN THE REFINEMENT.

Before discussing the refinement of the (001) projection in detail it is convenient to mention here two of the computer programs which were used extensively.

The first of these calculates structure factors and Fourier maps for the two-dimensional space group cmm and was adapted from one written by Miss A Sutherland of this

department. Structure factors are computed from atomic parameters fed into the program using the expression

$$F_c(h,k) = \Sigma_j f_j \; 8 \cos(2\pi hx) \cos(2\pi ky)$$

$$(h + k = 2n)$$

the summation being taken over all equivalent positions in the unit cell. The scattering factors are calculated from the expression

$$f_j = A_j \exp(- a_j x^2) + B_j \exp(- b_j x^2) + C_j$$

$$(x = \sin \theta/\lambda)$$

given by Forsyth and Wells (1959), who tabulate values of A_j, a_j, B_j, etc. for all atoms.

Fourier maps are computed from the expression

$$\rho(x,y) = \frac{1}{A}[F(00) + 4 \sum_{h=1}^{\infty} \sum_{k=1}^{\infty} KF_o(h,k) \cos(2\pi hx) \cos(2\pi ky)]$$

where K, the scaling factor, is calculated as

$$K = \Sigma |F_c| / \Sigma |F_o|$$

Difference maps ($F_o - F_c$) and maps from the calculated structure factor (F_c) may also be computed and output simultaneously with F_o maps. Reflections for which $K|F_o| > 3|F_c|$ are rejected from the computation, as having obviously indeterminate phases.

One interesting feature of the program is that reflections may be divided into two groups having values of sin θ less

than, or greater than, some specified value. Reflections in either the inner or the outer groups may be used alone to give Fourier and difference maps. Low-angle reflections are subject to extinction effects and may also be most in error, if the hydrogen atoms are not located; it is thus often useful to reject them in the final stages of a refinement. High-angle reflections are more sensitive to positional and temperature-factor changes and are often used on their own in the final refinement stages; but they may be rejected in the initial stages as their very sensitivity makes their phases difficult to determine.

One other useful feature enables the value of B, the overall temperature factor, to be recalculated as the refinement progresses. Values of $\Sigma|F_c| / \Sigma|F_o|$ for various ranges of $\sin^2\theta$ are output by the program. Now, since we may write

$$KF_o = F_c \exp(- B \sin^2\theta/\lambda^2)$$

then

$$\ln\left(\frac{\Sigma|F_c|}{\Sigma|F_o|}\right) = \ln(K) + \frac{B}{\lambda^2} \sin^2\theta$$

Thus, in a similar manner to the Wilson plot, values of B and K may be determined from a graph of $\ln(\Sigma|F_c| / \Sigma|F_o|)$ against $\sin^2\theta$.

The second program, used extensively in the refinement, was a minimum-residual refinement program (Bhuiya and Stanley, 1963). The method attempts to refine the structure merely by reducing the residual factor, $R = \Sigma(K|F_o| - |F_c|)/\Sigma|KF_o|$, which measures the agreement between the observed and

calculated structure factors. Each parameter of each atom is taken in turn and varied step by step over a discrete range of values. That value of the parameter, which gives the minimum value of R, is accepted as the refined estimate of the parameter. When all the parameters of all the atoms have been varied, the process is usually repeated, this time restricting a little more the range of variation of the parameters.

Several changes were incorporated into the standard minimum-residual refinement program. As in the Fourier program it was arranged that the reflections be divided into 'inner' and 'outer' groups. It was supposed that the inner reflections, when used alone, would allow a more rapid initial refinement of the structure. The outer reflections would be useful in the final stages for accurate positional-parameter refinement and the refinement of the temperature factors. In addition, certain rigid-body constraints were applied to the movement of the benzene ring as described below.

5.4.4 THE DERIVATION OF THE FIRST MODEL

As a first step towards the solution the weighted reciprocal lattice of the hk0 data was drawn (figure 5.3a). The black discs represent unitary structure factors, $|U(hk)| = |F_o(hk)| / \Sigma_j f_j$. The most striking feature of the weighted reciprocal lattice is the presence of the six strong peaks that are circled. These peaks are the characteristic indication of a benzene ring in the structure of the molecule, which is a distinct possibility since there are nine carbon

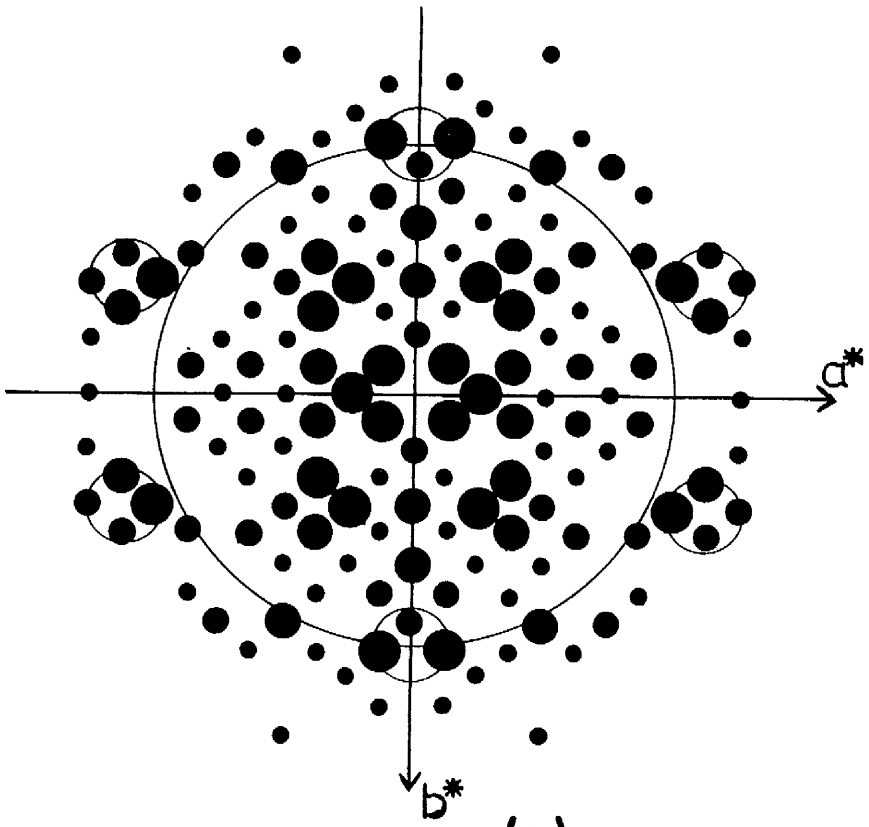

(a)

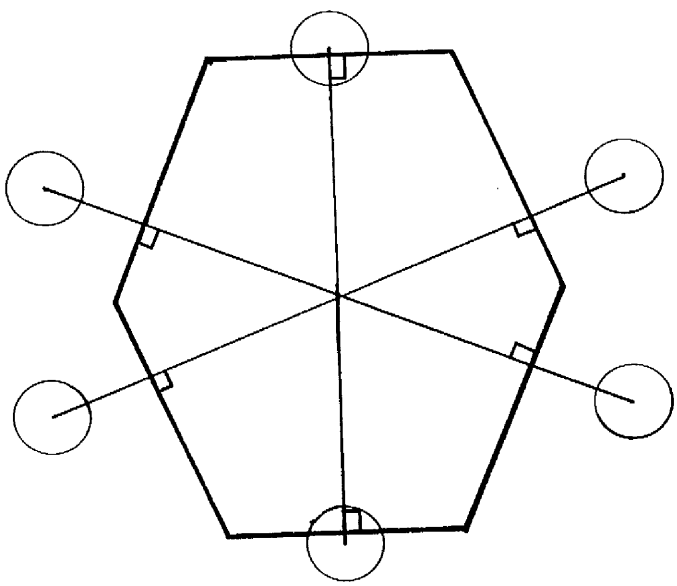

(b)

Fig.5.3

atoms in all. Assuming that there is in fact a benzene ring, it is evidently tilted about an axis parallel to the b axis. A benzene ring parallel to the hk0 plane would give six strong peaks all lying on the large circle in figure 5.3a; only two of the peaks lie on this circle (the benzene circle), and the remaining peaks are displaced from the circle and disposed symmetrically on either side of the b axis.

The angle of tilt of the benzene ring may be determined by a method given by Taylor and Lipson (1964). (The method can in fact be used to locate any general orientation of a benzene ring relative to a reciprocal-lattice plane). The centres of gravity of the six peaks in the reciprocal lattice are marked - A_1, A_2, A_3 ... A_6 - and these points are joined to the origin O (see figure 5.3b). Then points B_1, B_2 ... B_6 are marked on the lines OA_1 etc. such that OB_1 is inversely proportional to OA_1 and so on. Perpendiculars to the lines OA_1 etc. are drawn at B_1, B_2 ... B_6 and these then delineate the projected shape of the benzene ring. The method relies upon the inverse relation between the benzene-ring dimensions and the dimensions of its transform (see section 1.1).

Using Taylor and Lipson's construction, the tilt of the benzene ring about the b axis with respect the hk0 plane was calculated as 25°. Unfortunately, the optical transform of a benzene ring tilted in this way was found not to give a very good fit with the weighted reciprocal lattice; in fact, a slightly greater tilt seemed to be required. Transforms of benzene rings, tilted by various amounts in the range 25°-40°, were tried and the one having a tilt of 35° seemed to give the best fit. (It may be noted that in the fully refined structure the tilt was found to be 32° - a striking

example of the accuracy obtainable by optical methods).

It has already been noted that, since there are eight general positions in the unit cell and only four molecules, the molecules must be specially situated with respect to the symmetry elements. Six of the nine carbon atoms in the molecule are taken up by the benzene ring and obviously this ring must also be specially situated. The most likely position for the benzene ring is such that each 2-fold axis in the space group, parallel to b, lies in the plane of the ring and relates the two halves. All the benzene rings on the 2-fold **axes** are then related to each other by the centres of symmetry and the screw axes and are all in parallel orientation; the parallel orientation is confirmed by the clarity of the six peaks in the weighted reciprocal lattice. In addition, it can be concluded that at least one of the remaining carbon atoms must lie on the 2-fold axis.

In the (001) projection, symmetry cmm (figure 5.2b), a pair of 2-fold axes project on to the line x = 0 and another pair on to the line x = $\frac{1}{2}$. Therefore, on the line x = 0 in the projection there will be two benzene rings symmetrically orientated about this line and related to each other by the rotation diad at 0,0. Similarly two benzene rings are orientated about the line x = $\frac{1}{2}$ and related by the diad at $\frac{1}{2},\frac{1}{2}$.

The position of the benzene ring along the 2-fold axis now needed to be found; at first sight this would appear to be a simple one-parameter problem. The molecular-location method, described in section 5.4.6, was tried but gave no clear indication (probably owing to the difficulty in selecting the correct reflections).

However, two pieces of information suggested (unfortunately quite wrongly) a likely site for the benzene ring. First, pairs of benzene rings, such as those related by the diad at 0,0, would give regularly spaced fringes in the transform running perpendicular to the b-axis. Yet, the hk0 weighted reciprocal lattice does not show evidence of strong fringing. This would suggest that the two benzene rings are close together and probably overlapping. Secondly, the length of the c axis, 7.93Å, is such that the planes of these two benzene rings are 3.6Å apart. This distance is about the normal spacing (3.4Å) of aromatic rings, when stacked on top of each other; again, this suggests that the benzene rings are overlapping.

While this evidence, about the positions of the benzene rings, was by no means conclusive (and not even really circumstantial), in the absence of anything better it was decided to initially accept it as correct. A Fourier synthesis was calculated from the hk0 data using phases found from a trial model, in which the two benzene rings were exactly superimposed, and thus, situated such that the centre of the rings was at 0,0. Figure 5.4 shows the resulting electron-density map (one quarter of the total projected area of the unit cell). The peaks of the two superimposed benzene rings are returned strongly and other peaks appear (indicated by question marks) which could be possible atomic sites. The residual of 49% seemed quite promising, considering only half the atoms in the molecule have been included in the model, and a not unreasonable agreement between the structure factors was obtained.

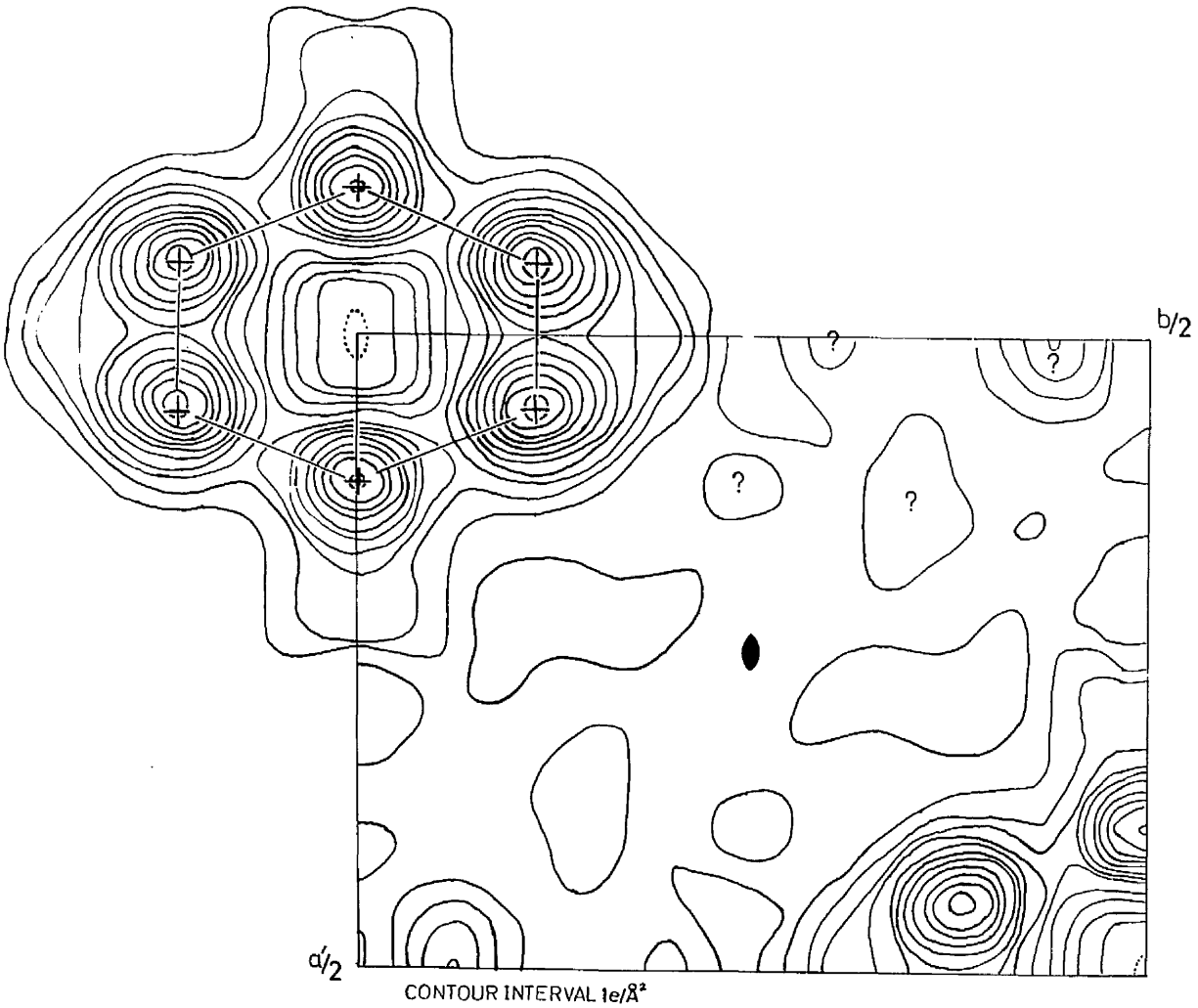

Fig. 5.4

Thus, although the model was based on somewhat insubstantial foundations, it seemed probable that it was near to the correct structure and was worth attempting to refine. Atoms were placed at the positions suggested by the Fourier map and agreement between the optical transform of this new model and the weighted reciprocal lattice was sought. However, it was found that the transform of the benzene ring so dominated the weighted reciprocal lattice, that the extra detail introduced into the optical transform, when other atoms were added to the model, appeared to be relatively insignificant.

At this point an impasse had been reached and, although a considerable amount of information had been gathered about the structure by purely physical methods, it was decided to seek guidance on the conformation of the molecule from the chemical evidence. This information on the chemical structure was given as

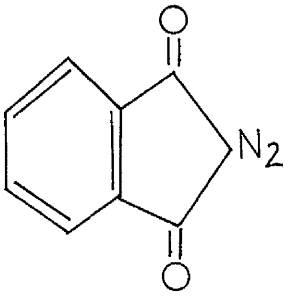

Owing to a misunderstanding, it was not realised that the two nitrogen atoms were supposed to be linked in a chain: C-N-N. The evidence from the Fourier maps appeared to suggest that the nitrogen atoms were linked thus:  and so this latter configuration was adopted, until it later became evident that it was wrong.

Using the information now available about the structure it was possible to assign atoms to certain peaks on the Fourier map of figure 5.4 and to calculate further Fourier

maps, putting additional atoms into the model, until all the atoms were located. A slight variation of this procedure was actually adopted. At each stage an optical transform was made of the trial structure and only those reflections, which corresponded to strong features on the optical transform, were used to calculate the Fourier maps; thus, only reflections with well-determined phases were used.

Figure 5.5 shows the Fourier map obtained when all the atoms were located. It should be noted that the benzene-ring peaks are of double height, since there are two such rings superimposed, belonging to the two molecules related by the diad at 0,0. Although this Fourier map appears to be not unreasonable in that the peaks appear in the correct places, are fairly well-rounded and of the right order of height, other evidence suggests that the model is quite wrong. First, although all the other atoms have been added, the residual, now 51, has slightly worsened from that obtained with the original model, in which only the benzene ring was located. Secondly, the agreement between the observed and calculated structure factors is not very good; for example, for one particular reflection (220) we have $F_c = 50$ and $F_o = 4$.

Attempts were made to refine this structure using optical methods, structure-factor graphs and error maps without success. While attempting to use structure-factor graphs to refine the structure, it was realised that only a drastic modification could correct the discrepancy in the 220 reflection, involving the movement of a number of atoms over considerable distances. Thus, it was realised correctly that the only way that the apparently reasonable Fourier map of figure 5.5, agreeing roughly with the known chemical

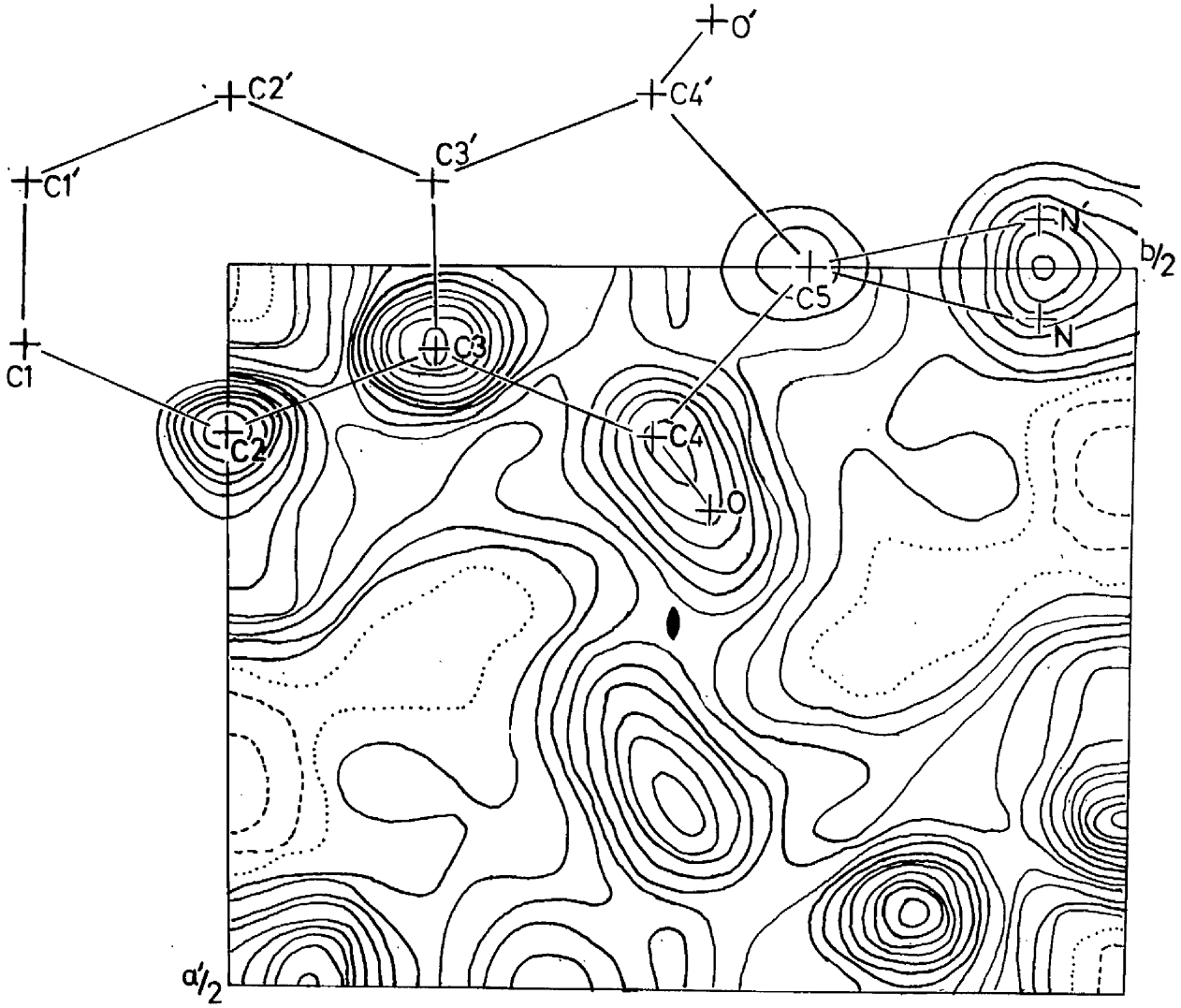

CONTOUR INTERVAL 1e/Å^2

Fig.5.5

structure, could be reconciled with the other indications that the structure was wrong was to assume that the model was basically correct but that it was in the wrong position in the unit cell.

5.4.5 AN EXPLANATION OF THE DERIVATION OF THE FIRST MODEL

An exactly similar situation was found by Pinnock et al. (1956) in a structure published by Klug (1950). The reasons advanced by Pinnock for Klug's result hold equally well in the present case.

If the shape and orientation of the molecule are substantially correct, then there will be good agreement for many of the large observed reflections but certain reflections will be seriously wrong. In terms of optical transforms the large reflections will correspond to intense areas of the transform of the individual molecule. However, the transform of the several molecules in the unit cell will be similar overall to the transform of the individual molecule but modulated by a fringe pattern. Reflections lying at the troughs of the fringes will be critically affected by small movements in the relative positions of the molecules; and these reflections will be ones showing the largest discrepancies, if the molecules are wrongly positioned in the unit cell.

Another way of approaching the situation is from the concepts of the Patterson function. In terms of a Patterson map the intermolecular vectors are wrongly identified but the intramolecular vectors are correct.

The existence of an apparently correct Fourier map is also explained by Pinnock as follows: "Fourier synthesis is not a good test of a proposed structure: it always tends to support the hypothesis on which it is based."

5.4.6 THE DERIVATION OF THE SECOND MODEL - THE MOLECULAR-LOCATION METHOD

Thus, assuming that the basic shape of the molecule is correct, it is now necessary to correctly position it in the unit cell; the molecular-location method of Taylor and Morley (1959) was used for this purpose. As indicated above certain reflections are critically dependent upon the relative positions of the molecules in the unit cell. Such reflections may be identified since they lie on strong regions of the optical transform of the single molecule but are themselves small in magnitude. In Taylor and Morley's molecular-location method such a reflection - h,k - is chosen and the quantity $||G(h,k)| - |F_o(h,k)||$ is evaluated at points covering the whole projected area of the unit cell. G(h,k) is the value of the calculated structure factor, $F_c(h,k)$, when the molecule is positioned at each of the points in the projected cell. (It is of course necessary to choose some reference point in the molecule, relative to which the molecule may be positioned over the unit cell). The correct position in the unit cell for the reference point in the molecule is marked by a dip in the contour map of the function $||G(h,k)| - |F_o(h,k)||$. If several such maps (using a number of different reflections) are superimposed, then the correct position should be unambiguously indicated.

For our purposes however it is not necessary to evaluate the function $||G(h,k)| - |F_o(h,k)||$ over all positions in the unit cell. Provided that the reference point is chosen such that it lies on the projection of 2-fold axis, it is only needed to evaluate the function along the line x = 0. A reference point at the centre of the benzene ring was therefore selected.

Figure 5.6a gives the results obtained, in graphical form, for Taylor and Morley's function evaluated along the x = 0 line, using only the 220 reflection. Two non-equivalent points appear to be indicated, which we shall refer to as A($y \approx -0.083$) and B($y \approx 0.167$). A further graph was plotted, figure 5.6b, in which several other reflections were used as well as 220, these were: 730, 370, 620 and 640. Troughs A and B are still present but B is now not so deep as A. There is also a further small trough, C, but this may be assumed to be spurious. Position B would appear to be less likely than A from the results of figure 5.6b. In fact, the optical transform produced, when position B was assumed, appeared quite wrong. The two molecules related by the diad at 0,0 were placed a good distance apart and the transform was heavily fringed. In addition, the residual remained high at position B and the agreement between F_o and F_c was poor.

However, at position A the two symmetry-related molecules overlap almost completely and their centres of gravity are quite close together. The heavy fringing present with position B was now found to be absent from the transform. Unfortunately, although the agreement between the structure factors was improved, the residual remained high (54).

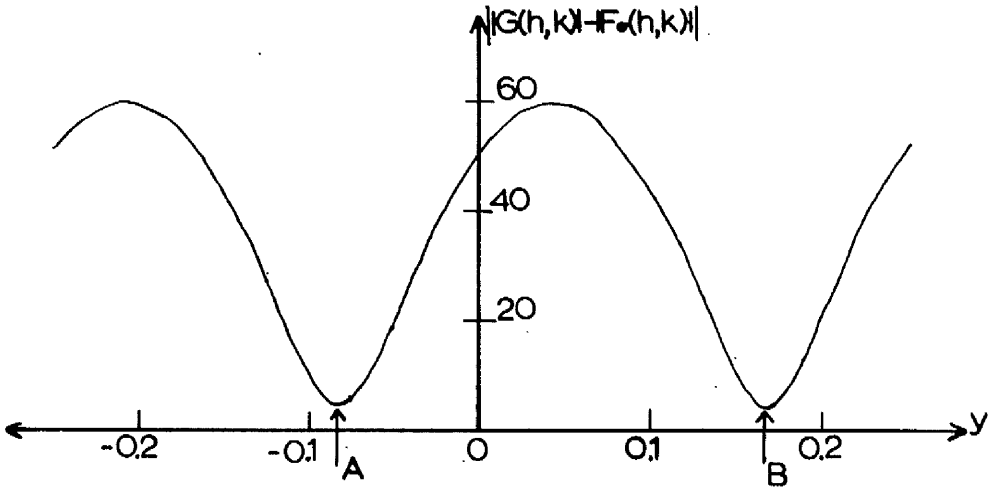
|G(h,k)|-|F₀(h,k)|
60
40
20
-0.2
-0.1
A
0
0.1
B
0.2
y

(a)

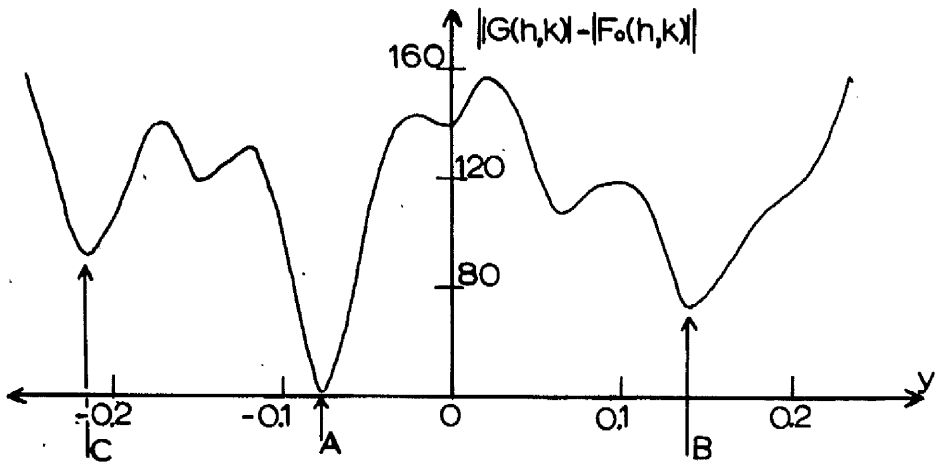
|G(h,k)|-|F₀(h,k)|
160
120
80
-0.2
C
-0.1
A
0
0.1
B
0.2
y

(b)

Fig.5.6

However, it was found that a small shift of the molecule from B to the point x = -0.107 produced a sharp drop in the residual to 39, and the Fourier map of fig. 5.7.

Accepting the molecule in its new situation, attempts were made to refine the structure. First, a difference map indicated that a shift was required in the position of the oxygen atom and a movement (deduced empirically) of 0.35Å in the positive a-axis direction decreased the residual from 39 to 36. A difference map then revealed the necessity for further movement of the oxygen atoms and also of the nitrogen atoms. Three cycles of minimum-residual refinement on these atoms alone produced some small adjustments in their position and a fall in the residual from 36 to 33.

Figure 5.8 shows the difference map corresponding to the structure at this point. The nitrogen atoms are in a sharp trough and it is evident that some movement in their position is required. The oxygen atoms are in a smaller hollow and also appear to need shifting. However, when an attempt was made to refine these atoms by the minimum-residual method, they refused to move. It was evident that, if in particular the nitrogen atom, which was obviously in an incorrect position according to the difference map, could not be refined, then there must be something wrong with the model.

5.4.7 THE REFINEMENT OF THE FINAL MODEL - THE PROGRAM 'BENZENETWIDDLE'

It was not difficult to trace the source of the error in the model. The most obviously incorrect feature on the difference map (figure 5.8) is in the region occupied by the

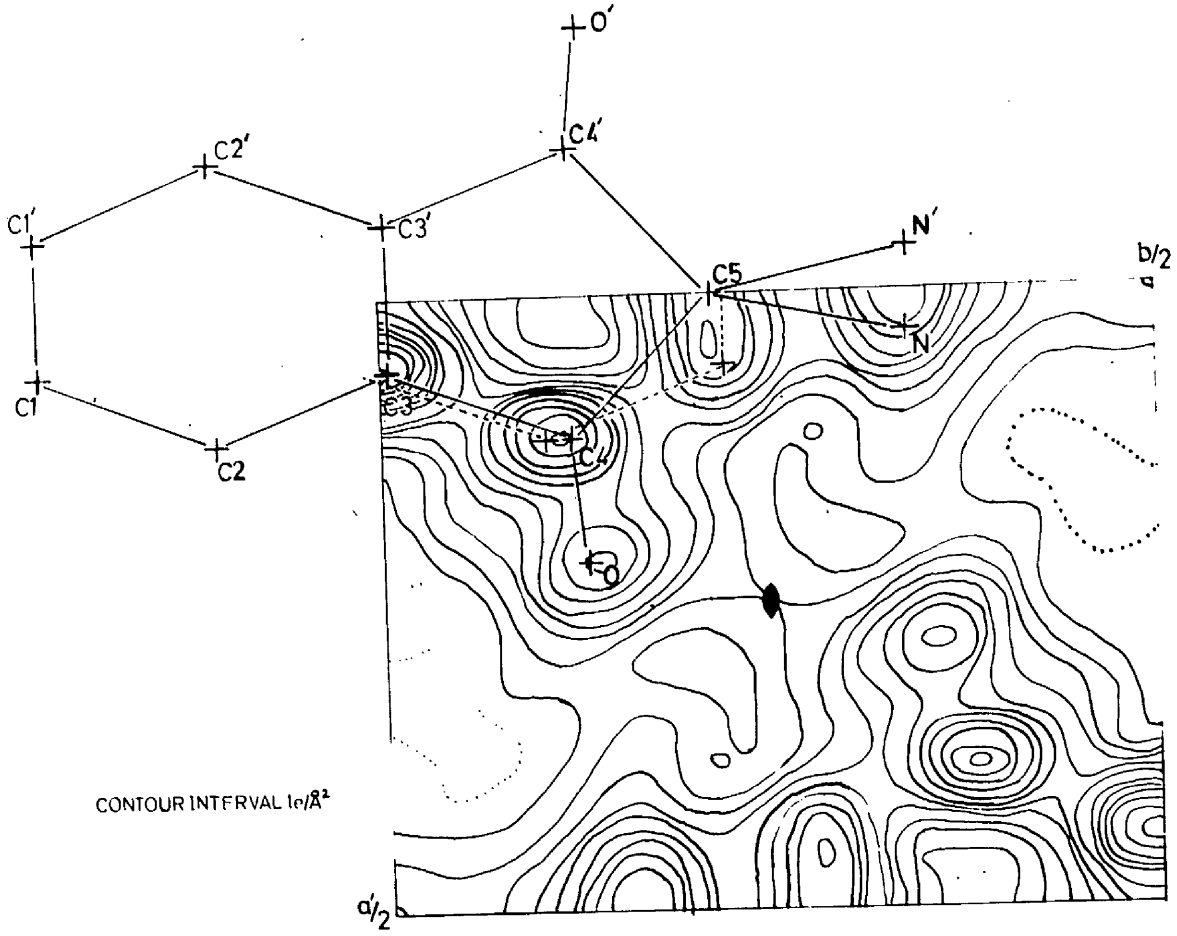

Fig.5.7

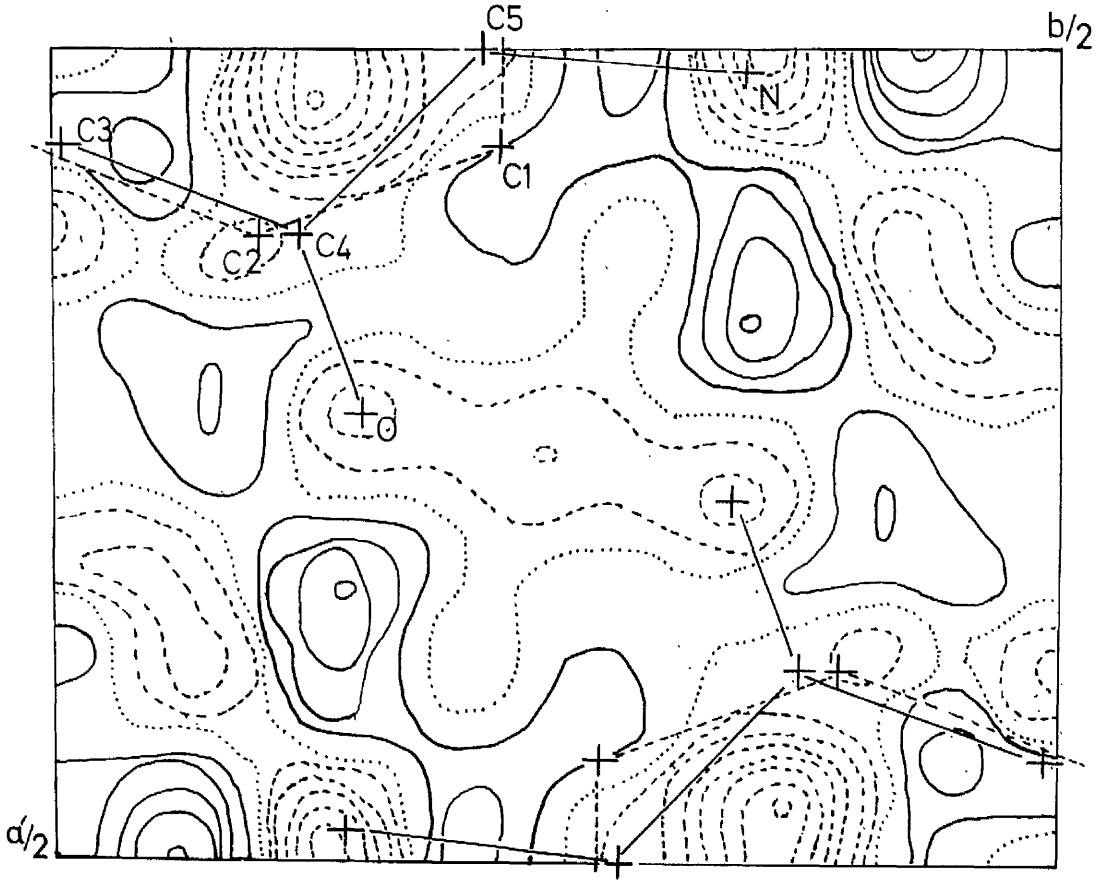

CONTOUR INTERVAL 0.5e/Å^2

Fig.5.8

nitrogen atoms. The difference map and the corresponding Fourier map showed that the electron density should be strongly elongated along the b-axis. This elongation suggested that instead of being situated on either side of the b-axis (C$\langle^{N}_{N}$) the nitrogen atoms were in fact positioned along the axis (C-N-N). The model was therefore altered to accord with this suggestion using bond lengths derived from the compound diazomethane

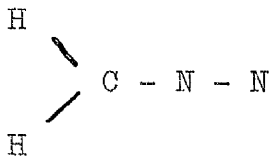

(Tables of Interatomic Distances, 1958), which contains the similar C-N-N grouping. The residual fell from 33 to 27.

Using the cmm Fourier program, a difference map and a Fourier map were calculated for this new model. The Fourier map returned peaks corresponding to the nitrogen atoms in their new positions but the difference map indicated that some adjustment was still necessary. A new temperature factor of 4.9 was calculated from the program data - up to this point the temperature factor of 4.5 derived from the Wilson plot had proved adequate.

Six cycles of minimum-residual refinement on the nitrogen atom positions alone, using inner reflections for which $\sin\theta/\lambda < 0.5$, brought the residual down from 27 to 24. Figure 5.9 shows the difference map corresponding to the structure at this point. This map now appeared to be quite reasonable, although shifts are indicated in several atoms including the nitrogens. The low value of the residual and the fairly good agreement between the structure factors indicated that the model was basically correct and

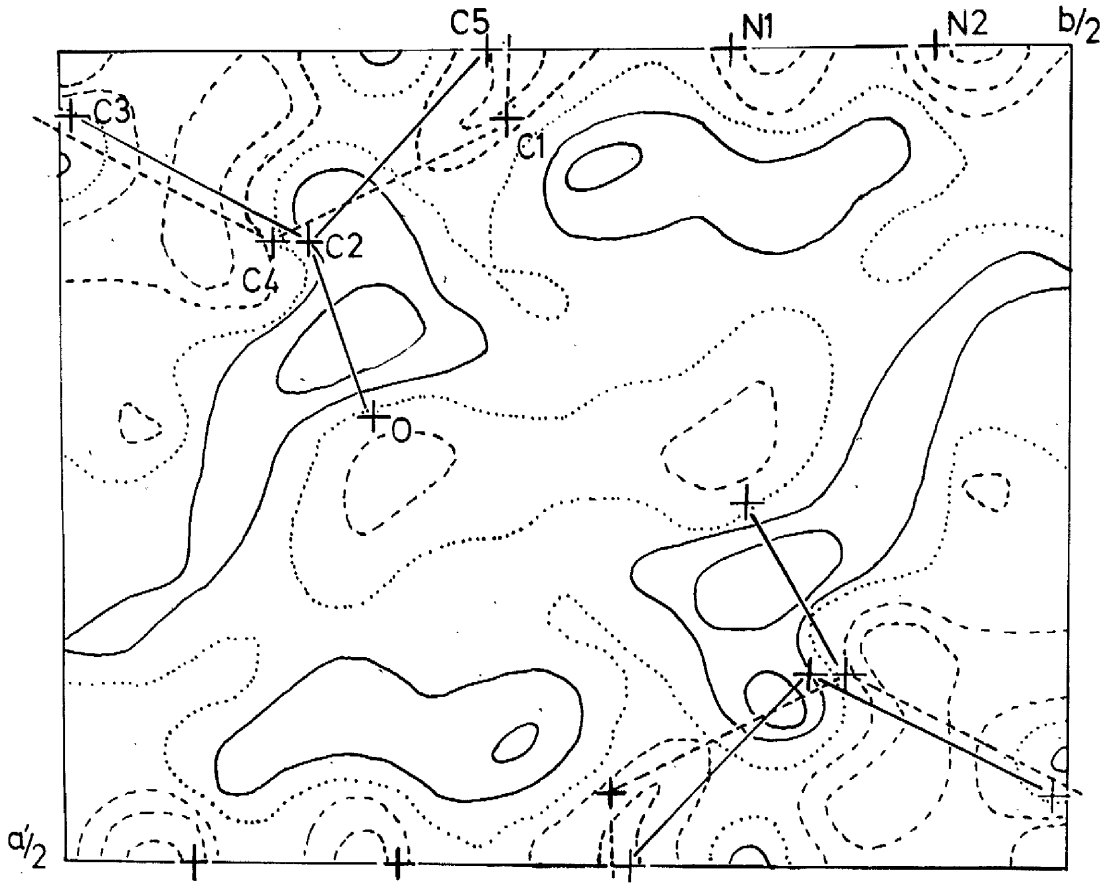

CONTOUR INTERVAL 0.5e/Å^2

Fig.5.9

should refine easily.

Acting upon a suggestion by Dr I G Edmunds it was decided to write a program for a minimum-residual refinement, which would treat the benzene ring as a rigid body - allowing it only to move along and rotate about the 2-fold axis keeping the relative position of the ring atoms fixed. This program, referred to as 'benzenetwiddle', allowed the atoms not contained within the benzene ring to refine normally. The minimum-residual refinement program often seems to work best if some such rigid-body constraints can be applied. At the suggestion of Miss A Sutherland the program was written such that a difference map was produced at the end of the refinement. This facility is extremely useful as it is possible to keep a check on the progress of the refinement - a difference map being a much more critical test of the results than the single numerical value of the residual.

The final refinement now proceeded relatively quickly in four separate stages.

Stage 1: Three cycles of the benzenetwiddle program were used, the benzene ring being allowed to move as a rigid body, as indicated above. The positional parameters of all the atoms not in the benzene ring were allowed to change freely (unless constrained by symmetry). The temperature factor for each atom was fixed at 4.9 and only reflections with $\sin\theta/\lambda < 0.5$ were used. The residual fell from 24 to 14, most of the change taking place in the first cycle!

Stage 2: A further three cycles of the benzene-twiddle program were used this time taking in all

reflections. Almost no change occured in the atomic parameters and the residual fell only by 0.1% The difference map output at the end of the refinement indicated an increase in the temperature factor for the nitrogen atom, N2, as the only big feature.

Stage 3: The benzenetwiddle program was now applied again, this time using only reflections for which $\sin \theta/\lambda > 0.25$. The isotropic temperature factors of all the atoms were allowed to vary independently. The residual for the outer reflections fell from 19.8 to 14.5 in three cycles and the total residual fell to 12.6 (the structure factors being scaled on the outer reflections only).

Stage 4: For this final stage of the refinement the benzene-ring atoms were now allowed to move freely, so that all the positional parameters and all the isotropic temperature factors of the atoms were varied independently. In six cycles of minimum-residual refinement only small changes of parameters were observed and the outer residual fell from 14.5 to 13.8 and the total residual from 12.6 to 12.3 At this point the refinement was stopped.

5.4.8 A DISCUSSION OF THE FINAL STRUCTURE OF THE (001) PROJECTION

The refinement was now essentially complete. The movements of the parameters were quite small and probably not significant. The agreement in the structure-factor

data was quite good apart from 200 ($|F_o|$ = 69.3, $|F_c|$ = 82.5) and extinction could easily cause this discrepancy.

Figure 5.10 shows the final difference map, in which only outer reflections, sin $\theta/\lambda > 0.25$, were included. The maximum height of the detail in the map is 0.6e/Å^2 and no atoms appear to lie on steep slopes which would indicate positional changes. One interesting feature in the 'butterfly' shape in the contours surrounding the nitrogen atom N2, which indicates an anisotropic temperature factor for this atom corresponding to a strong vibration perpendicular to the b-axis. This conclusion is confirmed by the final refinement of all the data in the next chapter. The positions of C4 (and C4') and O (and O') indicate that they lie close to the plane of the benzene ring; thus, the whole molecule is essentially planar. This conclusion was later found to be in agreement with the chemical data and was also confirmed by the final refinement.

The coordinates of the atoms in the molecule derived from the (001) projection are given in Table 5.1 below.

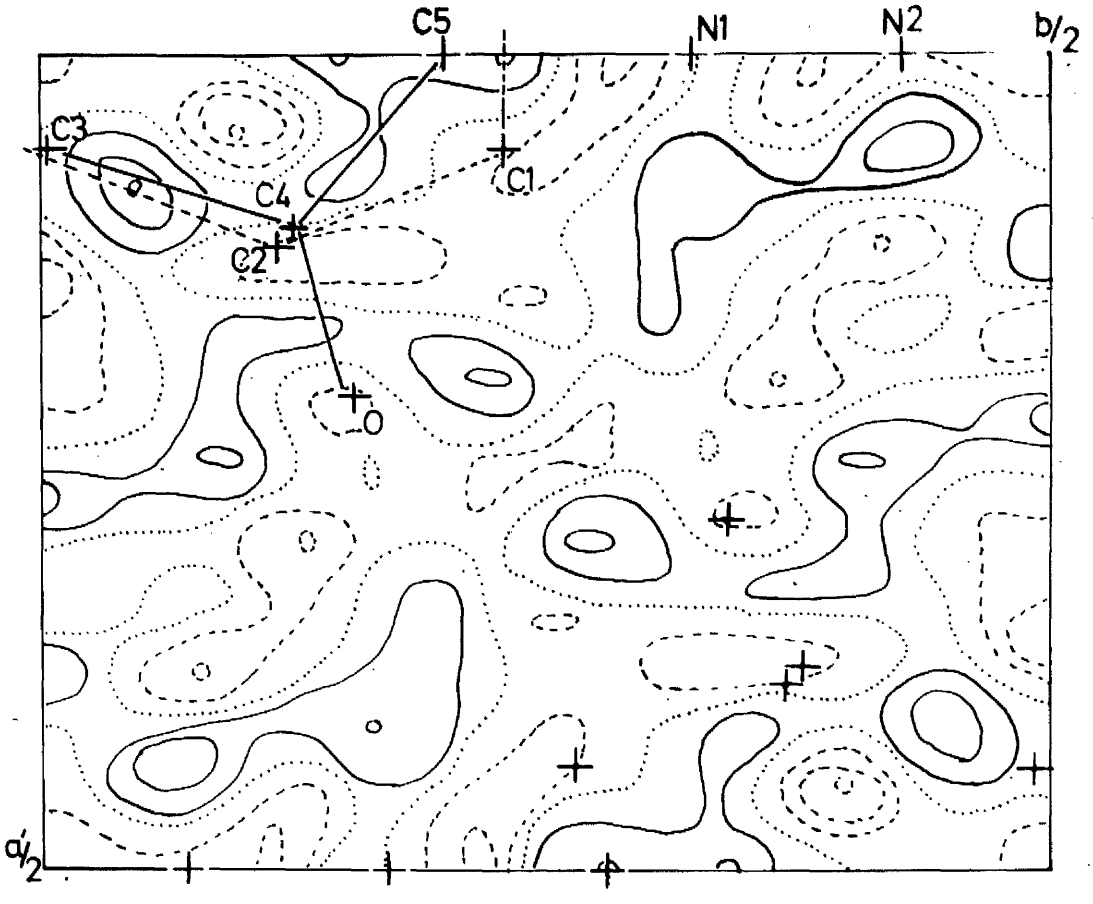

CONTOUR INTERVAL 0.2e/Å^2

Fig.5.10

TABLE 5.1

COORDINATES OF THE ATOMS IN THE (001) PROJECTION

	x	y	B
C1(C1^1)	±0.0603	-0.2341	4.52
C2(C2^1)	±0.1207	-0.1185	4.75
C3(C3^1)	±0.0603	-0.0085	3.78
C4(C4^1)	±0.1108	0.1283	4.19
C5	0	0.2022	5.05
O(O^1)	±0.2135	0.1566	4.83
N1	0	0.3253	5.69
N2	0	0.4316	6.58

CHAPTER 6

THE COMPLETION OF THE REFINEMENT OF THE STRUCTURE OF 2-DIAZOINDANE-1,3-DIONE

6.1 INTRODUCTION

The solution of the (001) projection, described in the previous chapter, enabled the x and y coordinates of all the atoms to be determined. It now remained to find the missing z parameter in order to specify the complete three-dimensional structure.

As has been noted in chapter 5, the molecule appeared to be planar from an examination of the (001) projection; and it will be shown later that the molecule is in fact very nearly planar. It is indicated below that approximate values of the z parameters can be deduced from the x parameters knowing a rough value for the orientation of the molecular plane. Also, it will be shown that this approximate orientation of the molecular plane can be found from the (001) projection of the benzene ring and a qualitative inspection of the h0l weighted reciprocal lattice.

Thus, it was possible to postulate a model for the (100) projection of the structure. The (100) projection was refined (with some difficulty owing to the small number of measured reflections) starting from this model. A residual of 15 and a not unreasonable difference map was

obtained for this projection. However, the y coordinates of the (100) projection differed by as much as 0.1Å from those in the (001) projection.

It was realised that good values for all the parameters would be obtained only if all the available data was used together in the refinement. Accordingly, all the reflections, from the three projections (001), (010) and (100), that had been measured up to this point, were used in a least-squares refinement. However, it was found that the x parameters of two atoms had approximately the same value and appeared to be strongly correlated. These two parameters would not refine at the same speed as all the other parameters and each had a high standard deviation. The hkl data were added to the least squares refinement and this appeared to have the effect of 'unlocking' this correlation.

The least-squares refinement now proceeded quickly to a residual of 18.6 when movements of the atoms ceased. Hydrogen atoms and anisotropic temperature factors were introduced and further refinement to a residual of 11.9 was obtained. The movements in the parameters at this point were much less than the standard deviation in the parameters and so the refinement was stopped. The difference maps, corresponding to the cross sections of the electron density taken through the atomic positions, also revealed no outstanding features requiring explanation. The atomic coordinates obtained were taken to be those of the final structure.

6.2 THE DEDUCTION OF THE ORIENTATION OF THE MOLECULAR PLANE FROM THE hOl DATA

A small crystal, approximately cubic in shape and of 0.16mm side, was cut from a larger one. The crystal was mounted on a Weissenberg camera and the hOl reflections were photographed using Ni-filtered $CuK\alpha$ radiation. The intensities were recorded on two packs of five films (exposures 24 hours and 120 hours) and they were measured and corrected in the same manner as the hkO data (see section 5.4.1). A total of 19 reflections out of a total possible of 51 were measured. Unobserved reflections were given intensity values of one half the weakest reflection recorded.

No Wilson plot was made of the data, because the statistical inaccuracy in the small number of reflections would have given poor results. However, the unitaries corresponding to the observed reflections were calculated and a weighted reciprocal lattice was drawn - figure 6.1.

It was shown in chapter 5 that the benzene rings in each molecule in the unit cell are all similarly orientated - the planes of the rings lying parallel to the b axis. It is possible to partly deduce the orientation of the benzene ring from the final structure of the (001) projection, if the reasonable assumption is made that the bond lengths of benzene are all 1.4Å. The projected length of the $C1C1^1$ bond is 1.16Å, which indicates that this bond is orientated at 33.7° to the hkO reciprocal-lattice plane. The $C2C2^1$ distance gives an almost identical result and thus the plane of the benzene ring must also be orientated at 33.7° to the hkO reciprocal-lattice plane. If the molecule is assumed to be planar, as has been indicated in chapter 5,

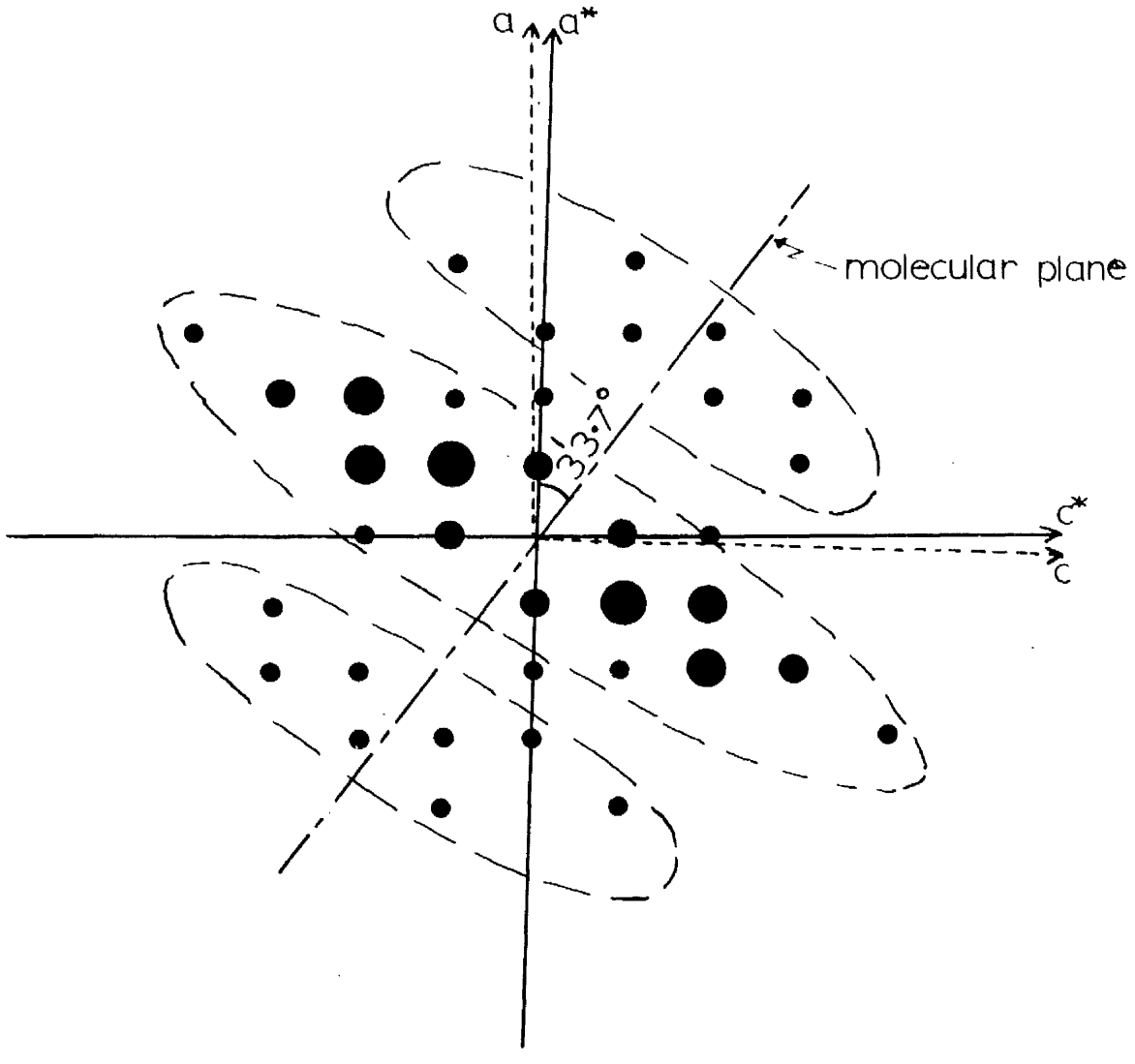

Fig.6.1

then all the atoms of the molecule must lie in the plane of the benzene ring.

It was now necessary to determine the absolute orientation of the molecular plane to the a and c axes and this can be done from an inspection of the h0l weighted reciprocal lattice. Looking down the b axis along the plane of the molecule the atoms will appear arranged in an irregular row. The optical transform of such a row of atoms is a series of streaks perpendicular to the row direction. If, therefore, such a series of streaks can be located in the h0l weighted reciprocal lattice, then the row direction and hence the orientation of the molecular plane can be fixed.

Figure 6.1 shows the presence of these streaks quite clearly—indicated by the dashed lines. The direction of the atomic row, also indicated on figure 6.1, is such that it cuts the obtuse (β) angle between the a and c axes.

No attempt was made to refine the (010) projection as the severe overlapping of the atoms and the small number of measurable reflections would have made this difficult.

6.3 THE SOLUTION OF THE (100) PROJECTION

6.3.1 THE DERIVATION OF A MODEL FOR THE PROJECTION AND THE COLLECTION OF THE DATA

The orientation of the plane of the molecule of 2-diazoindane-1,3-dione was found, as indicated above, to be at 33.7° to the hk0 plane. The h0l weighted reciprocal lattice then showed that the plane cuts the angle β between the positive a and c-axis directions. Simple geometry then

shows that the fractional z coordinates of the atoms are given by

$$z = \frac{a}{c} \frac{\sin(92.1 - 56.3)x}{\sin 56.3}$$

the angle 56.3° being the angle which the molecular plane makes with the c axis. Thus, the z parameters of the atoms in the molecule can be derived from the x parameters, using the equation above; and a trial model for the (100) projection can be found from these z coordinates and the y coordinates of the (001) projection.

A crystal, 0.204mm (needle axis) by 0.083mm by 0.074mm (rectangular cross section), was selected. The 0kl X-ray reflections were photographed in the same manner as the hk0 reflections (see section 5.4.1) using two packs of five films (200 hours and 24 hours exposure). The data were measured and corrected, again as in section 5.4.1, except that an absorption correction was also applied. Unobserved reflections were again given a value of half that of the weakest reflection recorded.

The computer program, that was used for the absorption correction, was written by Miss A Sutherland of this department. This program treats the data obtained by photographing zero layers of the reciprocal lattice by normal-beam, rotating-crystal methods. The cross section of the crystal perpendicular to the rotation axis must first be measured; if the cross section is not uniform then some average area must be considered. This cross-sectional area is then sampled by a lattice consisting typically of several hundred points. The reflections are considered in turn; and for each

reflection the incoming and diffracted beams are represented by the bundle of rays, which are scattered at the points of the sampling lattice. The path lengths within the crystal for each of these rays and hence the absorption factors of the rays are then determined. The absorption correction for the particular reflection under consideration is then taken as the average of the absorption factors for all the rays. All the remaining reflections are treated similarly.

The difference between the maximum and minimum absorption corrections to the intensities was about 10%, corresponding to a difference of about 3% in the structure factors.

Only a small number of reflections (29) could be measured despite the extremely long exposures used. The comparative shortness of the axes, which meant that there were few reflections (61) to be measured anyway, and the disintegration of the crystal during exposure, with a consequent loss in scattered intensity, probably account for the smallness of this number. A Wilson plot (see section 5.4.1) indicated an overall temperature factor of 3.9 for the projection and a scale factor of 4.3 for the data.

6.3.2 THE REFINEMENT OF THE (100) PROJECTION

A model of the (100) projection structure was found by calculating the y and z coordinates as indicated above. These trial parameters were then used to calculate the difference map of figure 6.2, on which the structure is outlined. It will be noted that the origin of the y coordinates is shifted one quarter of a unit cell translation from the origin used in the (001) projection, which is also

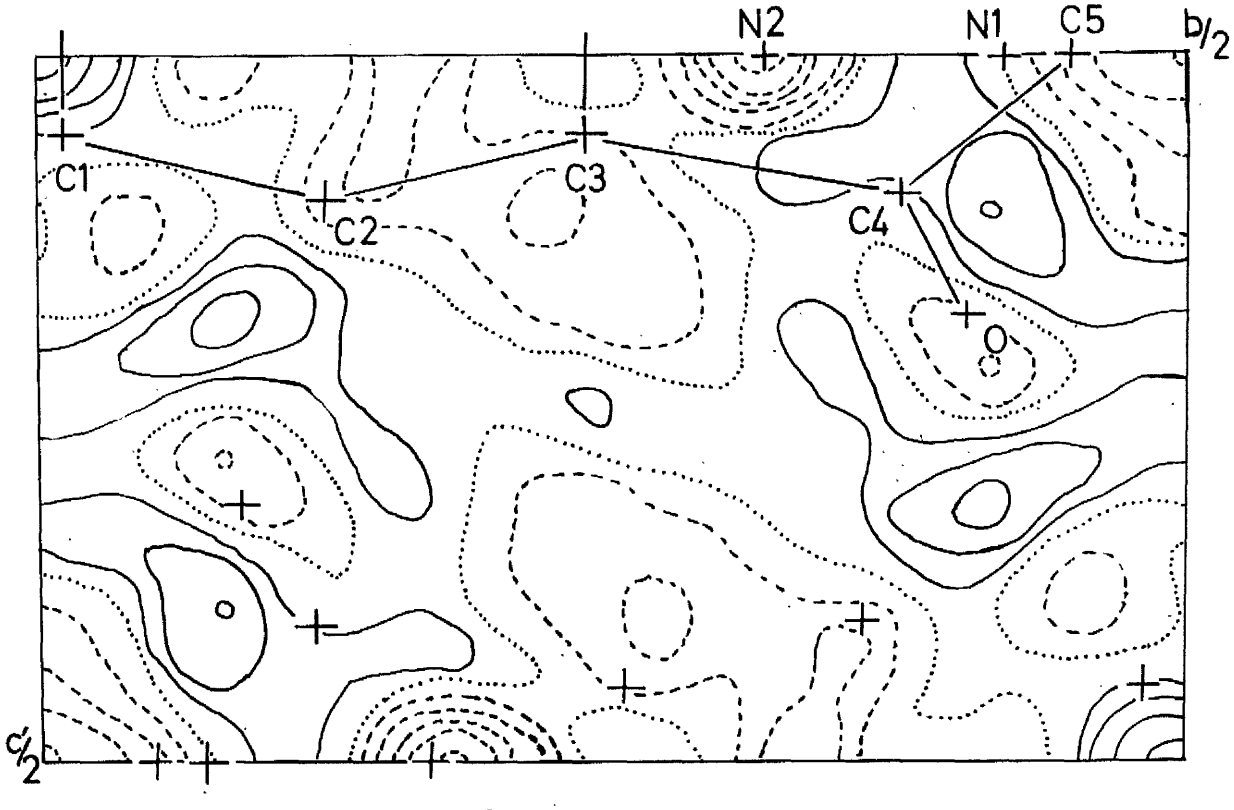

CONTOUR INTERVAL 0·5e/Å^2

Fig. 6.2

that of the three-dimensional cell. The atoms of the benzene ring are no longer overlapped in this projection by atoms of a symmetry-related molecule and in theory their positions should be easier to determine. However, the atoms C5 and N1 are overlapped by the atoms of a symmetry-related molecule in this projection.

The (100) projection proved to be extremely difficult to refine mainly owing to the small number of reflections. The parameters of different atoms often appeared to be strongly correlated, so that when one atom was moved this seemed to cause another atom to appear to be in an incorrect position.

If one isotropic temperature factor is allowed to each atom, then there are 21 independent parameters to be determined from the projection. Since there are only 29 measured reflections, the parameters are only slightly outnumbered by the reflections. In normal X-ray structure determinations the ratio of reflections to parameters is usually much greater. In theory, since the y parameters were known from the (001) projection, only 17 z and B parameters need be determined. In practice, it was found necessary to alter the y parameters in order to get the best possible fit to the data.

The refinement was carried out using the benzenetwiddle program, described in section 5.4.7, and the more-usual minimum-residual program. Difference maps proved useful at one point, where the expression given by Buerger (1960):-

$$\epsilon = \frac{\frac{d(\rho_o - \rho_c)}{dr}}{2\rho_o(0)p}$$

was used to calculate shifts in atomic positions. The factor ϵ is the amount the atom should move in the direction r, in which the slope, $d(\rho_o - \rho_c)/dr$, of the difference map is the steepest. The quantity $\rho_o(0)$ is the peak electron density, which may be estimated from the corresponding Fourier map, and p is a constant which was calculated by substitution in the expression (also given by Buerger, 1960):

$$\rho_o(0) = z(\frac{p}{\pi})^{\frac{3}{2}}$$

The model calculated for the (100) projection gave a residual of 29.3 and a temperature factor of 4.9. The difference map of figure 6.2 indicated that adjustments were necessary to the positions of the C5, N1 and N2 atoms in particular.

The first stage of the refinement was an attempt to achieve the same rapid progress towards the solution that was obtained for the final model of the (001) projection. The minimum-residual program was therefore used with low-angle reflections ($\sin\theta/\lambda < 0.52$). The z parameters of all the atoms were first refined alone, using the benzene-twiddle program to vary the tilt of the benzene ring. Some refinement occurred mainly in the oxygen atom whose z coordinates changed by 0.06Å.

The atoms C1, N1 and N2 were now refined by the minimum-residual program. The initial attempt was unsuccessful, producing unlikely nitrogen-nitrogen bond

lengths (less than 1Å), probably owing to the overlap about the C5 and N1 atomic sites. After several attempts it was found that the difference map could be smoothed in the region of the C5, N1 and N2 atoms, using the minimum-residual approach, if this group of atoms was moved as a whole along the 2-fold axis, with the C5 atom being shifted twice as fast as the N1 and N2 atoms. Shifts of 0.06Å for the nitrogen atoms and 0.12Å for the carbon atom were recorded. Some refinement of the y parameter of the benzene ring then seemed to be required by the difference map and a shift of 0.06Å was produced by the benzenetwiddle program.

Fourier and difference maps were calculated at this point using the cmm Fourier program. The difference map had improved considerably from that for the original model, although shifts still seemed to be required by the C5, N1 and N2 atoms. The residual had also fallen from 29.3 for the original model to 24.7, and a new temperature factor of 5.4 was calculated.

Further attempts to refine the molecule using inner reflections and the minimum-residual program now proved abortive. Some shifts in atomic position were recorded but none were greater than 0.04Å and the residual fell hardly at all.

The structure refinement now seemed to be 'sticking' and a second stage was reached when all the reflections were used in conjunction with the minimum-residual approach. At first the benzene ring still continued to be treated as a rigid body, using the benzenetwiddle minimum-residual program, but only quite small shifts ($\approx$ 0.02Å) could be obtained in any of the atomic parameters and the residual

fell by only 1% in three cycles.

Thus the benzene ring atoms were now released from the rigid-body constraints and allowed to move freely. Six cycles of minimum-residual refinement brought about a fall of approximately 3% in the residual and shifts in a number of atomic parameters of up to 0.04Å per cycle. The total shifts however were quite reasonable the largest being those in the z parameters of the C4 and C3 atoms (≈ 0.1Å).

At this point the difference map was inspected and it was found that the most incorrect feature was in the region of the atom N2, which was on the side of deep (1.8e/Å^2) 'hole '. The third stage of the refinement was an attempt to refine the parameters of this nitrogen atom by using difference maps, since the minimum-residual approach was obviously not working for this atom. A total shift of 0.096Å in the y coordinate was calculated from two successive difference maps. After these shifts had been made, the difference map showed that the nitrogen atom was at the bottom of a somewhat shallower hole than before. This feature was corrected by raising the isotropic temperature factor for the nitrogen atom to 7, which was approximately its value at the end of the refinement of the (001) projection.

Fourier maps and difference maps were calculated at this point using the cmm Fourier program. Although the residual was found to be as high as 20%, there were now no outstanding features on the difference map. It now seemed that the final stages of the refinement had been reached but that the residual would not fall as low as that for the (001) projection, probably owing to the poorer quality of the data.

In this final stage of the refinement some small adjustments were made to the atomic parameters by the minimum-residual program, using all the reflections in the calculations. Initially, the positional parameters of all the atoms were allowed to vary freely. After three cycles of refinement the residual had dropped by 2% but a number of atoms, particularly C1 and C2, appeared to have moved in incorrect directions, as judged from the difference map. In addition, the agreement between the structure factors of the reflections 004, 006 and 008 was not very good indicating that the z parameters of certain atoms must be incorrect. Since the difference map was considered to be a more stringent test of the refinement than the results from the minimum-residual program, those atoms, that appeared to be in incorrect positions, were removed to their original sites. This effected some improvement in the 004 and 006 reflections.

A further ten cycles of minimum residual refinement were tried this time allowing the isotropic temperature factors for each atom to vary independently. The residual fell by 3% to 16.7%. However, the atom C1 was moved in a direction opposite to that indicated by the difference map. A further five cycles of minimum-residual refinement were tried, starting from the atomic positions reached before the previous ten cycles of refinement, this time keeping the C1 atom fixed in position. The residual fell to 15.5. The C1 atom was now released and a further five cycles of refinement were attempted. A residual of 15.2 was reached after some quite small changes in the atomic parameters.

At this point the refinement of the (100) projection was stopped.

6.3.3 A DISCUSSION OF THE FINAL STRUCTURE OF THE (100) PROJECTION

The difference map of figure 6.3 shows the state of the structure of the (100) projection at the end of the refinement. Although some shifts in atomic positions are indicated, there are no major features requiring correction. The maximum difference density on the map is 1.0e/Å^2. Although a residual somewhat higher (15.2) than that of the (001) projection was obtained, the minimum-residual program was shifting the atomic parameters only by small amounts, which were probably not significant. A reasonable agreement between the structure factors was obtained. Thus, the (100) projection may be considered to be as fully refined as the available data made possible.

The final atomic parameters are given in table 6.1 with the y coordinates shifted $\frac{1}{4}$ of a unit cell translation in order to bring them into line with the coordinates on the unit cell axes. The y coordinates obtained from the (001) projection are also given for comparison. Differences of up to 0.1Å are obtained between the y coordinates of the (001) and (100) projections. Thus, the uncertainties in the atomic positions must also be about 0.1Å, which is quite a high value for modern structure determinations.

Therefore, although the (001) and (100) projections appeared to be as fully refined as possible, the accuracy was low. This situation was due to the comparatively small

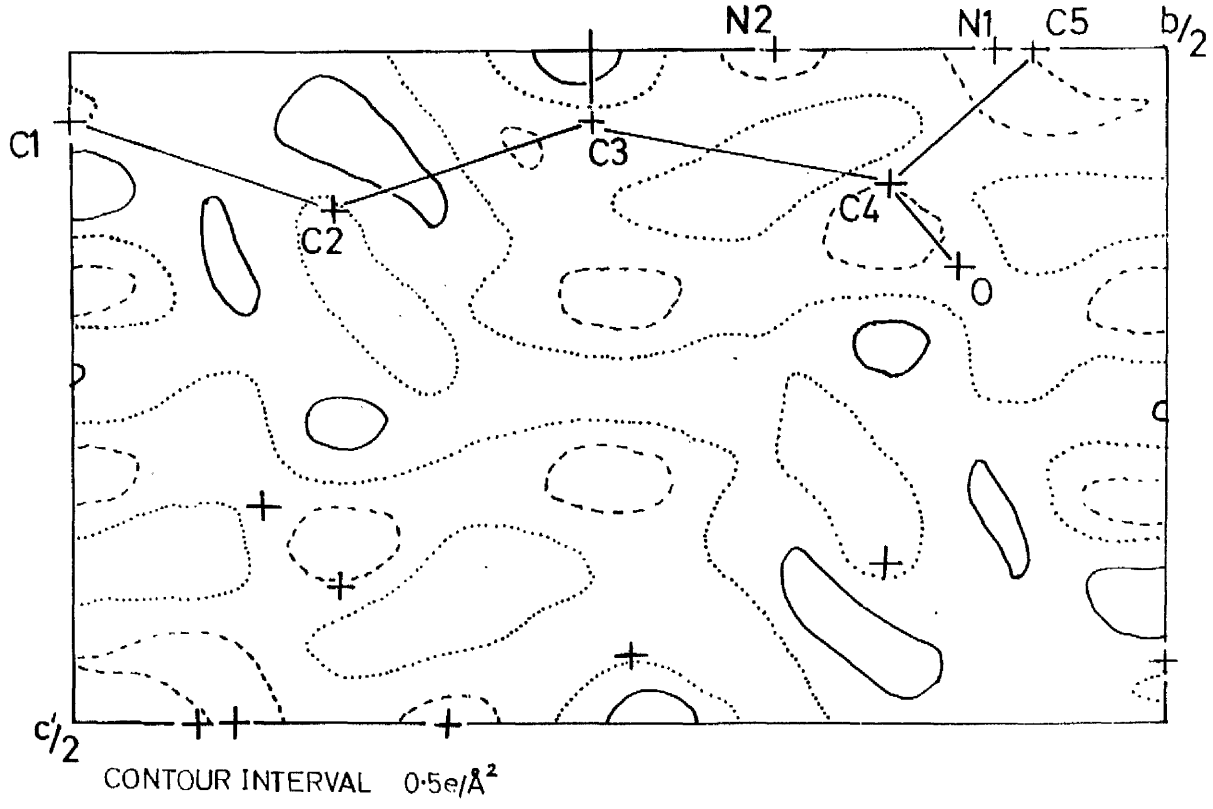

Fig.6.3

number of reflections, particularly in the (100) projection, that could be measured. It seemed at this point that better results would be obtained if all the measured data (including the h0l reflections) could be used simultaneously to refine the atomic parameters. Accordingly, the least-squares refinement, described below, was used for this purpose.

TABLE 6.1

COORDINATES OF THE ATOMS IN THE (100) PROJECTION

	y_{0kl}	y_{hk0}	z	
C1($C1^1$)	-0.2495	(-0.2341)	0.0459	5.32
C2($C2^1$)	-0.1268	(-0.1185)	0.1168	4.43
C3($C3^1$)	-0.0075	(-0.0085)	0.0560	5.38
C4($C4^1$)	0.1289	(0.1283)	0.1033	5.42
C5	0.1903	(0.2022)	0	3.87
O(O^1)	0.1589	(0.1566)	0.1628	6.30
N1	0.3227	(0.3253)	0	5.84
N2	0.4243	(0.4316)	0	8.44

6.4 THE LEAST-SQUARES REFINEMENT OF THE STRUCTURE

6.4.1 SHEARING'S LEAST-SQUARES PROGRAM

The least-squares method of refinement seeks to minimise some function of the difference between the observed and calculated structure factors with respect to the parameters of the molecular structure. The most commonly used function is

$$R = \sum_{hkl} W(|F_o| - |F_c|)^2 \qquad (6.1)$$

where W(hkl) is a weighting factor for the hkl reflection. If p_1, p_2, ... p_n are the n parameters, occuring in $|F_c|$, whose values are to be determined for R to be a minimum then:

$$\frac{\partial R}{\partial p_j} = 0 \quad (j = 1, \ldots n) \tag{6.2}$$

If $|F_c|$ were a linear function of p_1, p_2 ... p_n it would be possible, in the usual manner of the least-squares method, to derive from equations 6.2 and 6.1 a set of n simultaneous equations, the normal equations, whose solution would give the best values of p_1, p_2 etc. Unfortunately, most crystallographic parameters are not linearly related to the $|F_c|$ values; but, if the relationships are assumed to be linear over small ranges of the parameters, approximate corrections to the parameters, ϵ_1 ... ϵ_n, may be calculated from a set of a normal equations that may be written:

$$\sum_{i=1}^{n} \{ \sum_{hkl} W \frac{\partial |F_c|}{\partial p_i} \frac{\partial |F_c|}{\partial p_j} \} \epsilon_i = \sum_{hkl} W\Delta \frac{\partial |F_c|}{\partial p_j} \tag{6.3}$$

where $\Delta = |F_o| - |F_c|$.

The normal equations may be conveniently expressed in matrix notation as:

$$\sum_i a_{ij} \epsilon_i = b_j \tag{6.4}$$

where

$$a_{ij} = \sum_{hkl} W \frac{\partial |F_c|}{\partial p_i} \frac{\partial |F_c|}{\partial p_j} \tag{6.5}$$

and

$$b_j = \sum_{hkl} W\Delta \frac{\partial |F_c|}{\partial p_j} \tag{6.6}$$

The least-squares computer program used for this work was written by Dr G Shearing, formerly of the Mathematics Department of the University of Manchester. It is only necessary to give a brief outline of the program here but a comprehensive description is given in the manual for the program, obtainable from the Atlas Computing Laboratory of the University of Manchester.

Shearing's program will refine the following parameters:

(i) one or more scalefactors for the data,
(ii) the atomic coordinates,
(iii) an overall temperature factor,
(iv) the individual isotropic or anisotropic temperature factors of the atoms,
(v) the multiplicities of the atoms.

In addition the program deals with:-

(i) any type of symmetry,
(ii) anomalous scattering factors,
(iii) atoms in special positions,
(iv) any combination of isotropic or anisotropic temperature factors.

Atomic scattering factors are calculated by linear interpolation from a table of values fed in with the data. The actual scattering data used here were taken from the results of Hanson et. al. (1964).

The weighting factor W for each reflection may be fed in with the data or the user may add a routine to the program in order to calculate W from some functional relation. If

the estimated standard deviation of each $|F(hkl)|$ due to random errors is $\sigma(hkl)$, then the value of W which gives the lowest estimated standard deviation in the derived parameters is:

$$W = 1/\sigma^2(hkl)$$

Often however $\sigma(hkl)$ is unknown and some function of F(hkl) is used to calculate weights for the data. The weighting function used here was one suggested by Rollett (1965)

$$W = 1/(a + |F_o| + c|F_o|^2) \qquad (6.7)$$

The constants a and c are approximately $2F_{min}$ and $2/F_{max}$ respectively, where F_{min} is the smallest observed reflection and F_{max} the largest. Shearing's program outputs average values of $W\Delta^2$ in zones of $\sin\theta/\lambda$ and of F_o. A correct weighting function like that of equation 6.7 must be such that there are no systematic variations in $W\Delta^2$ from zone to zone. Unobserved reflections, which were fed in as one half the local minimum value of F_o, were given equal weights, which may be adjusted to ensure constant values for the average $W\Delta^2$.

Often the least-squares matrix a_{ij} may be too large to be accommodated in the fast-access store of the computer. In such a case certain off-diagonal elements of the matrix, which correspond to parameter pairs having a low correlation, may be ignored (the block-diagonal approximation). Shearing's program enables the full matrix or the block-diagonal approximation to be used and also allows the terms to be recalculated or retained each cycle. As the number

of parameters was reasonably small in this problem, the full matrix was used and recalculated for each cycle.

The output of the program consists of the corrections c_i to the parameters, their refined values and their individual estimated standard deviations. Also output is the residual and the reflections data with refined scaling factors.

6.4.2 THE REFINEMENT WITH THE PROJECTIONS DATA ALONE

For this first stage of least-squares refinement the parameter corrections were calculated using the 0kl, h0l and hk0 data, Each set of projection data had its own scale factor which was refined independently. Reflections common to different sets of data were regarded as independent observations.

An initial model for the structure was found from the coordinates obtained in the refinement of the (100) and (001) projections. The x and z coordinates were taken directly from these results and the y and B parameters were calculated as the weighted means of the results from both projections. (The weighting for this latter calculation was in the ratio of the number of observed reflections in each projection).

Initially, the coordinate parameters and one isotropic temperature factor for each atom were refined.

No weighting function was used for the first few refinement cycles with the aim of speeding up the refinement. In five cycles the residual fell from 21.3 to 18.8 with shifts in coordinates of up to 0.05Å at the beginning. However, it was noted that a small group of reflections had

been fed in wrongly and correcting this mistake gave a drop of 2% in the residual. Subsequent refinement showed that the effect of these incorrect reflections was quite small.

In the next stage of the refinement the reflections were weighted by means of the weighting function of equation 6.7 with $a = 2F_{min}$ and $c = 2/F_{max}$. Unobserved reflections were given a weighting of 0.05 in the first five cycles and 0.3 in cycles six to ten. The residual fell from 16.7 to 15.9 in these ten cycles. Quite large coordinate shifts up to 0.1Å were obtained in the first few cycles.

Although the refinement for most of the atoms appeared to have ceased at the end of the 10 cycles, quite large shifts were still being obtained in the x coordinates of the atoms C2 and C4. The estimated standard deviations for these two parameters (0.06 and 0.05)were several times larger than for the x coordinates of the other atoms. It was noted that the shifts for the two parameters at the end of the refinement, as well as being large (approximately $\frac{1}{3}$ the estimated standard deviations), were, on each cycle, approximately equal and always opposite in sign. Obviously the x parameters of the two atoms (which were nearly equal) were highly correlated. The effect is very similar to attempting to refine the coordinates of two nearly equal atoms for a projection in which they overlap.

Following this latter analogy the best way to 'unlock' these two atoms seemed to be to introduce extra data. Accordingly, the data from the hk1 reciprocal-lattice plane were introduced into the refinement.

6.4.3 THE REFINEMENT AFTER THE INTRODUCTION OF THE hk1 DATA

The hk1 reflections were photographed with the same crystal that was used for the hk0 reflections. Two five-film exposures (24 hours and 120 hours) were made and the data were measured and scaled in the same way as the hk0 intensities (see section 5.4.1).

A correction was made for the differences in estimated intensity due to the difference in spot shape, which occurs on opposite halves of Weissenberg photographs of upper layers of the reciprocal lattice (Phillips, 1954) - the spots being contracted on one half (Ic) and extended on the other (Ie). Reflections which could be measured on both halves of the film were averaged using the expression given by Phillips

$$Iav = 2Ie\ Ic/(Ie + Ic)$$

Other reflections were corrected by means of the expression

$$I = I\ meas\ (1 \pm K \cos \theta)$$

given by Rollett (1965) who attributes it to P G Owston. The sign depends on whether the reflection is extended or contracted and the constant K is determined empirically (for this data K = 0.127). The data were then corrected for the Lorentz and polarisation factors in the usual way.

The introduction of the hk1 data had precisely the desired effect on the refinement in causing the x coordinates of the atoms C2 and C4 to refine rapidly. Three cycles were sufficient to achieve the situation in which their movements were negligible. In addition the estimated

standard deviations of the two coordinates fell to the average value for the remaining x coordinates.

The same weighting function was used as before with the unobserved reflections again having weight of 0.3. In five cycles of refinement the residual fell from 20.5 to 18.6 at which point the movements in the parameters were negligible.

Although the refinement had now ceased, the weighting function required some adjustment. A number of further cycles of refinement were calculated so that the weighting could be adjusted empirically, until reasonable results were obtained for the average values of $W\Delta^2$ over the various ranges of F_o and $\sin\theta/\lambda$. The best results were obtained by using the weighting function of equation 6.7 with $a = 2F_{min}$ and $c = 8/F_{max}$ and giving the unobserved reflections a weighting of 0.9. No significant refinement of the structure resulted from this process and a final residual of 18.4 was obtained.

6.4.4 THE STRUCTURE AFTER REFINEMENT WITH ISOTROPIC TEMPERATURE FACTORS - THE BEST-PLANES AND CROSS-SECTION FOURIER PROGRAMS

Although further refinement was achieved, when anisotropic temperature factors were given to the atoms and hydrogen atoms were added, the structure parameters had for the moment ceased to refine. At this point it was of interest to examine the various features of the structure and several computer programs were written for the purpose.

First a program was written to evaluate the bond lengths and angles. The program transfers the crystallographic atomic coordinates to a set of orthogonal axes by means of a transformation matrix $\underline{L}$ (Rollett, 1965), enabling the simpler geometric relations for orthogonal axes to be used in the calculation of the bond lengths and angles. Thus:

$$\underline{x}_o = \underline{L}\underline{x}_c \qquad (6.8)$$

where $\underline{x}_o$ and $\underline{x}_c$ represent atomic coordinates on orthogonal and crystallographic axes respectively.

The bond lengths and angles appeared to be reasonable except for the distance between the symmetry-related atoms C3 and $C3^1$. This bond length had the value of 1.51Å, which is rather long for a bond in a benzene ring (normal bond length ≈ 1.4Å). However, this length shortened considerably in the later refinement to 1.42Å.

The second program to be written was one to determine the degree of planarity of the molecule and is referred to as the 'best-plane' program, since it calculates the mean plane through the atoms in the molecule. Again the atomic coordinates are transferred to orthogonal axes. Then the parameters A, B and C of the plane

$$A_x + B_y + C_z = 1$$

are determined by a least-squares fit to the atomic coordinates on the orthogonal axes. The program then determines the direction cosines of the perpendicular to this plane and the perpendicular distances of the atoms on to the plane.

Since the benzene ring could be reasonably assumed to be planar, the mean plane, passing through the six benzene-ring atoms and parallel to the b axis, was calculated. This plane lay at 56° to the c axis. The atoms C4 and O were at 0.05Å and 0.15Å respectively from the plane. Thus, since the uncertainty in the atomic positions was about 0.02Å, the C4 and O atoms would appear to lie well out of the molecular plane. However, the later refinement of the structure caused the two atoms to lie much closer to the plane.

Lastly, two programs were written to evaluate the difference density on planes passing through the atomic positions, using the values of $(|F_o| - |F_c|)$ output from the least-squares program for the calculation. The three-dimensional difference density for the space group $I\frac{2}{c}$ is given by

$$\rho_o - \rho_c = \frac{4}{V}\{\sum_{0}^{\ell=2n}\sum_{0}^{\infty}\sum_{0}^{\infty}\sum_{0}^{\infty} A \cos 2\pi ky + \sum_{0}^{\ell=2n+1}\sum_{0}^{\infty}\sum_{0}^{\infty}\sum_{0}^{\infty} A \sin 2\pi ky\}$$

where $A = [F_o(hkl) - F_c(hkl)] \cos 2\pi(hx + lz)$

$$+ [F_o(\bar{h}kl) - F_c(\bar{h}kl)] \cos 2\pi(-hx + lz)$$

One of the programs evaluates this difference density on the mean plane passing through the molecule. The second program evaluates the difference density on a series of planes perpendicular to the b axis and each passing through an atomic position.

Figure 6.4 shows the difference density in the plane of the molecule, on the left-hand side of the diagram, and in the sections perpendicular to b taken through the atomic positions, on the right-hand side. These difference maps show several interesting features.

First, the peak marked H indicates the presence of a hydrogen atom attached to the atom C2. It appears to lie in the plane of the benzene ring at about 1Å from the atom C2 and to be situated such that the C2-H bond bisects the external angle C1C2C3, all of which agrees with the most probable chemical configuration. There should also be a similarly situated hydrogen atom attached to C1 but this does not show up in the difference map. However, there are several, strong, spurious features in this area of the map which may be obliterating the hydrogen peak.

The second interesting feature of the difference maps is the indications of anisotropic temperature factors with a strong vibration perpendicular to the b axis, which are shown by the contours surrounding the atoms N1 and N2. The effect on the contours can be seen quite clearly in both the map of the cross section in the molecular plane and the two maps of the sections perpendicular to b passing through the N1 and N2 positions. It will be remembered that this anisotropic temperature factor was observed for the atom N2 in the final difference map for the (001) projection - figure 5.10.

One further feature that may be noted in the difference maps is the negative regions at the centres of both the benzene ring and the adjacent five-membered ring, which are

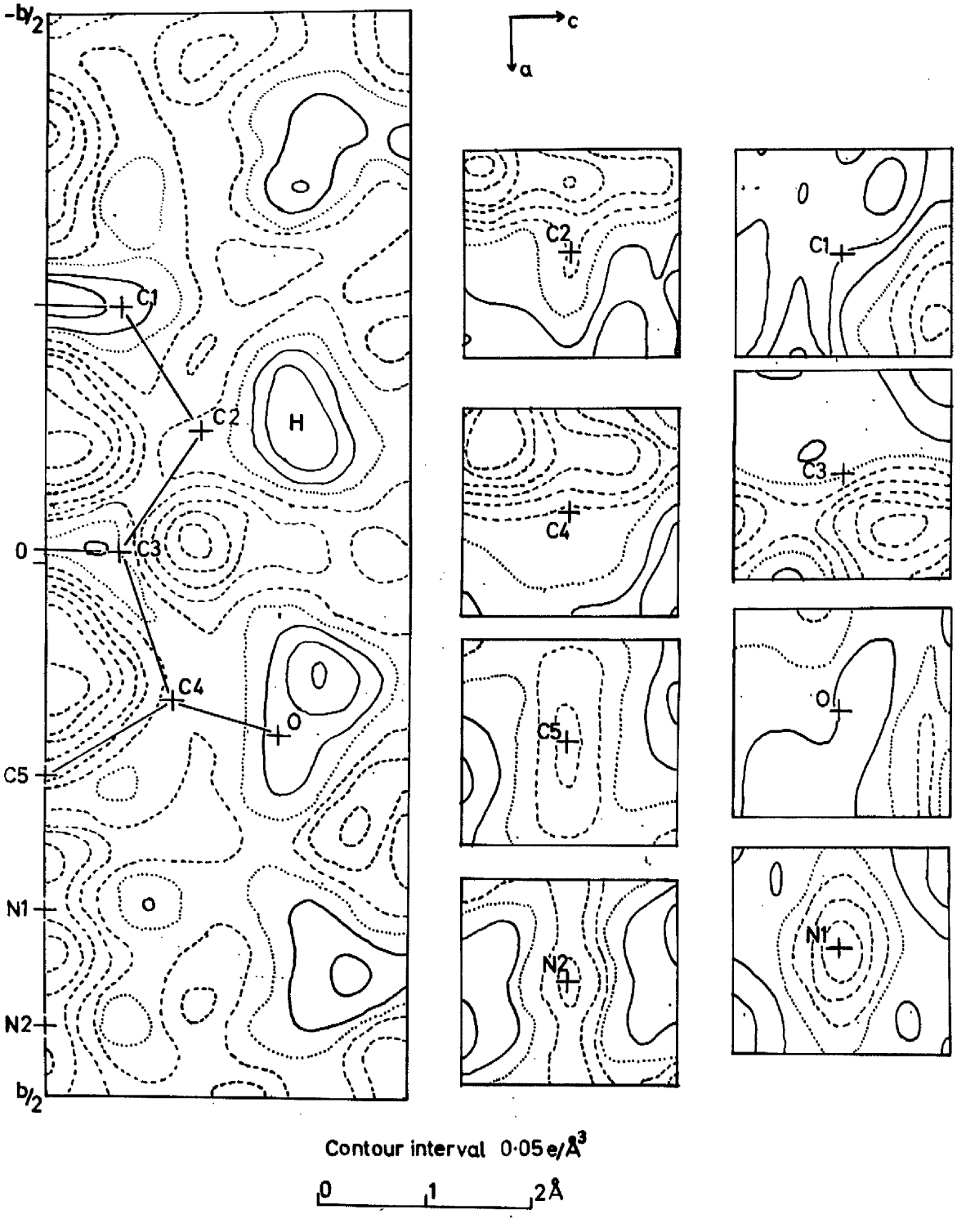
-b/2
c
a
C1
C2
H
0
C3
C4
O
C5
N1
O
N2
b/2
C2
C1
C4
C3
C5
O
N2
N1
Contour interval 0·05 e/Å3
0
1
2Å

FIG. 6.4

surrounded by positive regions following the lines of the atoms. This effect is common in difference maps of aromatic rings and has been noted previously by Cruickshank (1956) in anthracene. Cruickshank explains the feature qualitatively as being caused by a tendency for the electrons in the aromatic ring to be channelled along the bonds. The difference maps still show the negative region even after anisotropic temperature factors have been added.

6.4.5 THE FINAL REFINEMENT WITH ANISOTROPIC TEMPERATURE FACTORS AND HYDROGEN ATOMS ADDED

In the last stage of refinement the anisotropic temperature factors of all the atoms were refined together with the coordinate parameters and the scale factors for the data. Although only the atoms N1 and N2 indicated strongly that their temperature factors were anisotropic, it was felt that, since the number of atoms was small, it was reasonable to treat them all similarly.

In addition, hydrogen atoms were attached to the atoms C1 and C2 at a distance of 1.08Å. It was arranged that these two hydrogen atoms lay in the plane of the benzene ring and were orientated such that the carbon-hydrogen bond made equal angles with the adjacent carbon-carbon bonds. The hydrogen atoms were given isotropic temperature factors corresponding to those possessed by the carbon atoms, to which they were joined, at the end of the refinement with isotropic temperature factors (C1 = 5.40, C2 = 4.89). The addition of the hydrogen atoms to the structure caused a drop of 1.4% in the residual.

The succeeding refinement was carried out in a series of two-cycle steps and at the end of each step the hydrogen-atom positions were adjusted to take into account the movements of the C1 and C2 atoms. However, no attempt was made to refine the positions of the hydrogen atoms or their temperature factors with the least-squares program.

The weighting scheme which had been found suitable for the isotropic refinement above was used. In this scheme the weighting function of equation 6.7 was applied, with $a = 2F_{min}$ and $c = 8/F_{max}$ and the unobserved reflections having a constant weight of 0.9.

In the first two cycles of refinement the residual fell rapidly from 17.0 to 13.4. The changes in the atomic coordinates were quite small none being greater than 0.03Å. At the end of the two cycles the hydrogen atom positions were adjusted and two further cycles of refinement were carried out, in which the residual fell only to 13.3 with little variation in the parameters.

At this point the structure-factor data were examined and two reflections were found to have large discrepancies - the reflection 002 ($F_o = 87$, $F_c = 113$) from the 0kl data and the reflection 20-2 ($F_o = 170$, $F_c = 204$) from the h0l data. Both of these reflections are similar in that they are large in magnitude and at least twice as great as the other reflections in the group in which they were measured. Extinction immediately suggests itself as a possible explanation; but this is unlikely as the correction is large and no other reflections seem to require a correction which approaches this size. It may be noted that the 002

reflection occurs also in the h0l data with the larger 20-2 reflection and that here the agreement between F_o and F_c (for 002) is quite good. Some error in the measurement of these two reflections therefore seems likely and a possible explanation is that these reflections were not accurately scaled relative to the smaller reflections in the same group.

The values of F_o for these two reflections were therefore raised to the corresponding values of F_c at this point in the refinement. Although the residual now fell by 1.5%, the succeeding refinement was not greatly affected, since these reflections were very much downweighted.

The new positions of the hydrogen atoms were now recalculated and two cycles of least-squares refinement were carried out followed by a further readjustment in the hydrogen atom positions. A further two cycles were calculated and then the refinement was stopped. The residual was now 11.9% and the movements of all the parameters were well within their estimated standard deviations.

Table 6.2 gives the final refined values of all the atomic parameters together with their estimated standard deviations.

6.4.6 THE FINAL DIFFERENCE SYNTHESIS

Although no further refinement by least-squares seemed possible, it was decided to calculate the difference maps for this final structure to check for any remaining discrepancies. Figure 6.5 shows, on the left-hand side, the difference map for the section in the molecular plane

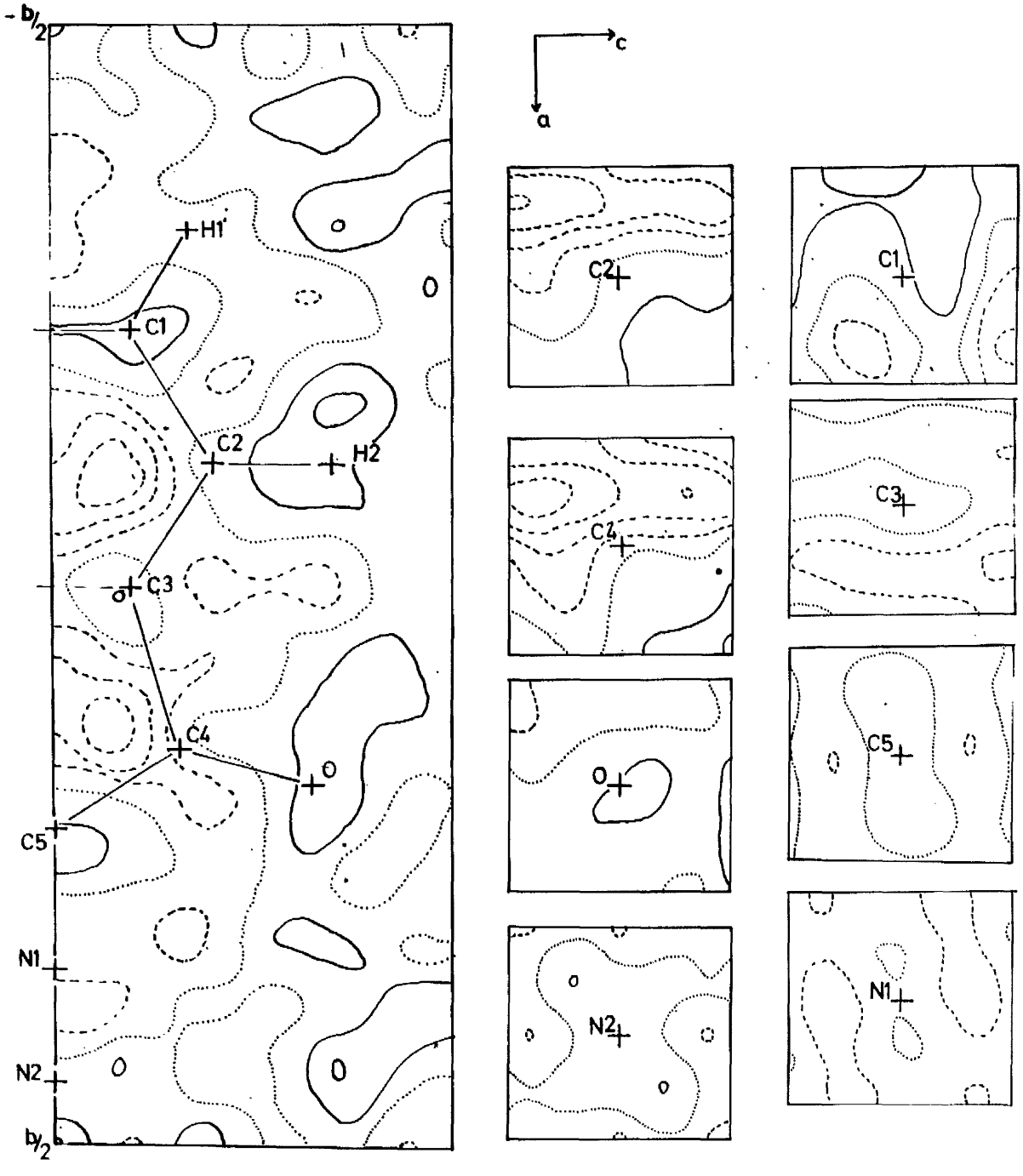
-b/2
c
a
H1
C1
C2
H2
C3
C4
O
C5
N1
N2
b/2
C2
C1
C4
C3
O
C5
N2
N1
Contour interval 0·05e/Å3
0
1
2Å

FIG. 6.5

and, on the right-hand side, the difference maps for the sections perpendicular to the b axis and passing through the atomic positions.

The contours indicating anisotropic temperature factors for N1 and N2 have now disappeared, as would be hoped. Still present, however, are the negative regions in the two rings surrounded by the positive areas at the atomic positions.

The hydrogen atom H1, whose position was unlocated in the map of figure 6.4, is in a fairly flat region of the map of figure 6.5. This feature would indicate that the position of this hydrogen atom is probably correct, since a wrongly positioned atom would produce a negative region in the map. The other atom H2 is on a slightly positive region, which could indicate that a lowering of its temperature factor was necessary. However, the accuracy of the data did not warrant refinement of the parameters of the hydrogen atoms.

No gross inaccuracies in the structure were however indicated by the difference syntheses in figure 6.5. Thus no further attempts were made to refine the structure.

TABLE 6.2

Final atomic parameters

Atomic coordinates

atom	x	y	z
C1	0.06184	-0.23695	0.04658
C2	0.12558	-0.12264	0.10221
C3	0.06170	-0.00926	0.05127
C4	0.10270	0.12409	0.07842
C5	0	0.19856	0
N1	0	0.32597	0
N2	0	0.42920	0
O	0.21091	0.15823	0.16080
H1	0.10807	-0.32698	0.08408
H2	0.22086	-0.12259	0.17971

Coordinate errors

atom	σ(x)	σ(y)	σ(z)
C1	0.00084	0.00082	0.00167
C2	0.00089	0.00077	0.00177
C3	0.00069	0.00081	0.00136
C4	0.00075	0.00074	0.00201
C5	0	0.00116	0
N1	0	0.00092	0
N2	0	0.00121	0
O	0.00058	0.00056	0.00115

Anisotropic temperature factors

atom	b11	b22	b33	b12	b13	b23
C1	0.0146	0.0106	0.0328	0.0021	0.0183	-0.0034
C2	0.0121	0.0111	0.0256	-0.0027	0.0054	0.0031
C3	0.0107	0.0109	0.0207	-0.0024	-0.0029	0.0059
C4	0.0103	0.0112	0.0278	-0.0021	-0.0090	0.0010
C5	0.0141	0.0103	0.0448	0	-0.0324	0
N1	0.0168	0.0102	0.0282	0	0.0302	0
N2	0.0278	0.0121	0.0977	0	0.0134	0
O	0.0164	0.0132	0.0222	-0.0037	-0.0030	-0.0025
H1	B=5.40					
H2	B=4.89					

TABLE 6.2 (continued)

Anisotropic temperature factor errors

atom	σ(b11)	σ(b22)	σ(b33)	σ(b12)	σ(b13)	σ(b23)
C1	0.0009	0.0007	0.0037	0.0013	0.0078	0.0041
C2	0.0008	0.0007	0.0025	0.0011	0.0047	0.0027
C3	0.0007	0.0006	0.0021	0.0012	0.0086	0.0021
C4	0.0008	0.0008	0.0032	0.0011	0.0047	0.0033
C5	0.0012	0.0009	0.0090	0	0.0086	0
N1	0.0012	0.0009	0.0049	0	0.0058	0
N2	0.0023	0.0012	0.0144	0	0.0142	0
O	0.0007	0.0006	0.0015	0.0012	0.0031	0.0022

CHAPTER 7

A DISCUSSION OF THE STRUCTURE

7.1 BOND LENGTH AND BOND ANGLE ERRORS

In a least-squares refinement, when relative weights and a full matrix are used, as in this case, the variance of a parameter p_i is given by

$$\sigma^2(p_i) = (a^{-1})_{ii} (\Sigma W\Delta^2)/(m - n) \qquad (7.1)$$

where m is the number of observations and n the number of parameters and $(a^{-1})_{ii}$ is an element of the matrix inverse to a_{ij} (Rollett, 1965). Values of the estimated standard deviation $\sigma(p_i)$ are output by Shearing's least-squares program for all the refined parameters (see table 6.2).

The variance in the bond length l between two atoms, A and B, is given by

$$\sigma^2(l) = \sigma^2(A) - 2 \text{ cov } (A,B) + \sigma^2(B) \qquad (7.2)$$

where $\sigma^2(A)$ and $\sigma^2(B)$ are the variances in the positions of A and B respectively in the direction AB. The covariance between the atomic positions of A and B, cov(A,B), is zero if both atoms are unrelated. However, certain bond lengths are evaluated in the present structure between atoms related by a 2-fold axis and here,

$$\text{cov}(A,B) = -\sigma^2(A) = -\sigma^2(B) \text{ and hence}$$

$$\sigma^2(l) = 4\sigma^2(A) \qquad (7.3)$$

If the unit cell coordinates of atom A are x, y, z then for the general case of oblique axes the variance in the position of the atom A along AB is given by

$$\sigma^2(A) = \sigma^2(x)\left(\frac{\partial l}{\partial x}\right)^2 + \text{------}$$

$$+ 2\sigma(x)\,\sigma(y)\,\frac{\partial l}{\partial x}\,\frac{\partial l}{\partial y}\,\text{cov}(x,y) + \text{------} \qquad (7.4)$$

Now cov(x,y), the covariance of the x and y coordinates, may be evaluated from

$$\text{cov}(x,y) = (a^{-1})_{ij}(\Sigma W\Delta^2)/(m - n) \qquad (7.5)$$

if x and y are assumed to be the i and j^{th} parameters in the least-squares refinement.

Thus, substituting the values for the estimated standard deviations in the atomic coordinates output by Shearing's program into equation 7.4, values of $\sigma^2(A)$ (and σ^2B) may be determined. Then using these values in equation 7.2 the estimated standard deviation of each bond length may be found.

However, this is rather a long procedure, particularly since equation 7.5 requires the least-squares matrix to be set up and inverted for the bond-length calculation. Considerable simplification is justified in this case, where the cell is almost orthorhombic, since for an orthorhombic cell the cross terms of equation 7.4 are zero.

In fact, Templeton (1959) shows that for oblique axes, when the errors are reasonably isotropic, $cov(x,y) = \cos \beta^*$ etc. Thus, for the present monoclinic cell, $cov(x,y) = cov(y,z) = \cos 90^\circ = 0$ and $cov(x,y) = \cos (88.9^\circ) \approx 0$.

Also, since the coordinate errors (in angstroms) appeared to be approximately the same, an average value σ_{av} was assumed, this being the average of all the coordinate errors. This assumption considerably simplified the bond length and angle calculations for atoms related by symmetry or where one or both were on a symmetry element. Hence for two atoms in general positions the bond length error was found from

$$\sigma^2(A) = \sigma^2(B) = 3(\sigma_{av})^2$$

and $$\sigma^2(l) = 6(\sigma_{av})^2$$

For two atoms related by the 2-fold axis

$$\sigma^2(A) = \sigma^2(B) = 2(\sigma_{av})^2$$

and $$\sigma^2(l) = 8(\sigma_{av})^2$$

The bond angle errors were calculated from an expression given by Cruickshank and Robertson (1953)

$$\sigma^2(\beta) = \frac{\sigma^2(A)}{AB^2} + \sigma^2(B)\left(\frac{1}{AB^2} - \frac{2\cos\beta}{AB.BC} + \frac{1}{BC^2}\right) + \frac{\sigma^2(C)}{BC^2} \qquad (7.6)$$

where $\sigma^2(A)$ and $\sigma^2(C)$ are the variances of A and C in the ABC plane perpendicular to AB and BC respectively and

$\sigma^2(B)$ is the variance of B in the direction tangential to the circle through ABC. Where the bond AB lay across the 2-fold axis the half length of the bond was used in place of AB in equation 7.5.

The estimated standard deviations in the bond lengths and angles are shown in figure 7.1.

7.2 BOND LENGTHS AND BOND ANGLES

The bond lengths and angles of the refined structure were calculated and compared with the values that might be anticipated for the structure proposed by Regitz and Heck. The significance test suggested by Cruickshank and Robertson (1953) was used when comparing measured bond lengths and angles with theoretical values. If δl is the difference between measured and theoretical values then if

$\delta l < 1.645\sigma$ the difference is not significant,
$2.327\sigma > \delta l > 1.645\sigma$ the difference is possibly significant,
$3.090 > \delta l > 2.327\sigma$ the difference is significant.
Theoretical bond lengths were found from a table of covalent radii given by Robertson (1953).

The bond lengths in the benzene ring are all within the standard deviation of the usual bond length of 1.394Å (Tables of Interatomic Distances). In the benzene ring however one angle, C1C2C3, is possibly significantly different from the usual 120°.

The bond C3C4 should have approximately a single carbon-carbon bond length of 1.54Å and is certainly significantly different at 1.47Å. The resonance structure indicates

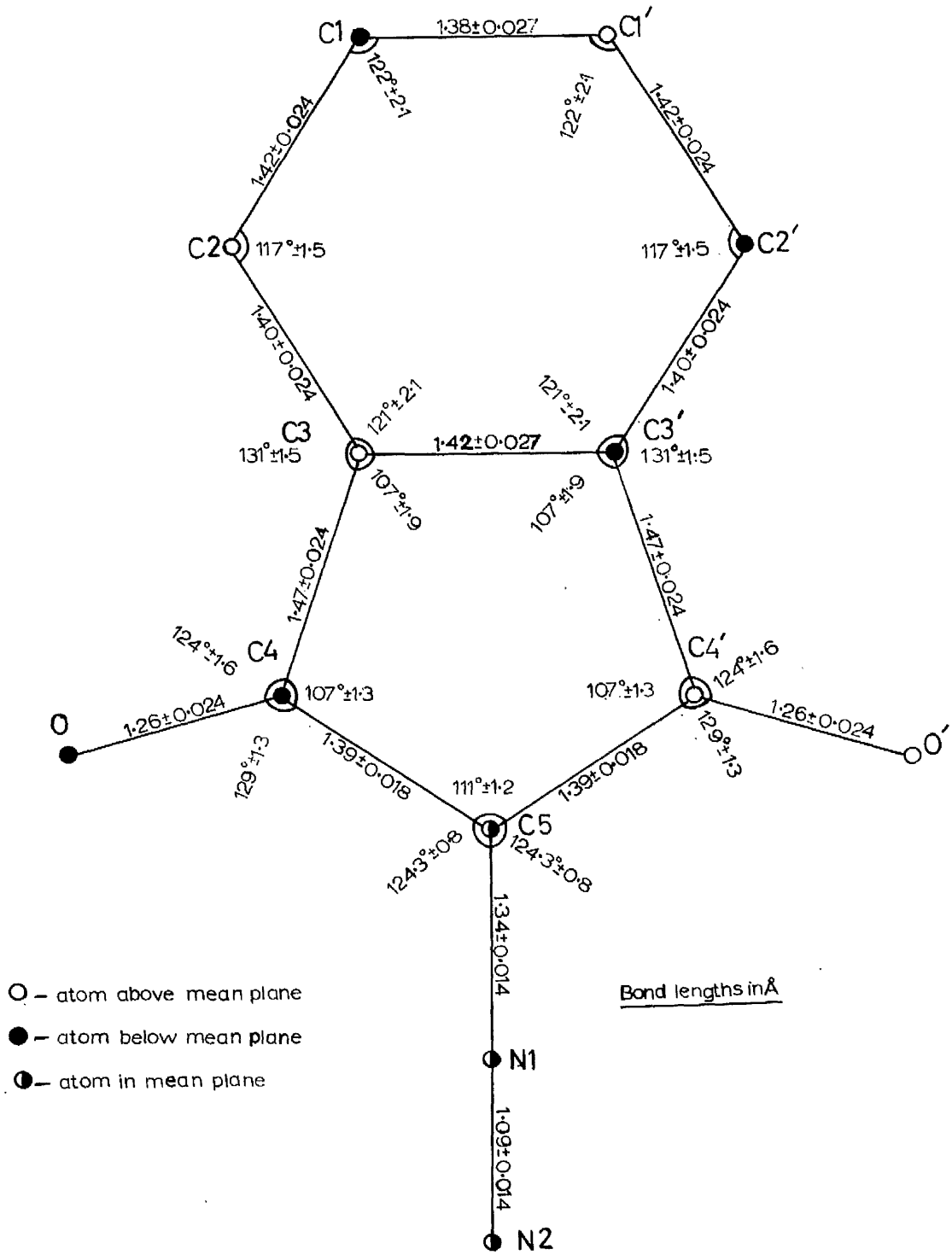
C1
1·38±0·027
C1′
122°±2·1
122°±2·1
1·42±0·024
1·42±0·024
C2
117°±1·5
117°±1·5
C2′
1·40±0·024
1·40±0·024
121°±2·1
121°±2·1
C3
131°±1·5
1·42±0·027
C3′
131°±1·5
107°±1·9
107°±1·9
1·47±0·024
1·47±0·024
124°±1·6
C4
C4′
124°±1·6
107°±1·3
107°±1·3
O
1·26±0·024
1·26±0·024
O′
129°±1·3
129°±1·3
1·39±0·018
1·39±0·018
111°±1·2
C5
124·3°±0·8
124·3°±0·8
1·34±0·014
N1
1·09±0·014
N2
O – atom above mean plane
● – atom below mean plane
◑ – atom in mean plane
Bond lengths in Å

Fig.7.1

that C4C5 should be intermediate in length between a single and a double carbon-carbon bond (1.54 and 1.33) but perhaps closer to the single bond length and it should be certainly shorter than C3C4. However, this bond is nearer to the double bond length, although it is certainly shorter than C3C4. Therefore, both C3C4 and C4C5 seem to be shorter than might be expected.

The C4O bond should be very close to the carbon-oxygen double bond length of 1.22Å; the actual value of 1.26Å is possibly significantly larger. The C5N1 bond should be intermediate between a single (1.47Å) and a double bond (1.27Å) and the actual length of 1.34Å agrees with this suggestion. The N1N2 bond should be intermediate between a double and a triple bond (1.20 and 1.09) but it is in fact equal to the triple-bond length.

Thus, not all bond lengths are entirely consistent with Regitz and Heck's structure. However, a definite conclusion on this point would require better theoretical and experimental estimates of the bond lengths.

7.3 THE PLANARITY OF THE MOLECULE

The best-plane program was used to find the mean plane passing through the atoms in the molecule. This mean plane, lying parallel to the b axis, was orientated at 59.2° to the c axis (32.9° to the a axis). The deviations of each atom from the mean plane are given in the table below (in angstrom units)

$C1(C1^1)$	0.008
$C2(C2^1)$	0.035
$C3(C3^1)$	0.024
$C4(C4^1)$	0.007
$O(O^1)$	0.015

The atoms not listed lie on the 2-fold axis and therefore in the mean plane. The directions of the deviations from the mean plane are shown in figure 7.1, where the open circles indicate atoms above the mean plane and full circles those below.

Cruickshank's significance test was applied to the above table of deviations assuming that the orientation of the mean plane is known absolutely. The average error in the atomic positions parallel to the a-c plane is 0.014Å. Thus, one atom, C2, is situated at a distance from the mean plane which is significant and another atom, C3, is situated a distance which is possibly significant. It will be remembered that the bond angle of the benzene ring at C2 was rather small, which would be expected if the benzene ring was slightly twisted there. Thus a slight twisting of the molecule seems to exist possibly caused by a reorientation of the bonds in order to attach the five-membered and six-membered rings together.

7.4 THE PACKING OF THE MOLECULE

The molecules can be pictured as lying in planes which are parallel to the a-b plane of the unit cell. Each

almost-planar molecule is orientated parallel to the b axis and at 32.9° to the a-b plane. Figure 7.2a shows the appearance of one plane of molecules at height z = 0 viewed down the c axis. The molecule outlined by the dashes is at height z = $\frac{1}{2}$ and shows the way in which the next plane of molecules is superimposed on the first.

The apparent contact points between the atoms of adjacent molecules in the plane are indicated by the dotted lines. The oxygen atoms of adjacent molecules appear to be in contact, although the separation of 3.31Å is fairly large compared to the average Van de Waal distance of 2.8Å (Robertson, 1953). The nitrogen atom N2 and the hydrogen atom H1 also appear to be in contact (2.84Å) and there is a possibility of a hydrogen bond existing between C1 and N2. However, this bond would be very weak since the C1-N2 distance is large (3.59Å). Also, the H1 and H2 atoms of adjacent molecules seem to be in contact but the probable distance of 2.76Å cannot be given accurately because of the uncertainty in the hydrogen atom positions.

Figure 7.2b shows from the projection down the b axis how the sheets of molecules stack. The spacing of the molecular sheets seems to be governed by the usual separation obtained between the planes of aromatic molecules. The molecules are stacked so that the edges of the five and six-membered rings of adjacent molecules overlap. If the five-membered ring is assumed to have the same thickness as is usually obtained for an aromatic ring, then the perpendicular distance between adjacent molecular planes would be about 3.4Å (Robertson, 1953); in fact, the actual distance is 3.36Å.

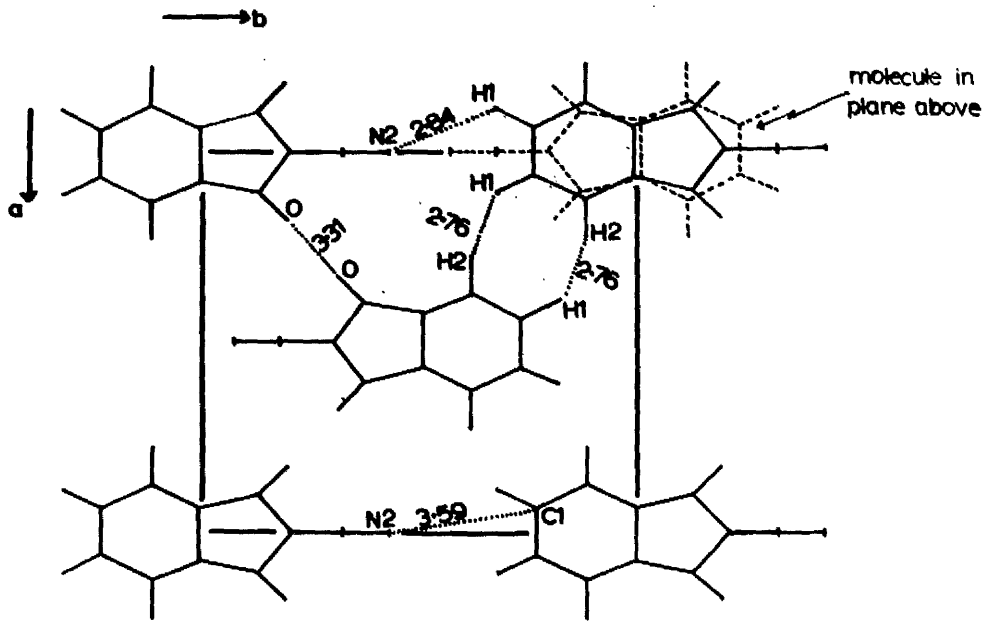

Intermolecular distances in Å

(a)

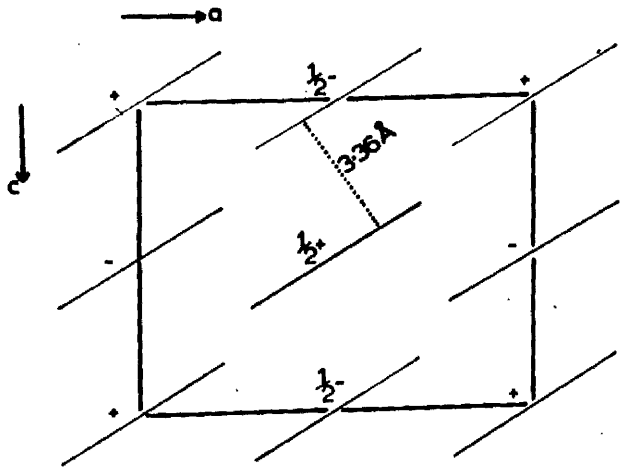

(b)

Fig.7.2

7.5 THE THERMAL VIBRATION ELLIPSOIDS

The anisotropic temperature factor term can be written:

$$\exp -(b_{11}h^2 + b_{22}k^2 + b_{33}l^2 + b_{12}hk + b_{23}kl + b_{13}hl) \quad (7.7)$$

The factors b_{11} etc. are refined and output by Shearing's least-squares program (see table 6.2). An alternative form of 7.7 is

$$\exp -(B_{11}h^2 + B_{22}k^2 + B_{33}l^2 + 2B_{12}hk + 2B_{23}kl + 2B_{13}hl)$$

$$\text{or} \qquad \exp - (\underline{h}^T B \underline{h}) \qquad (7.8)$$

where B is a matrix of the elements B_{11} etc. and $\underline{h}$ is the column vector (h,k,l). The matrix B may be referred to orthogonal axes in the same way as the atomic coordinates in equation 6.8, again using the matrix L. Thus, a new matrix V is produced where:-

$$V = LBL^T \qquad (7.9)$$

Rollett (1965) shows that the eigenvectors of V are the principal axes of the thermal vibration ellipsoid. Also, if λ_i is the i^{th} eigenvalue of V, the root-mean-square vibration amplitude $(\overline{u^2})^{\frac{1}{2}}$ along the principal axis corresponding to the i^{th} eigenvector is given by:

$$(\overline{u^2})^{\frac{1}{2}} = [\lambda_i/(2\pi^2)]^{\frac{1}{2}} \qquad (7.10)$$

A program was therefore written to determine the directions of the principal axes of the vibration ellipsoid for each atom and the corresponding r.m.s. vibration amplitudes.

The values of b_{11} etc. are read in by the program and the matrix B set up; and V is then determined from equation 7.9. The eigenvalues and the eigenvectors of V were found by Jacobi's method (Herriot, 1963). In Jacobi's method the off-diagonal elements of the matrix are progressively reduced to zero by means of a transformation $W^{-1}VW$, where W is an orthogonal matrix. When the off-diagonal elements are zero to within the working accuracy, then the diagonal elements are the eigenvalues and the product W_1W_2 ..... is a matrix whose columns are the eigenvectors.

The values of $(\overline{u^2})^{\frac{1}{2}}$ were therefore found from the eigenvalues using equation 7.10 and the coordinates of the principal axes (referred to the orthogonal axes) were determined from the eigenvectors of V. The coordinates of the principal axes were then transferred to the crystallographic axes by means of the transformation matrix L^{-1}.

Table 7.1 gives the values of $(\overline{u^2})^{\frac{1}{2}}$ for each atom. The angles made by the corresponding principal axes with the positive directions of the crystallographic axes are also given. As suspected there is a strong vibration direction perpendicular to the b axis for the atoms N1 and N2 - the root-mean-square amplitudes are 0.37Å and 0.56Å respectively.

TABLE 7.1

Parameters of vibration ellipsoids

atom	rms amplitudes (in Å units)	orientation of principal axes to crystallographic axes (in degrees)		
		a	b	c
C1	0.350	61	93	32
	0.253	64	29	102
	0.210	139	61	61
C2	0.291	101	103	161
	0.259	54	144	88
	0.221	142	123	71
C3	0.283	70	127	137
	0.226	89	40	130
	0.218	20	78	76
C4	0.313	66	97	157
	0.252	97	13	100
	0.201	25	79	70
C5	0.429	59	90	151
	0.241	90	0	90
	0.174	32	90	61
N1	0.372	49	90	43
	0.240	90	0	90
	0.164	139	90	47
N2	0.558	85	90	7
	0.359	5	90	97
	0.261	90	0	90
O	0.294	35	121	107
	0.279	80	48	137
	0.243	57	57	52

h	k	l	|Fo|	|Fc|	Fo-Fc	phase
0	2	0	37.93	39.02	-1.09	180
0	4	0	34.31	37.29	-2.98	180
0	6	0	25.40	25.36	0.03	0
0	8	0	16.51	17.44	-0.93	0
0	10	0	1.57	1.54	0.03	180
0	12	0	1.28	1.60	-0.32	0
1	1	0	62.04	68.43	-6.38	0
1	3	0	18.15	16.71	1.44	180
1	5	0	15.58	11.86	3.72	0
1	7	0	16.93	17.86	-0.93	0
1	9	0	22.51	21.29	1.22	0
1	11	0	6.35	4.65	1.70	180
1	13	0	0.96	0.51	0.45	180
2	0	0	68.59	78.04	-9.46	0
2	2	0	3.72	3.94	-0.22	0
2	4	0	48.16	42.84	5.32	0
2	6	0	10.42	11.70	-1.28	180
2	8	0	1.51	0.61	0.90	0
2	10	0	5.77	6.16	-0.38	0
2	12	0	1.25	1.35	-0.10	0
3	1	0	46.49	44.86	1.64	180
3	3	0	50.18	48.61	1.57	0
3	5	0	26.68	22.38	4.30	0
3	7	0	11.32	10.74	0.58	180
3	9	0	8.53	8.05	0.48	0
3	11	0	1.41	1.03	0.38	0
3	13	0	0.74	0.45	0.29	0
4	0	0	14.11	12.54	1.57	0
4	2	0	16.00	14.78	1.22	180
4	4	0	18.53	17.09	1.44	0
4	6	0	11.06	11.22	-0.16	0
4	8	0	18.44	18.18	0.26	180
4	10	0	1.51	1.60	-0.10	180
4	12	0	7.09	5.48	1.60	0
5	1	0	22.89	22.70	0.19	180
5	3	0	8.98	6.86	2.12	180
5	5	0	15.23	15.23	0.00	0
5	7	0	1.57	2.28	-0.71	180
5	9	0	7.09	8.43	-1.35	180
5	11	0	1.22	2.02	-0.80	0
6	0	0	12.89	12.89	0.00	180
6	2	0	6.99	6.64	0.35	180
6	4	0	4.39	4.01	0.38	180
6	6	0	1.57	1.64	-0.06	0
6	8	0	13.40	13.98	-0.58	180
6	10	0	1.31	0.80	0.51	0
6	12	0	0.45	0.38	0.06	0
7	1	0	16.74	17.03	-0.29	180
7	3	0	1.51	1.96	-0.45	0
7	5	0	13.27	10.52	2.76	180
7	7	0	5.48	5.23	0.26	180
7	9	0	1.35	1.51	-0.16	0
7	11	0	0.77	0.87	-0.10	180
8	0	0	1.57	1.83	-0.26	0
8	2	0	1.57	2.95	-1.38	180
8	4	0	19.98	18.50	1.47	180
8	6	0	1.57	2.02	-0.45	180
8	8	0	1.35	2.66	-1.31	180
8	10	0	0.83	1.09	-0.26	0
9	1	0	1.60	2.21	-0.61	0
9	3	0	16.00	13.18	2.82	180
9	5	0	10.97	9.07	1.89	180
9	7	0	1.28	2.05	-0.77	0
9	9	0	0.80	0.16	0.64	0
10	0	0	5.87	5.45	0.42	0

h	k	l	|Fo|	|Fc|	Fo-Fc	phase
10	2	0	4.71	3.91	0.80	180
10	4	0	10.58	9.75	0.83	180
10	6	0	1.19	1.41	-0.22	0
10	8	0	0.64	2.12	-1.47	180
11	1	0	1.28	2.28	-0.99	180
11	3	0	1.19	0.74	0.45	180
11	5	0	0.96	0.77	0.19	180
12	0	0	0.93	2.02	-1.09	180
12	2	0	0.87	0.58	0.29	180
0	0	2	106.81	114.57	-7.76	0
0	0	4	8.18	8.51	-0.33	180
0	0	6	2.10	2.57	-0.47	0
0	0	8	7.44	4.30	3.13	180
0	0	10	1.17	1.68	-0.51	180
0	1	1	29.70	30.82	-1.12	90
0	1	3	10.90	11.46	-0.56	-90
0	1	5	16.27	14.82	1.45	90
0	1	7	9.17	7.06	2.10	90
0	1	9	1.87	1.68	0.19	-90
0	2	0	40.97	39.00	1.96	180
0	2	2	6.83	6.22	0.61	180
0	2	4	1.64	1.82	-0.19	180
0	2	6	9.07	9.03	0.05	180
0	2	8	2.20	2.48	-0.28	180
0	2	10	0.98	0.75	0.23	180
0	3	1	32.78	32.74	0.05	90
0	3	3	12.72	11.27	1.45	90
0	3	5	2.01	1.08	0.94	90
0	3	7	6.50	3.23	3.27	-90
0	3	9	1.73	2.20	-0.47	-90
0	4	0	35.40	37.27	-1.87	180
0	4	2	26.42	21.89	4.54	0
0	4	4	28.57	26.14	2.43	0
0	4	6	2.24	1.22	1.03	180
0	4	8	2.06	2.48	-0.42	180
0	5	1	34.04	35.96	-1.92	-90
0	5	3	1.82	2.62	-0.80	90
0	5	5	6.55	8.28	-1.73	-90
0	5	7	2.24	2.20	0.05	-90
0	5	9	1.40	3.04	-1.64	90
0	6	0	26.24	25.35	0.89	0
0	6	2	1.87	1.92	-0.05	180
0	6	4	2.15	2.62	-0.47	180
0	6	6	7.34	6.31	1.03	0
0	6	8	1.78	1.12	0.65	180
0	7	1	20.62	19.64	0.98	90
0	7	3	2.15	2.24	-0.09	-90
0	7	5	2.29	2.95	-0.65	90
0	7	7	4.86	3.69	1.17	90
0	8	0	16.60	17.44	-0.84	0
0	8	2	5.71	5.80	-0.09	0
0	8	4	8.00	7.62	0.37	180
0	8	6	10.99	8.14	2.85	180
0	8	8	1.17	3.04	-1.87	180
0	9	1	12.39	12.25	0.14	-90
0	9	3	10.71	9.91	0.80	-90
0	9	5	2.10	1.31	0.80	-90
0	9	7	1.40	0.05	1.36	90
0	10	0	2.29	1.54	0.75	180
0	10	2	4.54	3.98	0.56	0
0	10	4	2.06	1.96	0.09	0
0	10	6	1.50	1.96	-0.47	180
0	11	1	2.15	2.85	-0.70	-90
0	11	3	1.96	3.18	-1.22	90
0	11	5	1.45	0.89	0.56	-90
0	12	0	1.87	1.59	0.28	0

h	k	l	$\|F_o\|$	$\|F_c\|$	F_o-F_c	phase
0	12	2	1.73	0.65	1.08	0
0	12	4	1.31	1.78	-0.47	0
0	13	1	1.31	1.73	-0.42	-90
0	13	3	0.75	1.45	-0.70	-90
0	0	2	105.74	114.58	-8.84	0
0	0	4	8.86	8.52	-0.47	180
0	0	6	3.83	2.58	1.25	0
0	0	8	3.99	4.30	-0.31	180
0	0	10	2.03	1.64	0.39	180
2	0	-10	1.88	0.55	1.33	180
2	0	-8	3.91	0.00	3.91	0
2	0	-6	3.83	2.89	0.94	180
2	0	-4	71.17	69.76	1.41	0
2	0	-2	196.00	202.80	-6.80	0
2	0	0	67.89	78.05	-10.17	0
2	0	2	2.19	2.42	-0.23	0
2	0	4	3.85	4.38	-1.25	0
2	0	6	13.53	13.30	0.23	180
2	0	8	3.83	0.94	2.89	180
2	0	10	1.49	1.41	0.08	0
4	0	-8	3.68	1.96	1.72	0
4	0	-6	32.54	31.21	1.33	0
4	0	-4	66.79	60.77	6.02	0
4	0	-2	15.95	15.88	0.08	0
4	0	0	15.95	12.51	3.44	0
4	0	2	2.82	4.15	-1.33	180
4	0	4	20.02	18.38	1.64	180
4	0	6	8.13	6.73	1.41	0
4	0	8	3.52	3.05	0.47	0
6	0	-8	12.20	11.73	0.47	0
6	0	-6	17.44	16.35	1.09	0
6	0	-4	3.83	3.21	0.63	0
6	0	-2	3.44	4.61	-1.17	0
6	0	0	13.22	12.90	0.31	180
6	0	2	8.60	7.90	0.70	180
6	0	4	18.93	17.13	1.80	0
6	0	6	3.99	3.13	0.86	0
6	0	8	2.74	1.72	1.02	180
8	0	-8	1.56	5.01	-3.44	0
8	0	-6	3.52	2.11	1.41	0
8	0	-4	4.87	0.78	3.28	180
8	0	-2	11.42	9.70	1.72	180
8	0	0	3.99	1.80	2.19	0
8	0	2	17.05	15.25	1.80	0
8	0	4	4.87	0.47	3.60	0
8	0	6	3.28	0.23	3.05	180
10	0	-6	2.11	0.55	1.56	180
10	0	-4	3.28	3.28	0.00	180
10	0	-2	3.75	2.74	1.02	0
10	0	0	3.83	5.47	-1.64	0
10	0	2	3.68	2.03	1.64	180
10	0	4	3.13	1.64	1.49	0
12	0	-2	2.11	0.31	1.80	0
12	0	0	2.35	2.03	0.31	180
12	0	2	1.80	1.72	0.08	0
12	1	1	1.85	0.89	0.96	90
12	3	1	1.37	0.27	1.09	-90
11	2	1	2.60	1.71	0.89	90
11	4	1	2.26	0.21	2.05	90
11	6	1	1.37	1.37	0.00	-90
10	1	1	6.15	8.61	-2.46	90
10	3	1	3.08	1.64	1.44	90
10	5	1	2.73	2.32	0.41	-90
10	7	1	1.98	1.16	0.82	-90
9	2	1	9.16	10.80	-1.64	90
9	4	1	3.28	4.99	-1.71	-90

h	k	l	$\|F_o\|$	$\|F_c\|$	F_o-F_c	phase
9	6	1	2.94	1.50	1.44	-90
9	8	1	2.26	1.09	1.16	90
8	1	1	16.13	16.13	0.00	90
8	3	1	3.35	2.32	1.03	-90
8	5	1	3.35	0.21	3.14	90
8	7	1	3.08	2.05	1.03	90
8	9	1	2.39	1.98	0.41	90
7	2	1	11.48	10.93	0.55	-90
7	4	1	3.35	1.91	1.44	90
7	6	1	6.49	9.36	-2.87	90
7	8	1	3.14	3.96	-0.82	-90
7	10	1	2.32	3.49	-1.16	90
6	1	1	2.80	1.64	1.16	90
6	3	1	13.26	14.90	-1.64	-90
6	5	1	18.66	20.78	-2.12	90
6	7	1	3.35	3.42	-0.07	90
6	9	1	3.14	4.03	-0.89	-90
6	11	1	2.19	0.96	1.23	90
5	2	1	11.14	11.34	-0.21	-90
5	4	1	9.91	7.52	2.39	-90
5	6	1	12.10	12.85	-0.75	90
5	8	1	3.35	1.91	1.44	-90
5	10	1	3.81	1.57	1.44	90
5	12	1	1.78	1.03	0.75	90
4	1	1	48.80	54.06	-5.26	90
4	3	1	2.39	2.73	-0.34	-90
4	5	1	11.82	11.21	0.62	-90
4	7	1	14.97	14.83	0.14	90
4	9	1	3.35	2.26	1.09	-90
4	11	1	2.80	3.01	-0.21	-90
3	2	1	1.91	3.14	-1.23	-90
3	4	1	10.66	10.59	0.07	-90
3	6	1	2.87	3.49	-0.62	-90
3	8	1	3.35	1.09	2.26	-90
3	10	1	3.28	3.83	-0.55	90
3	12	1	2.46	0.48	1.98	90
2	1	1	1.50	2.46	-0.96	90
2	3	1	16.13	17.15	-1.03	90
2	5	1	7.04	5.40	1.64	90
2	7	1	3.01	0.34	2.67	90
2	9	1	13.12	10.87	2.26	-90
2	11	1	3.08	3.35	-0.27	90
2	13	1	1.78	1.78	0.00	-90
1	2	1	41.48	45.38	-3.90	-90
1	4	1	7.86	7.59	0.27	90
1	6	1	8.54	7.93	0.62	-90
1	8	1	10.46	10.18	0.27	-90
1	10	1	3.35	3.01	0.34	90
1	12	1	2.73	2.53	0.21	90
0	1	1	26.58	30.82	-4.24	90
0	3	1	28.64	32.74	-3.90	90
0	5	1	31.57	35.95	-4.37	-90
0	7	1	19.55	19.68	-0.14	90
0	9	1	13.94	12.23	1.71	-90
0	11	1	3.21	2.87	0.34	-90
0	13	1	1.98	1.71	0.27	-90
-1	2	1	9.50	9.16	0.34	90
-1	4	1	37.45	35.88	1.57	-90
-1	6	1	16.68	15.38	1.30	-90
-1	8	1	8.88	9.02	-0.14	90
-1	10	1	3.35	3.96	-0.62	-90
-1	12	1	2.73	0.14	2.60	-90
-2	1	1	7.18	7.04	0.14	90
-2	3	1	25.22	24.74	0.48	90
-2	5	1	17.50	18.45	-0.96	-90
-2	7	1	12.85	13.46	-0.62	90

h	k	l	$\|F_o\|$	$\|F_c\|$	F_o-F_c	phase
-2	9	1	14.83	12.30	2.53	-90
-2	11	1	3.88	8.55	2.53	-90
-2	13	1	1.85	1.91	-0.87	-90
-3	2	1	44.90	44.35	0.55	-90
-3	4	1	14.63	14.88	0.55	90
-3	6	1	2.87	4.31	-1.44	-90
-3	8	1	12.78	18.11	2.67	-90
-3	10	1	3.28	4.65	-1.37	90
-3	12	1	2.46	1.91	0.55	90
-4	1	1	18.11	15.38	2.73	90
-4	3	1	12.83	11.87	0.96	90
-4	5	1	2.80	3.08	-0.27	-90
-4	7	1	3.21	4.72	-1.50	90
-4	9	1	6.77	5.67	1.09	-90
-4	11	1	2.80	1.50	1.30	90
-5	2	1	8.75	6.29	2.46	90
-5	4	1	15.65	9.84	5.81	-90
-5	6	1	3.21	1.57	1.64	-90
-5	8	1	3.35	1.85	1.50	90
-5	10	1	3.08	3.42	-0.34	90
-5	12	1	1.85	0.21	1.64	-90
-6	1	1	32.53	27.88	4.65	90
-6	3	1	8.54	4.24	4.31	-90
-6	5	1	3.21	1.57	1.64	-90
-6	7	1	12.10	9.16	2.94	90
-6	9	1	3.14	1.44	1.71	-90
-6	11	1	2.19	1.57	0.62	-90
-7	2	1	15.45	13.46	1.98	-90
-7	4	1	3.28	2.39	0.89	90
-7	6	1	10.32	10.05	0.27	90
-7	8	1	3.21	4.24	-1.03	-90
-7	10	1	2.39	2.73	-0.34	90
-8	1	1	3.35	2.39	0.96	90
-8	3	1	11.07	8.95	2.12	-90
-8	5	1	13.94	12.64	1.30	90
-8	7	1	3.14	1.37	1.78	90
-8	9	1	2.39	1.30	1.09	-90
-9	2	1	3.35	2.80	0.55	-90
-9	4	1	3.28	0.34	2.94	90
-9	6	1	3.01	3.96	-0.96	90
-9	8	1	2.32	1.30	1.03	-90
-10	1	1	12.98	10.11	2.87	90
-10	3	1	3.08	1.37	1.71	-90
-10	5	1	2.73	0.96	1.78	-90
-10	7	1	2.05	0.89	1.16	90
-11	2	1	2.67	4.03	-1.37	90
-11	4	1	2.32	1.16	1.16	-90
-11	6	1	1.57	1.57	0.00	-90
-12	1	1	1.91	3.42	-1.50	90
-12	3	1	1.57	0.82	0.75	90.

TABLE OF ACCIDENTALLY ABSENT REFLECTIONS

h	k	l	h	k	l	h	k	l	h	k	l
0	10	0	0	5	9	10	0	-6	2	7	1
0	12	0	0	6	2	10	0	-4	2	11	1
1	13	0	0	6	4	10	0	-2	2	13	1
2	8	0	0	6	8	10	0	0	1	10	1
2	12	0	0	7	3	10	0	2	1	12	1
3	11	0	0	7	5	10	0	4	0	11	1
3	13	0	0	8	8	12	0	-2	0	13	1
4	10	0	0	9	5	12	0	0	-1	10	1
5	7	0	0	9	7	12	0	2	-1	12	1
5	11	0	0	10	0	12	1	1	-2	11	1
6	6	0	0	10	4	12	3	1	-2	13	1
6	10	0	0	10	6	11	2	1	-3	6	1
6	12	0	0	11	1	11	4	1	-3	10	1
7	3	0	0	11	3	11	6	1	-3	12	1
7	9	0	0	11	5	10	3	1	-4	5	1
7	11	0	0	12	0	10	5	1	-4	7	1
8	0	0	0	12	2	10	7	1	-4	11	1
8	2	0	0	12	4	9	4	1	-5	6	1
8	6	0	0	13	1	9	6	1	-5	8	1
8	8	0	0	13	3	9	8	1	-5	10	1
8	10	0	0	0	6	8	3	1	-5	12	1
9	1	0	0	0	8	8	5	1	-6	5	1
9	7	0	0	0	10	8	7	1	-6	9	1
9	9	0	2	0	-10	8	9	1	-6	11	1
10	6	0	2	0	-8	7	4	1	-7	4	1
10	8	0	2	0	-6	7	8	1	-7	8	1
11	1	0	2	0	2	7	10	1	-7	10	1
11	3	0	2	0	4	6	1	1	-8	1	1
11	5	0	2	0	8	6	7	1	-8	7	1
12	0	0	2	0	10	6	9	1	-8	9	1
12	2	0	4	0	-8	6	11	1	-9	2	1
0	0	6	4	0	2	5	8	1	-9	4	1
0	0	10	4	0	8	5	10	1	-9	6	1
0	1	9	6	0	-4	5	12	1	-9	8	1
0	2	4	6	0	-2	4	3	1	-10	3	1
0	2	8	6	0	6	4	9	1	-10	5	1
0	2	10	6	0	8	4	11	1	-10	7	1
0	3	5	8	0	-8	3	2	1	-11	2	1
0	3	9	8	0	-6	3	6	1	-11	4	1
0	4	6	8	0	-4	3	8	1	-11	6	1
0	4	8	8	0	0	3	10	1	-12	1	1
0	5	3	8	0	4	3	12	1	-12	3	1
0	5	7	8	0	6	2	1	1			

REFERENCES

(In alphabetical order of authors' names)

ANDREWS, C.L.	1960	Optics of the Electromagnetic Spectrum, Prentice-Hall: New Jersey.
BABINET, A.	1837	C.r.hebd. Séanc.Acad.Sci.Paris, 4, 638 (see especially 643-644).
BEEVERS, C.A.	1965	J.Chem.Educ., 42, 273.
BHUIYA, A.K., and STANLEY, E.	1963	Acta.Cryst., 16, 981.
BOERSCH, H.	1951	Z.Phys., 131, 78-81.
BRACEWELL, R.	1965	The Fourier Transform and its Applications, McGraw-Hill: New York.
BRATHOVDE, J.R. and LINGAFELTER, E.C.	1958	Acta Cryst., 11, 729-732.
BUERGER, M.J.	1960	Crystal-Structure Analysis, Wiley: New York.
CHAUDHURI, B. and HARGREAVES, A.	1956	Acta Cryst., 9, 793-800.
CROWDER, M.M., MORLEY, K.A. and TAYLOR, C.A.	1959	Acta Cryst., 12, 108-115.
CRUICKSHANK, D.W.J. and ROBERTSON, A.P.	1953	Acta Cryst., 6, 698-707.
CRUICKSHANK, D.W.J.	1956	Acta Cryst., 9, 915-923.
DARLOW, S.F.	1960	Ph.D. Thesis, Univ. of Cambridge.
DITCHBURN, R.W.	1963	Light, Blackie: London.
DOSSIER, B., BOUGHON, P. and JACQUINOT, P.	1950	J.des Rech.du C.N.R.S., Paris, 11, 49-69.
DRUDE, P.	1902	Theory of Optics, Longmans: London.

FORSYTH, J.B. and WELLS, M.	1959	Acta Cryst., 12, 412-415.
GIACOMO, P., ROIZEN-DOSSIER, B. and ROIZEN, S.	1964	J.Phys.(France), 25, 285-90.
HANDBOOK OF MATHEMATICAL FUNCTIONS	1964	Ed. Milton Abramowitz & Irene Stegun, National Bureau of Standards (USA).
HANSON, H.P., HERMAN, F., LEA , J.D. and SKILLMAN, S.	1964	Acta Cryst., 17, 1040-1044.
HARBURN, G.	1961	Ph.D. Thesis, Univ. of Manchester.
HARBURN, G. and TAYLOR, C.A.	1961	Proc.Roy.Soc., A, 264, 339-54.
HARBURN, G., TAYLOR, C.A. and YEADON, E.C.	1965	Brit.J.Appl.Phys., 16, 1367-1375.
HERRIOT, JOHN G.	1963	Methods of Mathematical Analysis and Computation, Wiley: New York.
HINDE, ROBERT MALCOLM	1951	Ph.D. Thesis, Univ. of Manchester.
HOLT, G. and WALL, D.K.	1965	J.Chem.Soc., 1965(Feb.) 1428-31.
HOSEMANN, R. and BAGCHI, S.N.	1962	Direct analysis of Diffraction of Matter. North Holland: Amsterdam.
HOWELLS, E.R., PHILLIPS, D.C. and ROGERS, D.	1950	Acta Cryst., 3, 210-214.
HUET, P.	1960	These, Fac.Sci.Caen, France.
HUGHES, W. and TAYLOR, C.A.	1953	J.Sci.Inst., 30, 105-9.
HUGHES, W. and TAYLOR, C.A.	1958	J.Sci.Inst., 35, 261-4.
IBALL, J. and MACKAY, K.J.H.	1962	Acta.Cryst., 15, 148-156 (also 157-160).
INTERNATIONAL TABLES FOR X-RAY CRYSTALLOGRAPHY	1962	Kynoch Press: Birmingham.
JACQUINOT, P.	1950	J.Phys.Rad., 11, 361-2.

JACQUINOT, P. and ROIZEN-DOSSIER, B.	1964	Progress in Optics (North Holland: Amsterdam), 3, 31-186.
JENKINS, F.A. and WHITE, H.E.	1957	Fundamentals of Optics, McGraw-Hill: New York.
KLUG, A.	1950	Acta Cryst., 3, 165-175.
KRONROD, ALEKSANDR SEMENOVICH	1965	Nodes and Weights of Quadrature Formulas. Consultants Bureau: New York.
LANCZOS, C.	1957	Applied Analysis. Pitman: London.
LANSRAUX, G. and BOIVIN, G.	1961	Can.J.Phys., 39, 158-88.
LIPSON, H. and COCHRAN, W.	1966	The Determination of Crystal Structures. Bell: London.
LIPSON, H. and TAYLOR, C.A.	1958	Fourier Transforms and X-Ray Diffraction. Bell: London.
LIPSON, H. and TAYLOR, C.A.	1965	Progress in Optics. (North Holland: Amsterdam), 5, 287-350.
LIPSON, H. and WALKLEY, K.	1968	Optica Acta, 15, 83-91.
LONGHURST, R.S.	1967	Geometrical and Physical Optics, Longmans: London.
MASCART, M.E.	1889	Traite D'Optique. Tome 1, Gauthier-Villars et Fils: Paris.
MEYER, CHARLES F.	1949	The Diffraction of Light, X-Rays and Material Particles. J.W.Edwards: Ann Arbor, Michigan.
MICHELSON, A.A.	1927	Studies in Optics. Univ. of Chicago Press.
PHILLIPS, D.C.	1954	Acta Cryst., 7, 746-751.
PINNOCK, P.R., TAYLOR, C.A. and LIPSON, H.	1956	Acta Cryst., 9, 173-8.
REDMAN, D.	1968	Science Journal, 4, 50-57.
REGITZ, MANFRED and HECK, GERHARD	1964	Chem.Ber., 97, 1482-1501.

ROBERTSON, J. MONTEATH	1953	Organic Crystals and Molecules. Cornell Univ.Press: New York.
ROBERTSON, J.M. and WHITE, J.G.	1945	J.Chem.Soc., 607-617.
ROLLETT, J.S.	1965	Methods in Computing Crystallography. Pergamon: Oxford.
SINTON, W.M.	1952	J.Opt.Soc.Am., 42, 284.
SOMMERFELD, A.	1964	Optics. Academic Press: New York.
STERN, PAUL GEORGE	1966	Ph.D. Thesis, Univ. of Manchester.
STONE, J.M.	1963	Radiation and Optics. McGraw-Hill, New York.
TABLES OF INTERATOMIC DISTANCES AND CONFIGURATIONS IN MOLECULES AND IONS.	1958	The Chemical Society: London.
TAYLOR, C.A.	1965	J.Sci.Inst., 42, 533-535.
TAYLOR, C.A. and LIPSON, H.	1957	Acta Cryst., 10, 739.
TAYLOR, C.A. and LIPSON, H.	1964	Optical Transforms. Bell: London.
TAYLOR, C.A. and MORLEY, K.A.	1959	Acta Cryst., 12, 101-5.
TAYLOR, C.A. and THOMPSON, B.J.	1957	J.Sci.Inst., 34, 439-447.
TEMPLETON, DAVID H.	1959	Acta Cryst., 12, 771-3.
VERDET, E.	1869	Leçons D'Optique Physique, Tome 1. Levistal: Paris.
WEBB, J.H.	1933	J.Opt.Soc.Amer., 23, 157.
WILSON, A.J.C.	1942	Nature, 150, 151-2.
WILSON, A.J.C.	1949	Acta Cryst., 2, 318-321.
WILSON, A.J.C.	1950	Acta Cryst., 3, 258-262.
YOUNG, THOMAS	1845	Lectures on Natural Philosophy. Taylor and Watton: London.

ACKNOWLEDGEMENTS

I should first like to thank my two supervisors, Professor H Lipson and Dr G Harburn, for their unfailing help and guidance during the course of the work described in this thesis. I am also grateful to Professor C A Taylor for his considerable assistance to me especially during my first year as a rather inexperienced research student. In addition, I should like to thank the staff and research students of this department, in particular Dr S F Darlow, Dr A Hargreaves and Miss A Sutherland, for their continual helpfulness. Thanks is also due to the members of the Department of Computation. Lastly, I should like to acknowledge the award of a Research Studentship by the Science Research Council and a Temporary Demonstratorship by the Institute, which have enabled me to carry out this work.

(*Reprinted from Nature, Vol.* 205, *No.* 4976, *pp.* 1095–1096, *March* 13, 1965)

Gas-phase Laser as a Source of Light for an Optical Diffractometer

THE commercial availability of gas-phase lasers giving a continuous output in the visible region of the spectrum solves a problem that has been troubling users of optical diffractometers for some time. It is sometimes necessary to study a region of a diffraction pattern which is so far removed from the centre that it subtends an angle which is large compared with that subtended by the detail to be resolved. If, for example, the distance between the region to be studied and the centre is 100 times the size of the detail to be resolved, it is clear that $\lambda/100$ is the maximum bandwidth that can be tolerated. The usual combination of mercury-vapour lamp and interference filter often gives too wide a band because of both the high-pressure broadening of the spectral lines and the problems of narrow-band filtering without undue reduction in effective source brightness. If the output of a helium–neon laser is focused on the pinhole of the diffractometer the necessary brightness is easily obtained with an extremely small bandwidth. Using a laser with an output of about 3 mW, photographic exposures are comparable with those for a 250-W compact-source mercury-vapour lamp in conjunction with a 70-Å bandwidth interference filter, even though the film is appreciably less sensitive to the laser wave-length (6328 Å) than to the usual mercury–yellow wave-length (5780 Å).

A striking illustration of the improvement in resolution of detail that can be obtained by using the laser is shown in Fig. 1. Harburn, Yeadon and Taylor have developed a method for controlling the effective phase of the light passing through different regions of a half-tone transparency used as a diffracting mask (unpublished work). This involves translation of a half-tone screen through a vector distance of one-half the diagonal of one of the square elements of the screen; the required pattern is then observed, not as usual around the zero order of the diffraction pattern of the screen, but around one of the first-order peaks. Since the screen is very fine the first-order peak is at a distance from the centre which is large compared with the detail to be resolved, and hence the method as originally reported[1] suffers greatly from the effect of wave-length spread.

In Fig. 1, *a* is a mask of holes. Its diffraction pattern, which is a continuous function involving only phases 0 and π since it is centrosymmetrical, was photographed and a half-tone mask prepared representing the pattern in both amplitude and phase. An image of the original object can then be observed in the appropriate region of

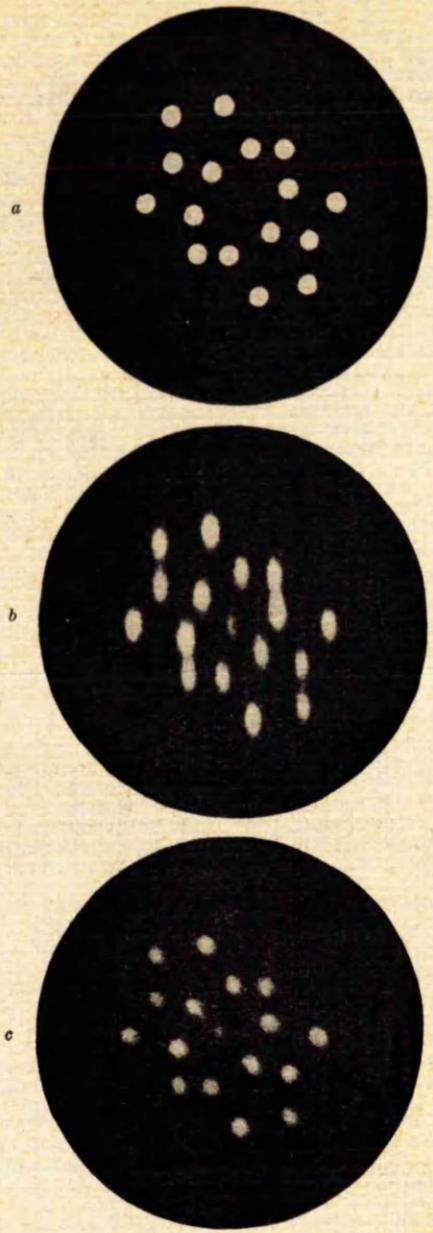

Fig. 1

the diffraction pattern of the half-tone mask. The image using conventional illumination is shown in *b* and the elongation of the peaks due to the wave-length spread is clearly visible. The considerable improvement in resolution when the laser is used as the source is shown in *c*.

G. HARBURN
K. WALKLEY
C. A. TAYLOR

Physics Department,
Faculty of Technology,
University of Manchester.

[1] Taylor, C. A., and Lipson, H., *Optical Transforms* (Bell, London, 1964).

Printed in Great Britain by Fisher, Knight & Co., Ltd., St. Albans.

OPTICA ACTA, 1968, VOL. 15, NO. 1, 83–91

On the Validity of Babinet's Principle for Fraunhofer Diffraction

H. LIPSON and K. WALKLEY

Physics Department, University of Manchester Institute of Science and Technology, Manchester 1, England

(*Received* 17 *February* 1967)

Abstract. Some misconceptions concerning Babinet's principle are pointed out. The Fraunhofer diffraction patterns of complementary screens are not similar unless the detail in the screens obeys certain conditions, which are not easily fulfilled. Some examples of the diffraction patterns of complementary screens are given, illustrating the extent to which Babinet's principle is valid in practice.

A way in which the principle can be used to give the diffraction patterns of three-dimensional crystal-structure models is indicated.

1. Introduction

The authors' interest in Babinet's principle arose when an attempt was made to apply it in developing the use of optical-transform techniques [1, 2] in crystal-structure determination. In these techniques, a representation of the x-ray diffraction pattern is compared with the optical transform (the Fraunhofer diffraction pattern) of an opaque screen pierced by an arrangement of holes representing the projection of a possible structure. According to Babinet's principle, it should be possible to replace the screen by a three-dimensional model of the structure and obtain the same transform; in practice the transform of the screen and of the model are different, although they have some features in common.

Few authors of text-books (except Ditchburn [3]) seem to be aware that there are any limitations to Babinet's principle, and none produces any illustration of it. These limitations have, however, been pointed out by Boersch [4] and Hosemann and Joerchel [5]. It is the aim of the present paper to extend their ideas and to give some experimental illustrations of the principle, obtained by means of the optical diffractometer [6].

2. Babinet's principle

Babinet's principle is concerned with the diffraction patterns of complementary screens—screens in which the opaque parts of one correspond to the clear parts of the other and vice-versa; such screens are supposed to give identical diffraction patterns except for a small region in the centre. In fact, this statement is far wider than was given by Babinet [7], a free translation from his original statement being as follows:

" Suppose that the eye observes a point source of light. If a small opaque object is placed just off the line of sight, the effect of this object is the same as that of a precisely similar aperture illuminated from the same source." This statement has been extended over the years to include the concept of complementary screens, although it is obviously a special case.

A typical 'proof' of Babinet's theorem applied to complementary screens states that the vector amplitude A_1 produced at any point in the diffraction pattern of one screen, when added to that, A_2, produced at the same point in the diffraction pattern of the other, gives the amplitude, A_0, produced by the unscreened wave; since, for Fraunhofer diffraction, this amplitude is zero except for a bright spot at the centre, we have:

$$\begin{aligned} A_1 + A_2 &= A_0 \\ &= 0. \end{aligned}$$

Thus $A_1 = -A_2$ and $|A_1|^2 = |A_2|^2$, giving equal intensities.

The fallacy in this 'proof' lies in the statement that $A_0 = 0$ except at the centre.

3. The diffraction pattern of a circular aperture

This fallacy can be explained by considering the two screens to have a circular boundary. It is often thought that the larger this aperture, the sharper the spot at the centre and thus the less the effect at other points (8). But in fact, as pointed out by Boersch [4], although the *relative* effect is less, the absolute effect increases with radius of aperture, as the following theory shows. The diffraction pattern of a circular aperture is given by the familiar relation:

$$A = 2\pi a^2 J_1(2\pi ya)/(2\pi ya), \tag{1}$$

where y is the distance from the centre of the pattern. The Bessel function $J_1(x)$ may be approximated by:

$$J_1(x) \approx \sqrt{\left(\frac{2}{\pi x}\right)} \cos\left(x - \frac{3}{4}\pi\right). \tag{2}$$

Hence

$$A \approx \frac{1}{\pi y} \sqrt{\left(\frac{a}{y}\right)} \cos\left(2\pi ya - \frac{3}{4}\pi\right). \tag{3}$$

Therefore the peak height of the pattern is given by:

$$|A|_{\max} \approx \frac{1}{\pi y} \sqrt{\left(\frac{a}{y}\right)}. \tag{4}$$

Hence, as the radius of the aperture increases, the average peak height of the pattern at any point at a distance y from the centre also increases, but only as the square root of the radius.

The effect of this result is illustrated in figure 1, which shows the diffraction patterns of a hexagonal arrangement of discs enclosed in circular apertures of increasing size.

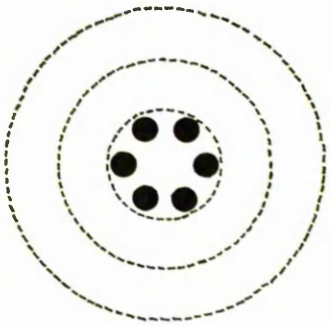

(*a*)

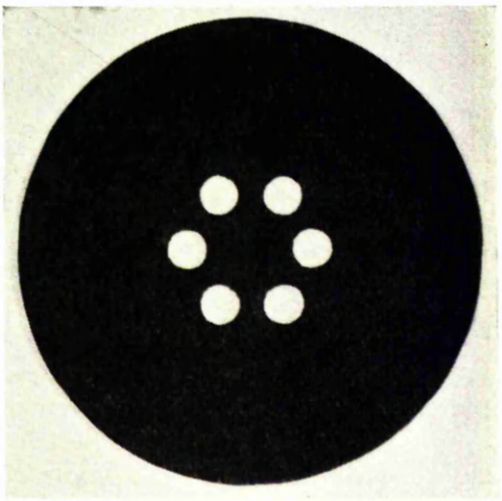

(*b*)

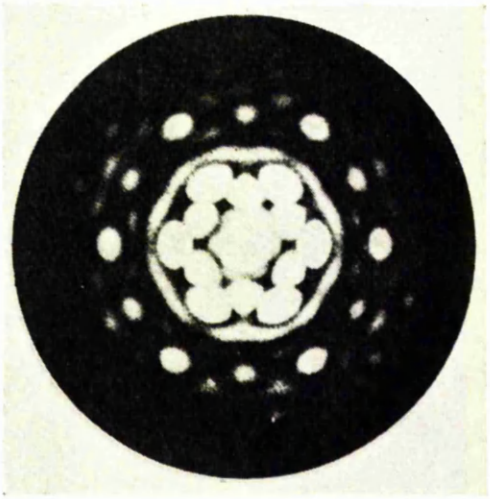

(*c*)

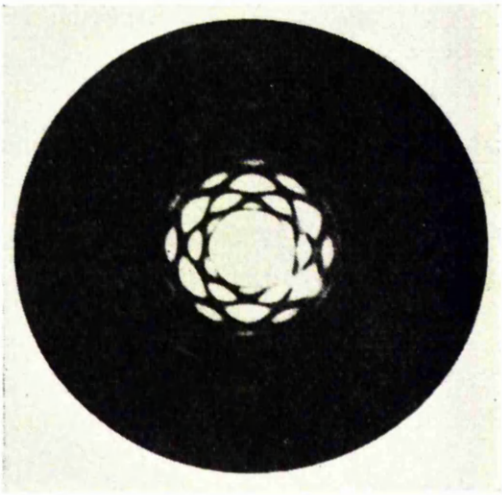

(*d*)

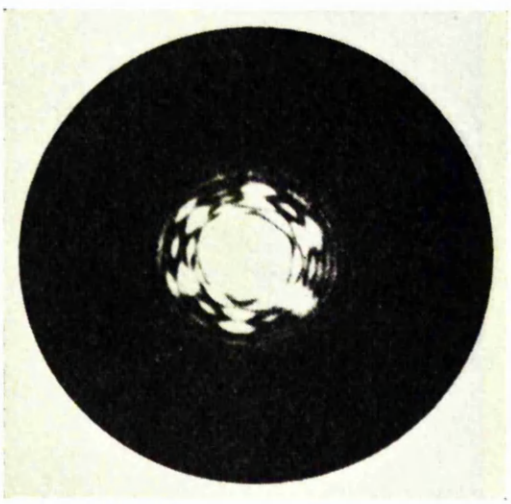

(*e*)

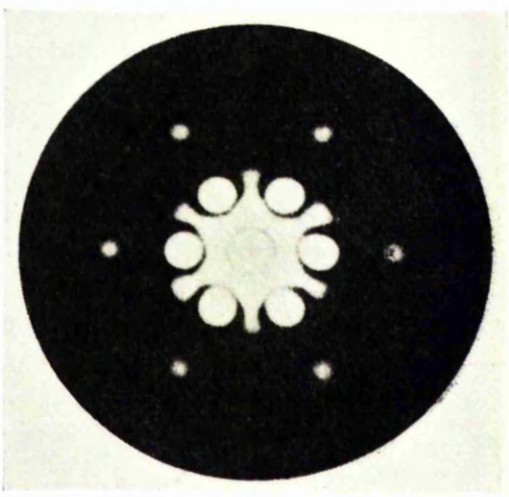

(*f*)

Figure 1. This shows the effect of placing a hexagonal arrangement of circular obstacles (*a*) in successively larger apertures (dotted lines). The corresponding optical transforms are respectively (*c*), (*d*) and (*e*). The complementary screen (*b*) and its transform (*f*) are also given for comparison.

4. Conditions for the validity of Babinet's principle

This theory suggests the following conditions for the production of two complementary screens that will give similar diffraction patterns.

1. The two screens must obstruct approximately half of the total aperture. This condition assures that both diffraction patterns will be as strong as possible.

2. The fine detail in the screens must be small compared with the dimensions of the total aperture. This condition assures that the diffraction patterns will have appreciable intensity for values of y at which the intensity of the diffraction pattern of the total aperture is negligible.

3. The fine detail must be evenly distributed. This condition helps to assure that the second condition is reasonably effective at every point in the diffraction pattern.

These three conditions may be simply derived for centrosymmetric complementary screens in a centrosymmetric aperture. The condition that the two complementary screens have the same diffraction pattern is that over a large section of the pattern:

$$|A_1|^2=|A_2|^2, \tag{5}$$

A_1 and A_2 being defined in § 2. The quantity A_0 in the expression

$$A_1+A_2=A_0 \tag{6}$$

must be zero over a considerable area of the diffraction pattern. From equation (6) we may write:

$$\begin{aligned}|A_2|^2&=A_2A_2^*\\&=A_1A_1^*+A_0A_0^*-2\,\mathrm{Re}\,(A_1A_0^*).\end{aligned} \tag{7}$$

For centrosymmetric complementary screens in a centrosymmetric aperture:

$$|A_2|^2=|A_1|^2+A_0(A_0-2A_1) \tag{8}$$

Hence the condition that the diffraction patterns of the complementary screens are similar, if any general centrosymmetric shape of aperture is assumed, is that

$$A_0-2A_1\approx 0. \tag{9}$$

A_1 may be re-written:

$$A_1=\sum_{n=1}^{N} F_n\cos(2\pi i\mathbf{r}_n\cdot\boldsymbol{\rho}) \tag{10}$$

if the diffracting screen 1 consists of a centrosymmetric distribution of N apertures each with scattering factor f_n and position vector $\mathbf{r}_n$. The vector $\boldsymbol{\rho}$ is the position vector in the plane of the diffracting pattern.

A_0 and A_1 are two independent oscillating functions of $\boldsymbol{\rho}$. Condition (5) can be satisfied for the largest number of values of $\boldsymbol{\rho}$ if

(a) $|A_0|_{\max}$, the maximum value of A_0, and $2|A_1|_{\max}$ are equal,

(b) (A_0-2A_1) oscillates through zero as frequently as possible.

Since $|A_0|_{\max}$ is proportional to S, the area of the aperture enclosing the screens, and $|A_1|_{\max}$ is proportional to ϵS, the clear area of screen 1, then condition (a) implies that $\epsilon=\frac{1}{2}$, condition (1).

Condition (b) implies that A_1 must oscillate as rapidly as possible if we assume that A_0 is fixed. In general the oscillation of A_1 is more rapid for larger values of

N, since the number of spatial frequency components in the diffraction pattern is increased. Also if the apertures are widely distributed, the oscillations of A are again more rapid since the average period of these spatial frequency components is decreased. It is obvious that condition (*b*) therefore corresponds to conditions (2) and (3).

5. Experimental studies

Figure 2 shows two one-dimensional complementary screens (*a*), (*b*) and their Fraunhofer diffraction patterns (*c*), (*d*). It will be seen that the centres of the diffraction patterns are quite dissimilar, and that even at higher angles there is only a general similarity.

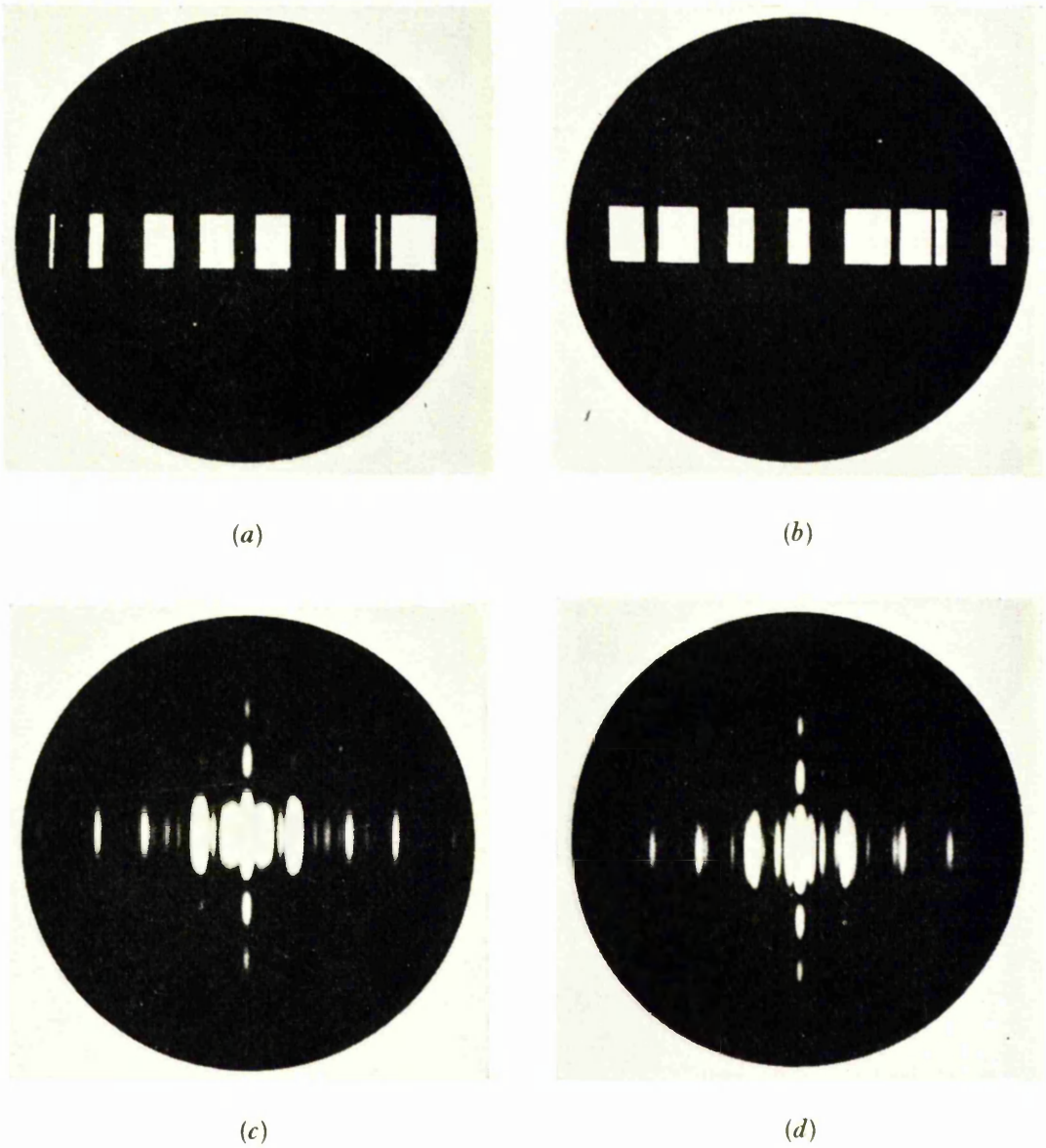

Figure 2. Illustration of two coarse complementary screens (*a*) and (*b*) and their respective optical transforms (*c*) and (*d*).

Figure 3 shows two two-dimensional complementary screens (*a*), (*b*) and their Fraunhofer diffraction patterns (*c*), (*d*). Here again the similarity is absent around the origin, but becomes clearer near the periphery of the diffraction patterns.

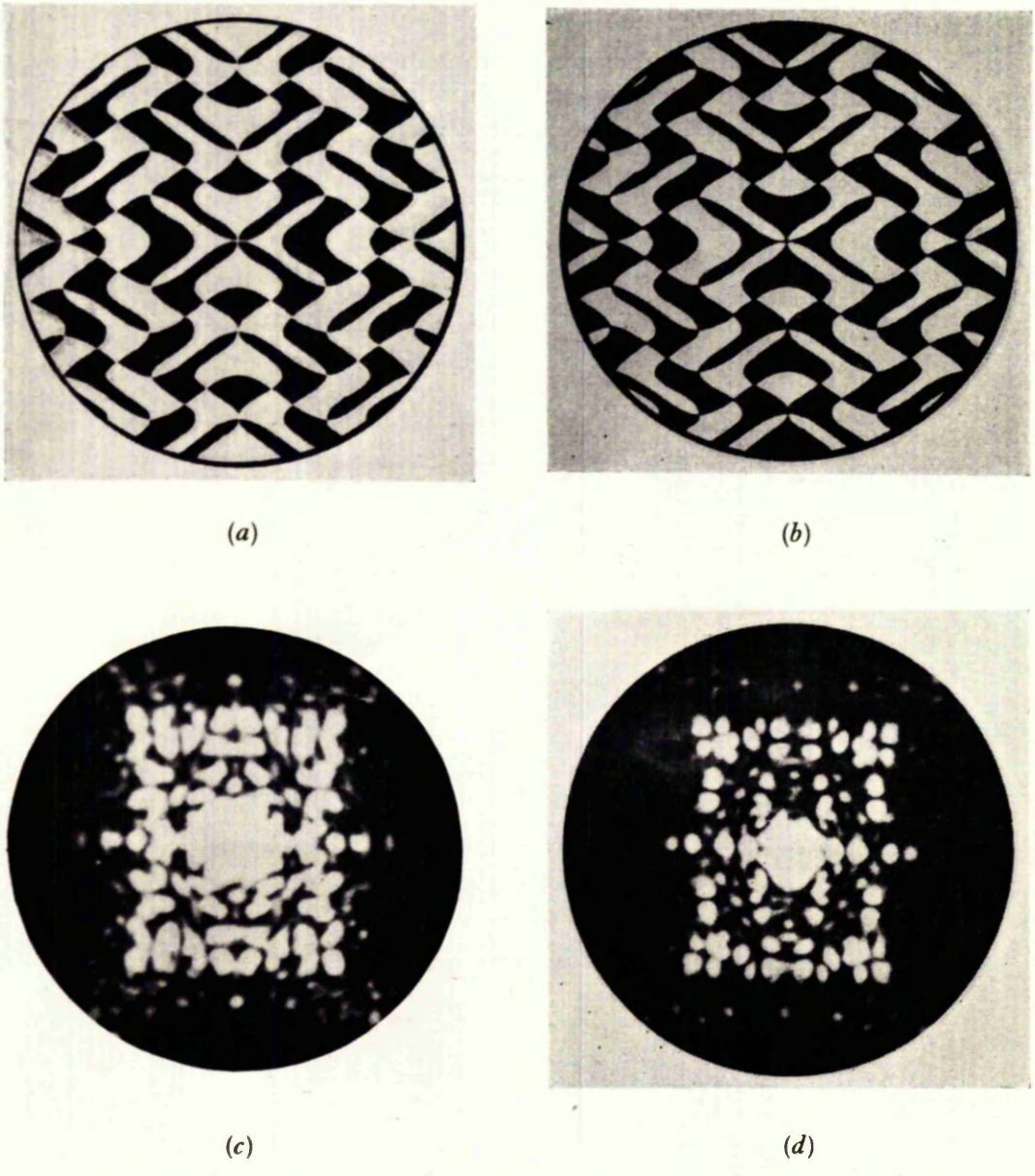

Figure 3. Two complementary screens (*a*) and (*b*), with detail finer than in figure 2, and their respective transforms (*c*) and (*d*).

6. Complementary gratings

Complementary gratings are defined as gratings with the same periodicity but in which the scattering points in one correspond to absence of scattering points in the other. Such gratings can be produced by punching holes (figure 4 (*a*), (*b*)) and if both gratings contain approximately equal numbers of holes the

correspondence of their diffraction patterns should be exact. Figure 4 (*c*), (*d*) shows that this result is very accurately fulfilled.

These gratings have some relation to the theory of homometric structures in crystallography (9).

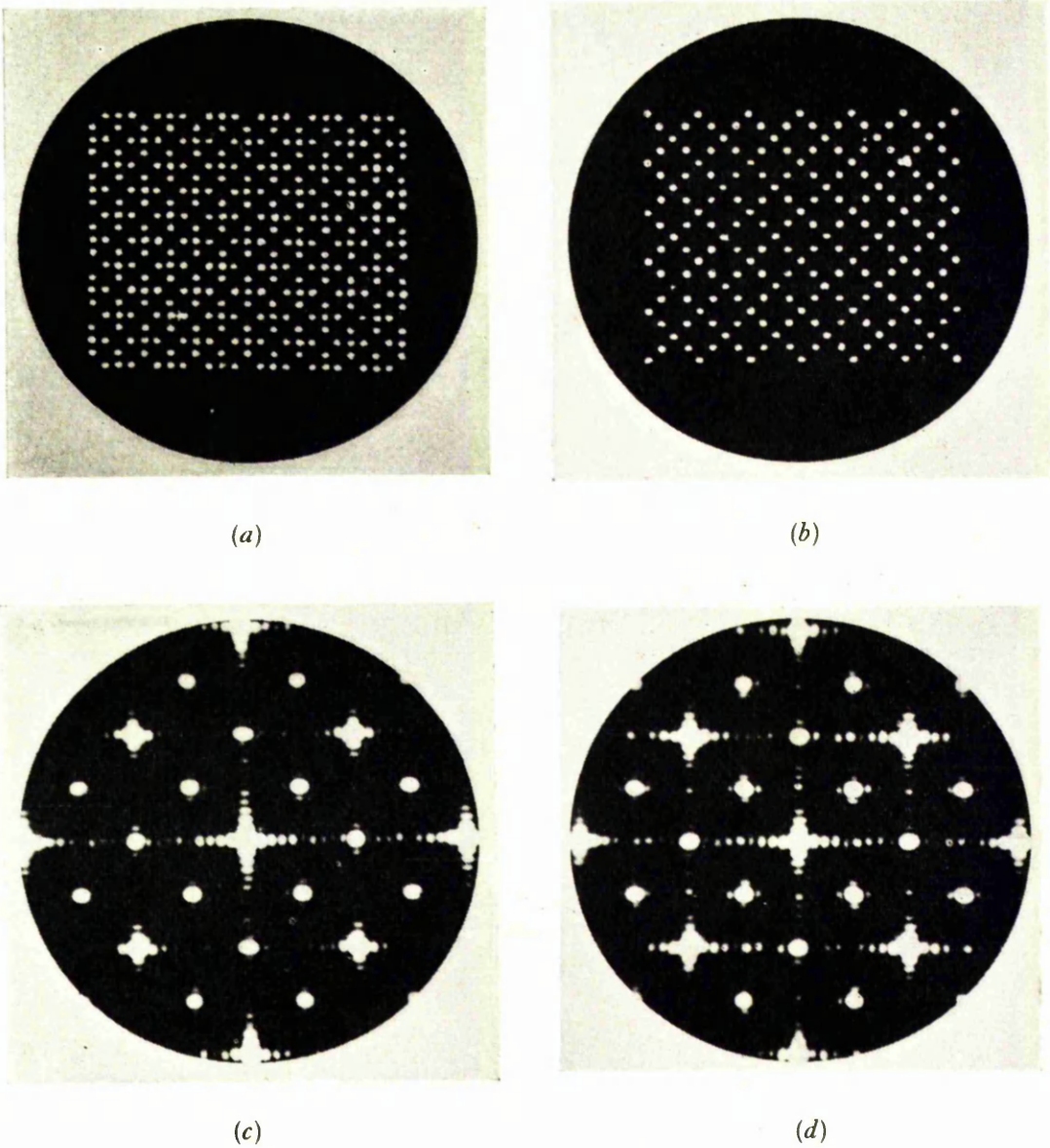

Figure 4. Two complementary gratings (*a*) and (*b*) and their respective transforms (*c*) and (*d*).

7. The production of diffraction patterns from coarse screens

Since the main reason for the invalidity of Babinet's principle is the presence of fringes (equations (1), (2)) in the diffraction pattern of a circular aperture, if these fringes could be eliminated, the principle would be better obeyed. In principle, fringes will not occur if the transmission function of the aperture is so

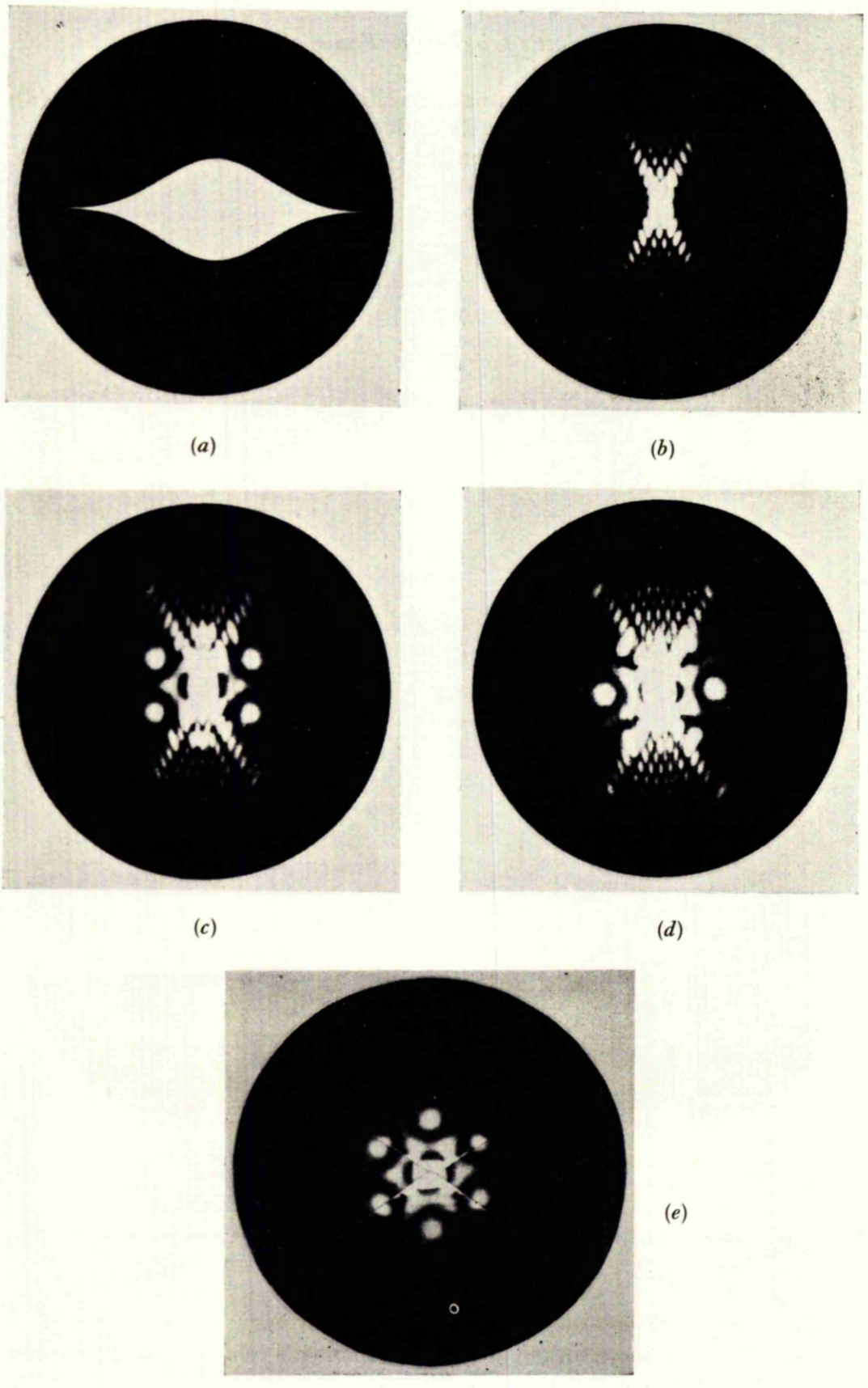

Figure 5. (*a*) represents an aperture whose diffraction pattern is near zero over a finite angle in the transform (*b*). The hexagonal arrangement of obstacles in figure 1 (*a*) gives a transform in the zero region which does not contain any effect due to the aperture (*c*). (*d*) shows the transform of the obstacles in a different orientation. (*c*) and (*d*) may be combined to give the total transform of the obstacles, cf. figure 1 (*f*).

adjusted that the diffracted intensity approaches zero asymptotically (apodization). Although it has not been found possible to prepare such an aperture, a one-dimensional function can be represented (figure 5(*a*)) and fringes will be absent from its diffraction pattern over a finite angle (figure 5 (*b*)). By piecing together several diffraction patterns (figure 5 (*c*)) with the model in different orientations within the aperture a fairly good representation of the diffraction pattern of the model can be obtained (cf. figure 1 (*a*)).

On indique quelques idées erronnées concernant le principe de Babinet. Les figures de diffraction de Fraunhofer d'écrans complémentaires ne sont pas semblables si le détail dans les écrans n'obéit pas à certaines conditions, qui ne sont pas facilement remplies. On présente quelques exemples de figures de diffraction d'écrans complémentaires, illustrant jusqu'à quel point le principe de Babinet est valable en pratique. On indique une façon suivant laquelle on peut utiliser le principe pour obtenir les figures de diffraction de modèles tridimensionnels de structures cristallines.

Es wird auf die Gefahr von Fehlschlüssen aus dem Babinetschen Prinzip hingewiesen. Die Fraunhoferschen Beugungserscheinungen komplementärer Schirme sind nur dann gleich, wenn die Schirme im Einzelnen gewisse Bedingungen erfüllen, die gar nicht leicht einzuhalten sind. Es werden einige Beispiele von Beugungserscheinungen an komplementären Schirmen gezeigt, die den Umfang der Gültigkeit des Babinetschen Prinzips in der Praxis verdeutlichen.

Das Babinetsche Prinzip kann dazu benutzt werden, die Beugungserscheinungen von Modellen dreidimensionaler Kristallstrukturen zu bestimmen.

References

[1] Lipson, H., and Taylor, C. A., 1958, *Fourier Transforms and X-ray Diffraction* (London : Bell).
[2] Taylor, C. A., and Lipson, H., 1964, *Optical Transforms* (London : Bell).
[3] Ditchburn, R. W., 1963, *Light* (London : Blackie), p. 205.
[4] Boersch, H., 1951, *Z. Phys.*, **131**, 78.
[5] Hosemann, R., and Joerchel, D., 1954, *Z. Phys.*, **138**, 209.
[6] Taylor, C. A., and Lipson, H., 1964, *Optical Transforms* (London : Bell), p. 29.
[7] Babinet, A., 1837, *C. r. hebd. Séanc. Acad. Sci., Paris*, **4**, 638.
[8] Meyer, C. F., 1949, *The Diffraction of Light, X-rays and Material Particles* (Ann Arbor : J. W. Edwards), p. 233.
[9] Patterson, A. L., 1944, *Phys. Rev.*, **65**, 195.